2013

Understanding multidrug resistance in Gram-negative bacteria -- A study of a drug efflux pump AcrB and a periplasmic chaperone SurA

Meng Zhong
University of Kentucky, meng_raul7@hotmail.com

STUDENT AGREEMENT:

I represent that my thesis or dissertation and abstract are my original work. Proper attribution has been given to all outside sources. I understand that I am solely responsible for obtaining any needed copyright permissions. I have obtained and attached hereto needed written permission statements(s) from the owner(s) of each third-party copyrighted matter to be included in my work, allowing electronic distribution (if such use is not permitted by the fair use doctrine).

I hereby grant to The University of Kentucky and its agents the non-exclusive license to archive and make accessible my work in whole or in part in all forms of media, now or hereafter known. I agree that the document mentioned above may be made available immediately for worldwide access unless a preapproved embargo applies.

I retain all other ownership rights to the copyright of my work. I also retain the right to use in future works (such as articles or books) all or part of my work. I understand that I am free to register the copyright to my work.

REVIEW, APPROVAL AND ACCEPTANCE

The document mentioned above has been reviewed and accepted by the student's advisor, on behalf of the advisory committee, and by the Director of Graduate Studies (DGS), on behalf of the program; we verify that this is the final, approved version of the student's dissertation including all changes required by the advisory committee. The undersigned agree to abide by the statements above.

Meng Zhong, Student

Dr. Yinan Wei, Major Professor

Dr. John Anthony, Director of Graduate Studies

UNDERSTANDING MULTIDRUG RESISTANCE IN GRAM-NEGATIVE BACTERIA--A STUDY OF A DRUG EFFLUX PUMP ACRB AND A PERIPLASMIC CHAPERONE SURA

THESIS

A thesis submitted in partial fulfillment of the requirements
for the degree of Doctor of philosophy in the College of
Arts and Sciences at the University of Kentucky

By

Meng Zhong

Lexington, KY

Director: Dr. Yinan Wei, Professor of Chemistry

Lexington, KY

2013

ABSTRACT OF THESIS

UNDERSTANDING MULTIDRUG RESISTANCE IN GRAM-NEGATIVE BACTERIA--A STUDY OF A DRUG EFFLUX PUMP ACRB AND A PERIPLASMIC CHAPERONE SURA

Multiple drug resistance (MDR) has been a severe issue in treatment and recovery from infection.Gram-negative bacteria intrinsically exhibit higher drug tolerance than Gram-positive microbes. In this thesis, two proteins involved in Gram-negative bacterial MDR were studied, AcrB and SurA.

Resistance-nodulation-cell division pump AcrAB-TolC is the major MDR efflux system in Gram-negative bacteria and efficiently extrudes a broad range of substances from the cells. To study subtle conformational changes of AcrB *in vivo*, a reporter platform was designed. Cysteine pairs were introduced into different regions in the periplasmic domain of the protein, and the extents of disulfide bond formation were examined. Using this platform, an inactive mutant, $AcrB_{\Delta loop}$, was created that existed as a well-folded monomer *in vivo*. Next, random mutageneses were performed on a functionally compromised mutant, $AcrB_{P223G}$, to identify residues that restored the function loss. The mechanism of function restoration was examined.

SurA is a periplasmic molecular chaperone for outer membrane biogenesis. Deletion of SurA decreased outer membrane density and bacterial drug resistance. The dependence of SurA function on structural flexibility and stability was examined. In addition, the effect of molecular crowding on SurA interaction with its outer membrane protein substrates was examined.

KEYWORDS: Multidrug resistance, multidrug efflux pump, chaperone, AcrB, SurA

Meng Zhong

Apr. 26th , 2013

UNDERSTANDING MULTIDRUG RESISTANCE IN GRAM-NEGATIVE BACTERIA--A STUDY OF A DRUG EFFLUX PUMP ACRB AND A PERIPLASMIC CHAPERONE SURA

By

Meng Zhong

Yinan Wei, Ph.D.
Director of Thesis

John Anthony, Ph. D.
Director of Graduate Studies

May 2nd, 2013

ACKNOWLEDGEMENTS

I would like to express my deepest gratitude to my graduate advisor, Dr. Yinan Wei, for her tremendous support and guidance through the whole process. Whenever I face difficulties in my research, she is always there giving me insightful advices, instructions and encouragements. Thank her for taking all the time and efforts to correct my writings and help me with fellowship application. I would like to thank Dr. Rymond, Dr. Miller, Dr. Atwood, and Dr. Dziubla for sharing their expertise and knowledge and supervising my dissertation work. Without their guidance and help, this thesis would not have been possible.

I would like to thank Dr. Wei Lu, Dr. Jun Fang for teaching me all the molecular biology techniques. Thank my labmates for their help in my research.

I would like to acknowledge University of Kentucky, department of chemistry, and National Science Foundation (1158036) for their financial support.

Last but now least, I would like to thank my family for their unconditionally caring, love, encouragement, support throughout all these years. I can't tell how lucky I am to have you all in my life. Thanks everyone for making this thesis possible.

Table of Contents

List of Tables

List of Figures

List of Abbreviations

MDR: multidrug resistance

RND: Resistance-Nodulation-cell Division

OMP: Outer Membrane Protein

MRSA: Methicillin Resistant *Staphylococcus Aureus*

NDM-1: New Delhi Metallo-beta-lactamase-1

CRE: Carbapenem-Resistant *Enterobacteriaceae*

ATP: Adenosine Triphosphate

ITC: isothermal titration calorimetry

MFP: Membrane fusion protein

CD: Circular dichroism

DDM: n-dodecyl-β-maltoside

PMSF: phenylmethylsulfonyl fluoride

SDS: Sodium dodecyl sulfate

PAGE: Polyacrylamide gel electrophoresis

BN-PAGE: blue native polyacrylamide gel electrophoresis

IPTG: isopropyl-β-D-1-thiogalactopyranoside

EDTA: Ethylenediaminetetraacetic acid

Ni-NTA agarose: Nickel nitrilotriacetic acid agarose

IAM: Iodoacetamide

NBT: Nitro-blue tetrazolium chloride

BCIP: 5-bromo-4-chloro-3’-indolyphosphate p-toluidine salt

SLS: Sodium lauryl sulfate

SSB: Single stranded DNA binding protein

sfGFP: Super folded green fluorescent protein

NHS: N-Hydroxysuccinimide

DSP: Dithiobis(succinimidylpropionate)

EB: ethidium bromide

E.coli: *Escherichia coli*

H. pylori: helicobacter pylori

CHAPTER I. INTRODUCTION

1.1 A Brief History of Antibiotics Development

Long before the invention of the word "antibiotic", application of mold and plant extracts have been documented in disease treatment in ancient Greek and ancient Egypt.[1] In 1928, Alexander Fleming discovered the bactericidal property of penicillin in a *staphylococcus aureus* plate, suggesting that a particular group of compounds extracted from microbes could be used to treat infection effectively.[2] This kind of compounds were later named antibiotic. The urgent need of antimicrobials in treating wounded soldiers in World War II stimulated the beginning of the antibiotic era.[3] Till 1960s, more than 100 antibiotics became commercially available and were used extensively in the treatment of infectious disease.[4] This period of time was considered as the golden age of antibiotics.

Based on the mechanism of action, antibiotics are categorized into several classes. Antibiotics can be bactericidal or bacteriostatic through inhibiting the synthesis of cell wall, DNA, RNA, and protein, cell growth, and cell division.[5-8] Table 1.1 listed major classes of antibiotics and their working mechanisms.[5-10] At the beginning, antibiotics were mostly natural products isolated from microorganisms. Later compounds derived or synthesized from natural products were used. Finally, taking advantage of the structures of known natural products, scientists successfully designed and synthesized a great variety of antibiotics by substituting different functional groups.[11-13] Despite the remarkable success in exploring the natural product scaffolds, the pace of the advancement of antibiotic development slowed down in 1960s.[14, 15] The pre-existed drug resistance of structurally related antibiotics killed most new antibiotics in the cradle. The partial to complete failures in the mining of novel antibiotics drove away most pharmaceutical companies and financial investments.[16-18] As a result, no new class of antibiotics was developed

from 1962 to 2002. Since 2002, only four new classes of antibiotics have been approved and are available commercially. [19-22]

Table 1.1 List of Antibiotics by their classes and mechanisms of action.[5-10]

Classes	Examples	Mechanism
Aminoglycosides	Gentamicin, Kanamycin, Neomycin, Spectinomycin	Bind to ribosome subunits, inhibit protein synthesis, and disrupt bacterial cell membrane
β-lactam antibiotics	Penicillin, Cephalosporins, Carbapenems	Inhibit bacterial cell wall synthesis
Glycopeptides	Vancomycin, Teicoplanin	Inhibit peptidoglycan synthesis in bacterial cell wall
Lincosamides	Lincomycin, Clindamycin	Bind to 50s subunit of ribosome, inhibit protein synthesis
Lipopeptides	Daptomycin, Polymixin B	Bind to bacterial membrane, inhibit protein, DNA, and RNA synthesis
Macrolides	Erythromycin, Azythromycin	Bind to 50s subunit of ribosome, inhibit protein synthesis
Oxazolidonones	Linezolid, Torezolid	Inhibit protein synthesis
Polypeptides	Bacitracin, Colistin	Alter gram negative bacterial outer membrane and cytoplasmic membrane permeability
Quinolones	Ciprofloxacin, Levofloxacin	Inhibit DNA replication and transcription
Sulfonamides	Sulfadiazine, Sulfisoxazole	Inhibit folate synthesis
Tetracyclines	Tetracycline, Doxycycline	Bind to 30s subunit of ribosome, inhibit protein synthesis

1.2 Current Situation of Multiple Drug Resistances

Since the discovery of penicillin, antibiotics were considered as “magic bullets” in curing infectious diseases. They have been misused and abused in the clinical treatment. For example, antibacterial drugs were inappropriately prescribed to patients with viral infection due to misdiagnosis. Premature cessation of therapy failed to eradicate the pathogens, instead provoking resistance in the surviving bacteria. Additionally, in some countries, especially developing countries, antibiotics are sold as over the counter drugs without prescription. Another major factor that causes drug resistance is the large scale usage of antibiotics in animal farming which later consumed by human and accumulated in food chain.[23-26] Consequently, microbes developed cross-resistance to a series of structurally and functionally unrelated drugs. In the past decade, multidrug resistance (MDR) has been found toward all available antibiotics, presenting one of the biggest threats to public health.

In the pre-antibiotic era, antibiotic resistance was only identified in a very small portion of bacterial strains that have intrinsic and constitutive high drug tolerance, such as *Pseudomonas aeruginosa*.[27, 28] Gradually, usage of antibiotics served as an environmental selective pressure to select for strains with elevated drug tolerance. Mutations may first occur as random errors in replication. Bacteria with higher drug resistance were able to survive. Those genes who confer high antibiotic resistance were amplified and accumulated in pathogens under the selection process.[29] The horizontal transfer of genetic materials enables the wide spread of resistance. The resistant genes can be transferred by naked DNA transformation, phage-mediated transduction and cell-to-cell conjugation.[30] MDR is often found in organisms that acquired plasmids encoding genes for multidrug resistance.

Undoubtedly, the prevalence of MDR increased the morbidity, mortality of bacteria infection, making the treatment more difficult. In 2010, Center of Disease Control reported that bacterial infection results approximately 30,000 deaths each year in the United States. It is estimated that annual cost to treat infections of six major bacteria was over $1.87 billion.[31] nowadays, the increasing frequency of communication between countries makes MDR an international epidemic problem. Every year, species with new antibiotic resistance are identified and spread all over the world, attracting great public concern. The word "superbug" becomes more and more prevalent. Methicillin resistant *Staphylococcus aureus* (MRSA) is one of the most well-known examples of superbug. Surveys conducted in 2006 estimated more than 53 million people were carriers of MRSA globally, and the number is increasing each day.[32] Another alarming example is the fast spread of New Delhi metallo-beta-lactamase-1 (NDM-1) gene in a variety of strains of bacteria. It was first detected in colonies of *Klebsiella pneumonia* in India. Within a year, it has been found in more than 30 countries. So far, three years since the detection of the first case, effective treatment for infections caused by bacteria harboring NDM-1 gene is still lacking.[33, 34] Most recently, it is reported that another deadly superbug, carbapenem-resistant *Enterobacteriaceae* (CRE) was found in Virginia in December 2012. The mortality of infections caused by CRE can be as high as 40%.[35] These superbugs present great challenge in the treatment of bacterial infection. Unfortunately, under current medical condition, there is still a shortage of valid methods to combat superbug infection. Numerous efforts have been devoted in conquering this problem. Many strategies have been developed targeting different mechanisms of bacterial drug resistance.

1.3 Mechanisms Of Resistance To Antibacterial Agents

Multiple biochemical factors contributed to the fast spread of the MDR, presenting tremendous challenges in the fight against infectious diseases. There are five major mechanisms from which microbes acquire drug resistant. (Figure 1.1)[36] First, an organism can gain resistance to a drug target via mutation or enzymatic alteration. For example, due to an alteration of the ribosomal target, *Acinetobacter* developed resistance to two aminoglycosides: streptomycin and spectinomycin.[37] An additional example is MRSA. Acquisition of *mecA* gene helped express penicillin-binding protein 2a which cannot interact with methicillin or other β-lactam antibiotics, thereby leading to extremely strong drug tolerance.[38] Second, some drugs are inactivated by enzymatic degradation and modifications. The inactivation could be achieved by hydrolysis, group transfer, and redox mechanism.[39] Till now, more than 200 different β-lactamases have been identified, which is the major reason for resistance of β-lactam group antibiotics.[40] Third, bypass of the inhibited mechanism of antibiotics conferred high drug resistance to certain group of antibiotics.[41] One of the well-studied examples is a glycopeptide, vancomycin. Vancomycin inhibits cell wall synthesis by binding to the D-Ala-D-Ala in the pentapeptide of peptidoglycan. Vancomycin-resistant Enterococcus reprograms the synthesis pathway to produce D-Ala-D-Lac, so that the binding affinity of vancomycin to the peptide is reduced by 1000-fold.[42] Fourth, overexpression of drug targets exhibits titration effects on antibiotics, leading to reduction of drug efficiency. Fifth, drug penetration can be slowed down or inhibited by certain group of proteins and cell walls. For instance, multidrug efflux pumps can export a broad spectrum of compounds, including antibiotics, dyes, detergents, fatty acids, biocides, and organic solvents.[43] A low permeability barrier can provide a shield in order to decrease the influx of different drugs.[44] Among these five mechanisms, the first four mechanisms are specific towards a single drug or drugs with similar structures, while the last mechanism apply more generally. Therefore,

the latter mechanism is more difficult to target, which is my main research focus in this thesis. Moreover, microbes may employ more than one mechanism, making it even more challenging to combat multidrug resistance.

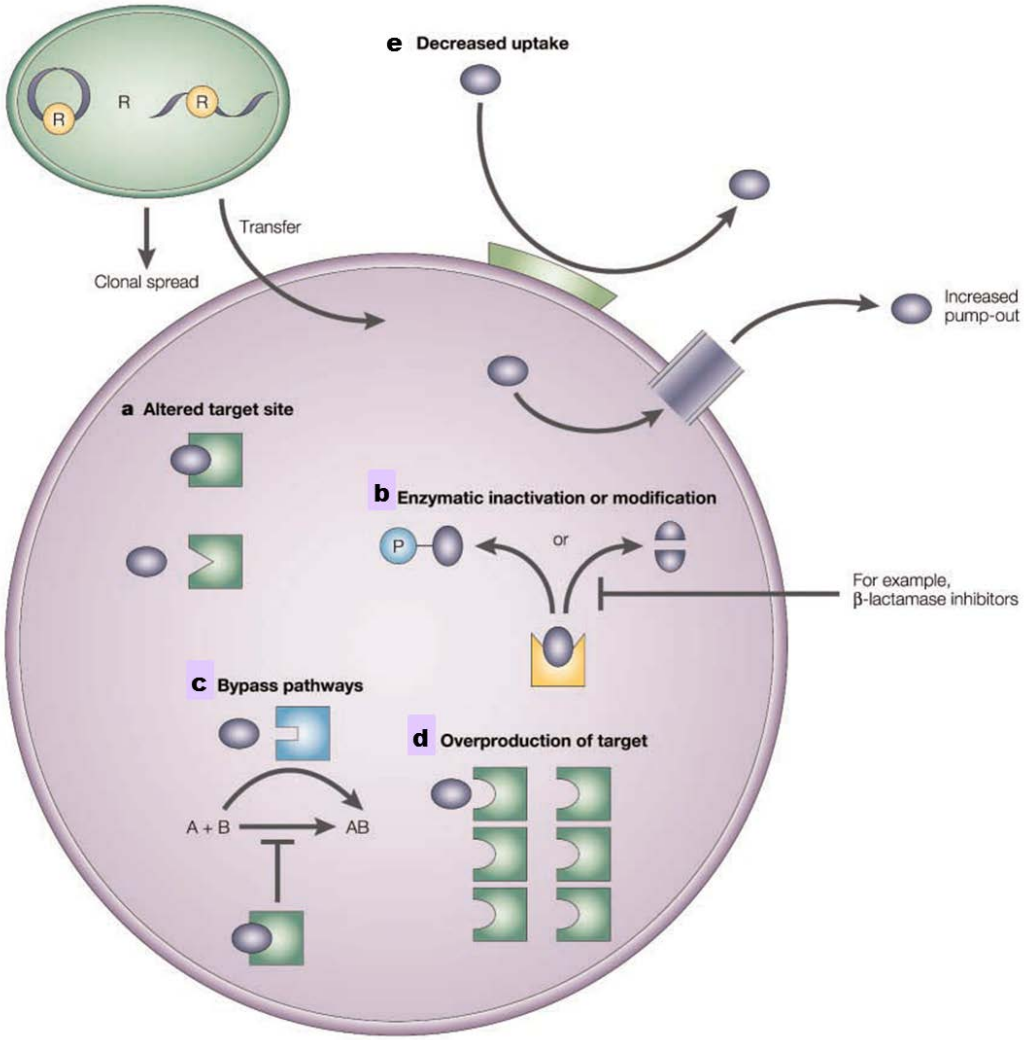

Figure 1.1 Mechanisms confer antibiotic resistance in bacteria.[45] Reprinted by permission from Macmillan Publishers Ltd: *Nat. Rev. Drug. Discover.*, ©2002

1.4 Gram Negative Bacterial Infection *vs* Gram Positive Bacterial Infection

Bacteria can be grouped into Gram-negative and Gram-positive strains based on Gram staining. Gram-negative bacteria are those that do not retain crystal violet dye after staining. The

difference between the two groups of bacteria lies in their cell walls (Fig. 1.2).[46] Gram-positive bacteria cells are covered with a thick layer of peptidoglycan, whereas Gram-negative bacteria have a more complex cell envelope structure. Gram-negative bacterial cell wall contains two phospholipid membranes, between which lies a thin intermediate layer of peptidoglycan. Lipopolysaccharide is bound to the outer leaflet of the outer membrane and stablizes the entire membrane structure. The non-covalent linkage between lipid A and divalent cations is highly polarized, preventing the entrance of hydrophobic molecules. At the same time, the high hydrophobicity of the phospholipid bilayer slows down the penetration of hydrophilic compounds.[47] The extra layer provides such a good protection that 90% of antibiotics effective against Gram-positive bacteria showed much lower activity against Gram-negative bacteria.[48] Additionally, a large group of inner and outer membrane proteins embedded in the two membranes. The majority of outer membrane proteins (OMPs) served as transportation channels for small hydrophilic substances. Some of the outer membrane proteins assemble together with inner membrane proteins to selectively pump out a broad range of compounds out of the cells. Therefore, these proteins could potentially be drug targets in combating MDR in the bacteria.

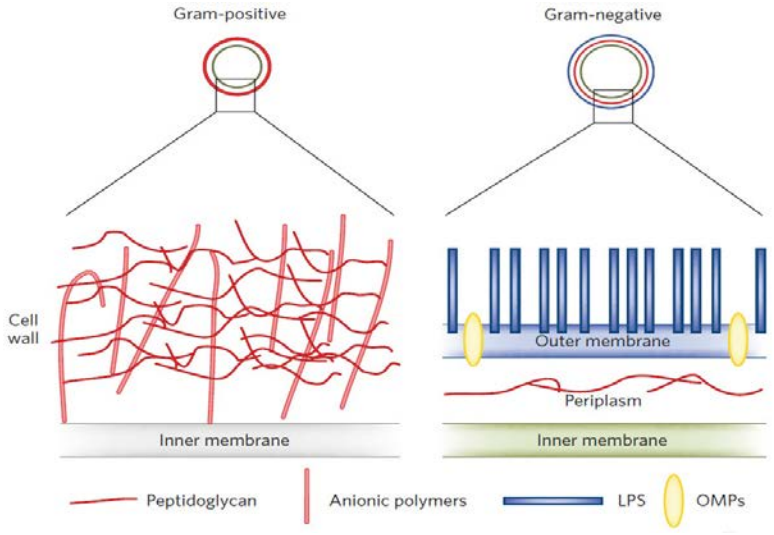

Figure 1.2 Cell envelope of Gram-negative (left) and Gram-positive (Right) bacteria.[46] Reprinted by permission from Macmillan Publishers Ltd: *Nat. Chem. Biol.* (1) © 2011

1.5 Bacterial Multidrug Efflux Pump

Based on sequence homology, bacterial efflux system can be grouped into five classes[49]: a) The major facilitator (MF) superfamily, also known as uniporter-symporter-antiporter family. Transporters in the MF family are the dominate substance excluding pumps in Gram-positive bacteria. They are responsible for transporting small solutes powered by chemiosmotic ion gradient. b) The ATP-binding cassette (ABC) family. Hydrolysis of adenosine triphosphate (ATP) provides energy for both the uptake and efflux of small molecules and macromolecules. c) The small multidrug resistance (SMR) family. These transporters shared a similar structure containing four transmembrane helices and driven by proton motive force. d) The multidrug and toxic compound extrusion (MATE) family. The efflux of this group of transporters is mediated by sodium gradient. e) The resistance-nodulation-division (RND) family, which is the major contributor to drug resistance in Gram-negative bacteria.[50] My research is focused on exploring structure and assembly of one of the most extensively studied RND pump, AcrAB-TolC.

1.6 AcrAB-TolC Tripartite Efflux Pump

AcrA, TolC in AcrAB-TolC system

AcrAB-TolC is one of the most extensively studied Gram-negative RND pump. In the complex, AcrA is a membrane fusion protein that facilitates the interaction between AcrB and TolC, and assembly of the entire pump. The α-helical hairpin domain of AcrA is the TolC binding domain. The exact interface of AcrA and AcrB remains unknown, but the α-β-barrel domain on AcrA is

thought to be the AcrB binding domain. AcrA may exist as a trimer or hexamer *in vivo*, which remains controversial .[51]

TolC is the outer membrane component of the pump and the final exit of the substrates. It is a trimeric protein composed of three 428-residue protomers. TolC trimer forms a long tunnel-like structure of 140 Å in length, transversing the entire outer membrane and the majority of the periplasmic space (Fig. 1.3). The transmembrane domain of TolC is consisted of 12 anti-parallel β-strands. They forms a 40 Å long β-barrel tunnel. The periplasmic part is composed of 12 α-helices, extending about 100 Å into the periplasm. The internal diameter of TolC is 35 Å. When TolC is recruited by an inner membrane complex, conformational rearrangements in the inner H7/H8 coiled coils and the outer H3/H4 coiled coils are induced. This opens the tunnel by approximately 30 Å, allowing the protein to transport molecules as large as full-length proteins.[52] Besides its role in the AcrAB-TolC tripartite efflux system, TolC is associated with several other inner membrane translocase complexes to export a large variety of substrates out of the cell, including enzymes, metals, antibiotics and toxins.[53, 54]

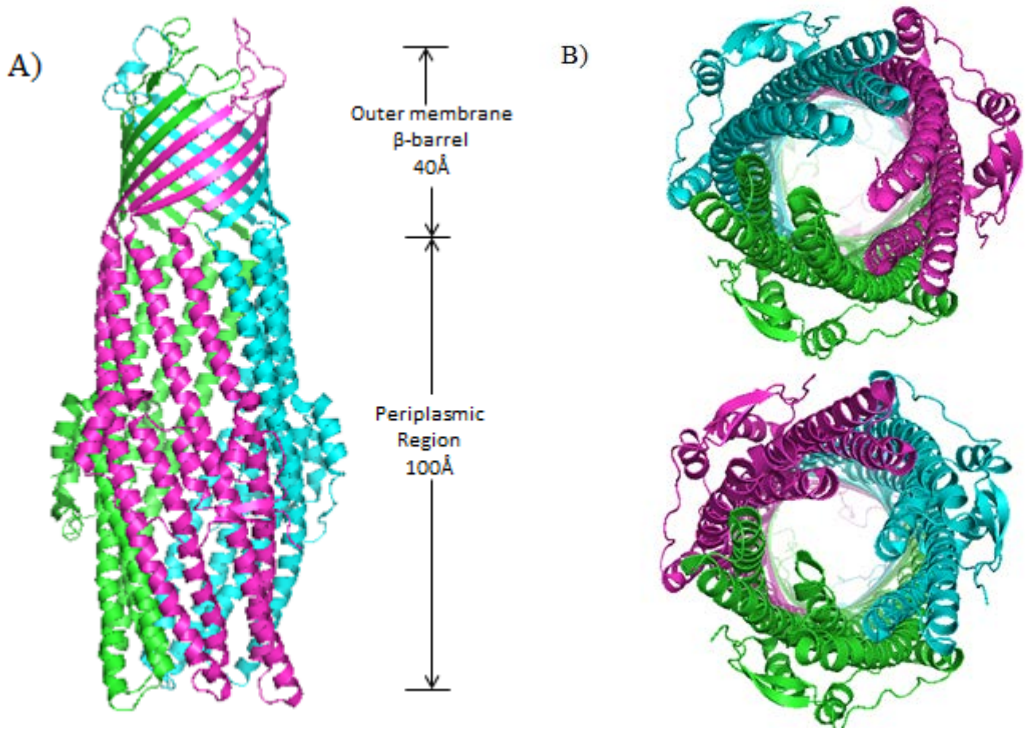

Figure 1.3 A) crystal structure of outer membrane protein TolC. Each protomer of TolC trimer is marked in different color. The 40 Å β-barrel domain is embedded in the outer membrane, while the 100 Å α-helical domain inserted into the periplasm. B) Top view of close-state (Top) and open-state confirmation (bottom) of TolC. Open-state of TolC allows passage of substances. Crystal structures were obtained from protein data bank. Protein data bank ID of close-state structure: 1TQQ, open-state structure: 2VDD. Structures created using Pymol.

AcrB in the AcrAB-TolC system

The third component in the AcrAB-TolC efflux pump is the inner membrane protein, AcrB. AcrB is the engine of the pump. It determines substrate specificity and provides the energy to drive the pump. So far, the substrates of AcrAB-TolC include antibiotics, detergents, dyes and organic solvents.[55]

The AcrB gene was first discovered during a genomic screen conducted by Nakamura *et al.* in 1978. Upon its deletion, the cell became hypersensitive to acriflavine. It was the second protein identified which caused elevated cell sensitivity to acriflavine. This is why the protein was named AcrB.[56] It was not until 1990s that scientists began to realize its crucial role in drug resistance. Since then, the protein has been studied extensively.

The crystal structure of AcrB was first solved by Yamaguchi and his group in 2002. AcrB is a trimeric protein, of which each protomer containing 1049 amino acids. The overall shape of AcrB is like an asymmetric jellyfish. The scheme of the arrangement of secondary structure elements in a single protomer was shown in Fig 1. 4. [57]

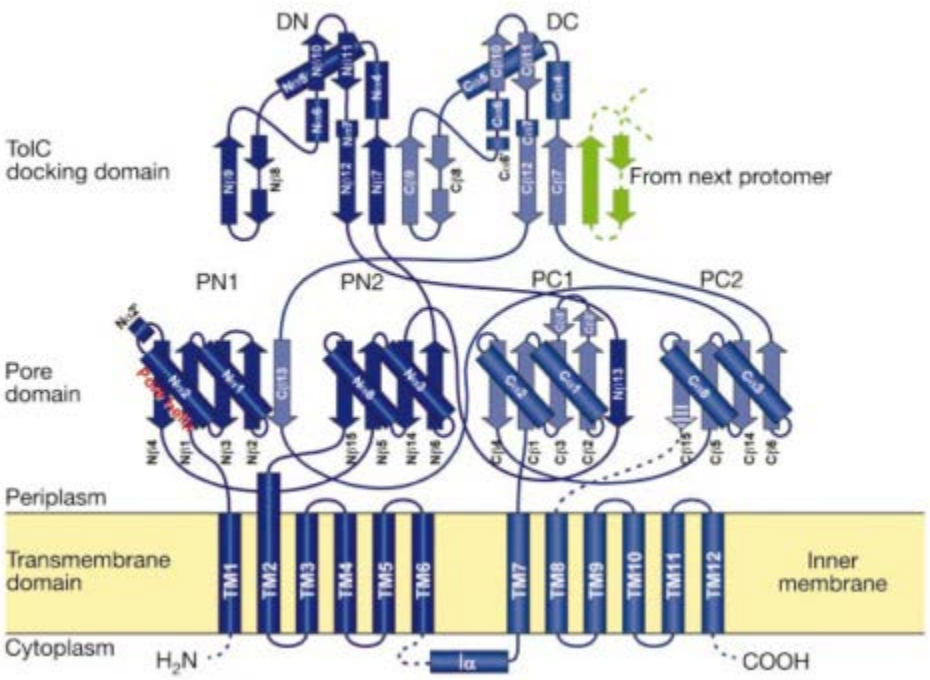

Figure 1. 4 Topology of a single protomer of AcrB. Secondary structures were indicated by cylinder (α-helic) and arrow (β-strand). Pore domain is divided into four regions: PN1, PN2, PC1, and PC2. TolC docking domain is composed by two subdomains, DN and DC. Two periplasmic loops lies in between TM1 and TM2, TM7 and TM8, respectively. [57] Reprinted by permission from Macmillan Publishers Ltd: Nature (419) ©2002

Each monomer AcrB contains 12 transmembrane (TM) α-helices and two large hydrophilic periplasmic loops. The two periplasmic loops reside in between TM1 and TM2 and TM7 and TM8, respectively. The periplasmic region of AcrB can be divided into two parts, the TolC docking domain and the porter domain, based on proposed functionality. The overall length of the AcrB periplasmic head piece is approximately 70 Å, of which the porter domain is 40 Å in length. The two subdomains between TM1 and TM2 were named PN1 and PN2; while the other two subdomains between TM7 and TM8 were PC1 and PC2. In AcrB trimeric state, PC1 and PC2 subdomain are at the outside surface. Though how AcrB interacts with AcrA remains unknown, it is often believed the cleft between PC1 and PC2 is the AcrA association region. Between PN2 and PC2 subdomains there are open vestibules which are later proven to be the central cavity for substrate binding. At the top of AcrB structure, 8-stranded β-sheets form TolC docking domain. In each monomer, an antiparallel β-sheet loop extends approximately 35 Å and inserted into the neighboring AcrB (Fig 1.5).[57] Our group demonstrated that this protruding loop is essential for the stabilization of AcrB trimer. Deletion of a fragment of the loop led to dissociation of trimeric AcrB and accumulation of inactive monomer AcrB, resulting in compromised drug resistance.[58] The bottom α-helix-turn-α-helix structure of TolC seems to fit perfectly with the tip of the TolC docking domain of AcrB through manual fitting.[59] The transmembrane domain is formed by 12 α-helices of 50 Å.[59] Asp407, Asp 408, Lys940 were buried in TM4 and TM10. These charged residues formed ion pairs which were involved in proton translocation.[60]

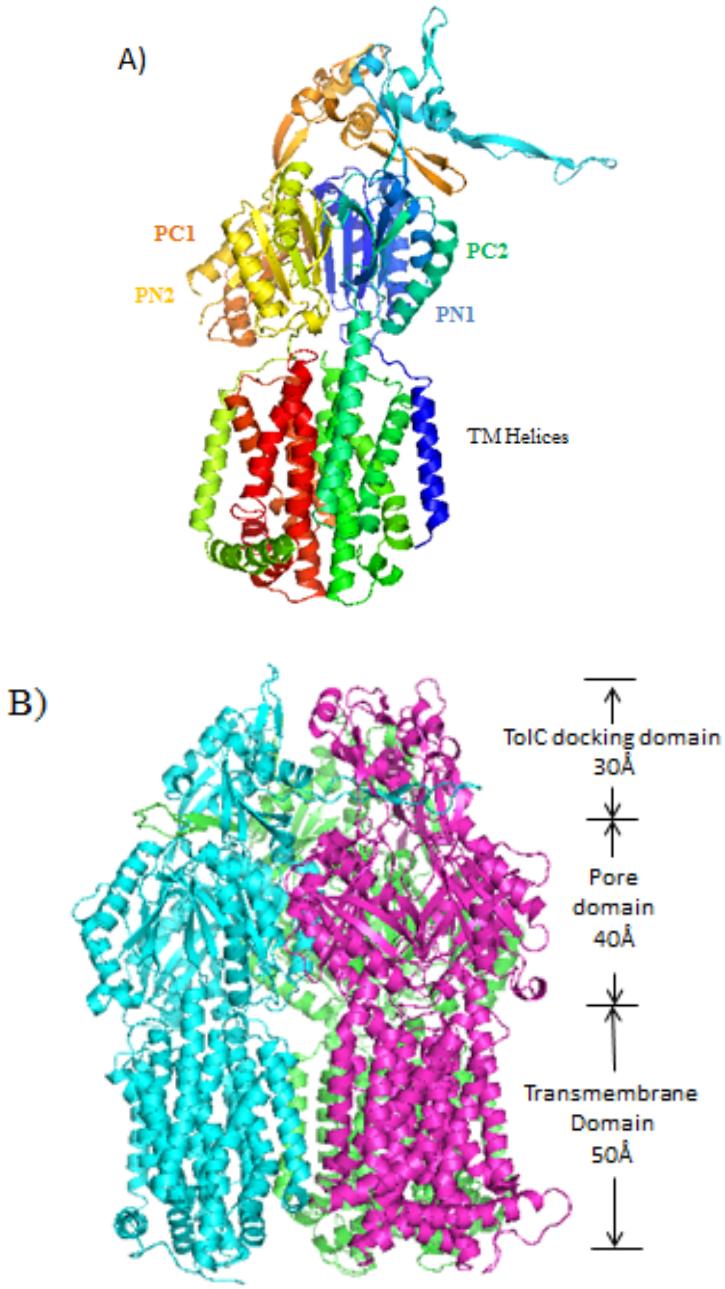
A)
PC1
PC2
PN2
PN1
TM Helices
B)
TolC docking domain
30Å
Pore
domain
40Å
Transmembrane
Domain
50Å

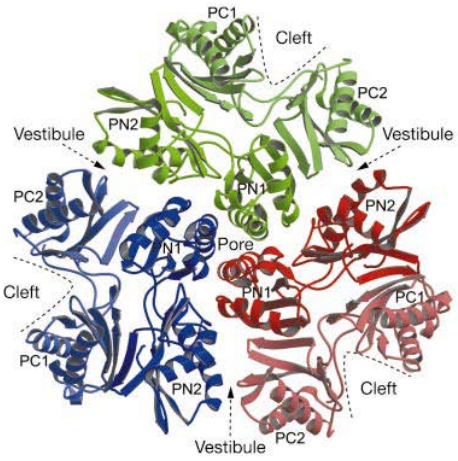

C)

Figure 1.5 A) Crystal structure of a single AcrB monomer. (Protein data bank ID: 1IWG). B) Assembly of AcrB trimer. Based on the function and position, AcrB is divided into three domains: TolC-docking domain (30 Å), Pore domain (40 Å), and Transmembrane domain (50 Å). Structure was drawn by Pymol from 2GIF in protein data bank. C) Top view of boundaries between each protomer in AcrB oligomer.[56] Reprinted by permission from Macmillan Publisher Ltd: Nature (419) ©2002

The conformational differences between each protomer were observed in the trimeric AcrB. From the observation, a three-stage functional rotation mechanism was postulated by two different groups at approximately the same time.[61, 62] Each monomer exhibits different confirmation upon different substrate activity: Access, Binding and Extrusion, which corresponding to Loose (L), Tight (T) and Open (O) in the other literature (Fig. 1.6). The transition of each monomer between different states is driven by proton relay. In the access state, the vestibule between PN2 and PC2 subdomains is open and accessible to substrates. Substrates enter the vestibule from periplasm or the groove at the top of TM8 and TM9, and bind loosely to the protein. In the binding state, the binding pocket expanded so that substrates could further

move upwards into the extended deep substrates channel. At this stage, the vestibule remains open and the central α-helix tilted approximately 15° towards the PN2 subdomain, which blocks the exit pathway. Finally, incline of the central helix in the extrusion state opened the exit and allowed the substrate to be excluded from the pump. The confirmation change from binding state to extrusion state required energy, which is generated from proton gradient force. [61, 62]

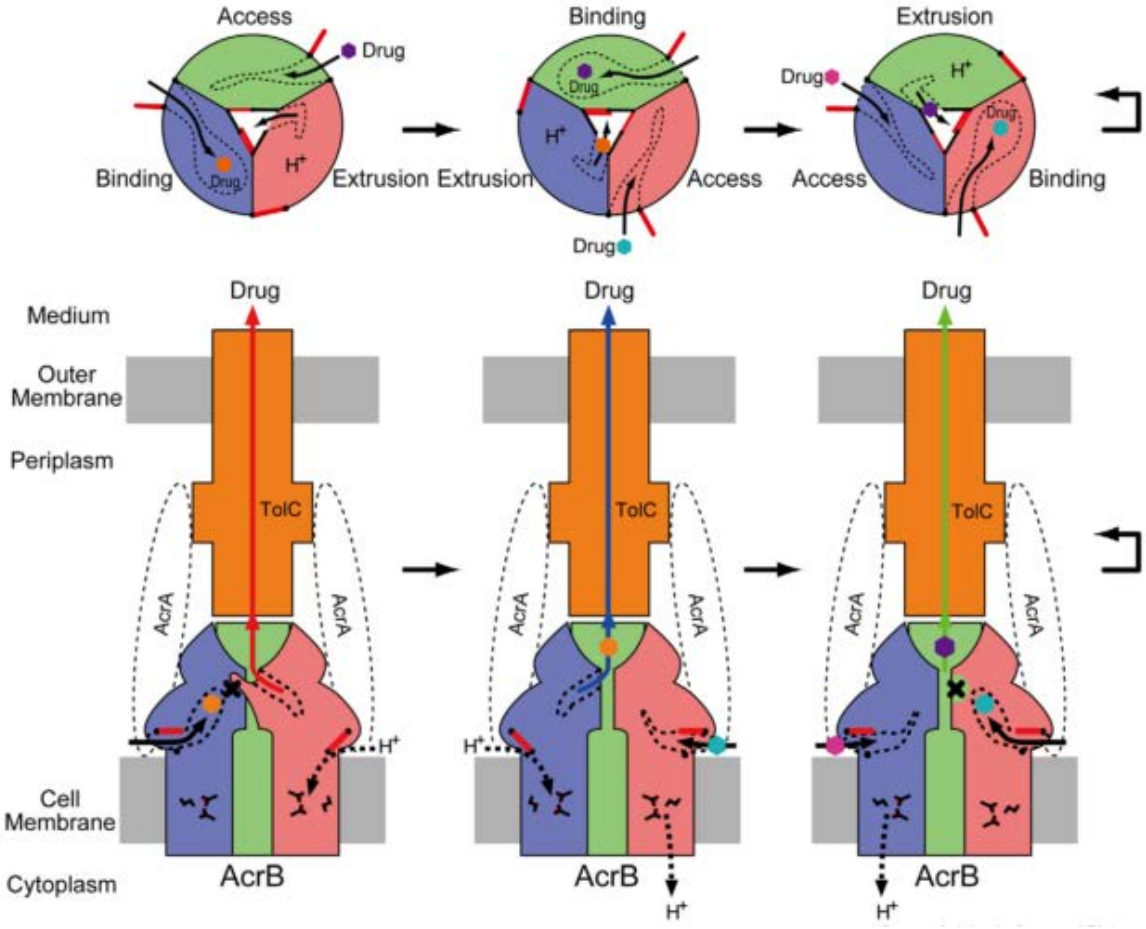

Figure 1.6 Schematic illustrations of substrate and proton pathways in the functionally rotation mechanism of AcrB.[63] When substrate enter AcrB pathway, three states of confirmation is induced: access, binding, and extrusion. The top views are from the periplasmic region of AcrB. Substrate and proton uptaken process are noted by dotted lines. Reprinted from *Curr Opin Struct*

Biol **18**, Murakami, S. Multidrug efflux transporter, AcrB--the pumping mechanism. 459-465 ©2008, with permission from Elsevier.

The pump transports substances from low concentration to high concentration, and hence energy is needed for the efflux of AcrAB-TolC. Proton motive force is primary energy source. Three amino acids, Asp407, Asp408, and Lys940 are crucial in the proton translocation pathway. Substitutions of each of the three residues with alanine lead to complete function loss of the pump.[57, 64] The three residues exhibit different configuration in each state of substrate efflux. In the access and binding states, Asp407 and Asp408 form a salt bridge with Lys940. When the protomer shifts to extrusion state, the salt bridge is dissociated and Lys940 forms hydrogen bond with another highly conserved residue Thr978. At this time, Asp407 and Asp408 are exposed so that they can interact freely with proton. It was proposed that energy released from twisting in transmembrane α-helices would lead to further conformational change in porter domains.[57] However; the exact mechanism of how the energy induces structural change is still unknown.

Exploration of the interaction between AcrB and its substrates is another active topic of research. Switching the periplasmic domain of AcrB and AcrD altered the substrate specificity of the two pumps, indicating the substrate specificity is determined by the periplasmic loop.[65] Next, mutagenesis studies identified a phenylalanine rich hydrophobic binding pocket, containing Phe178, Phe610, Phe615, Phe617, Phe664 and Phe666.[66] The position of the interaction site was consistent with Murakami and co-workers' finding by X-ray crystallography. Using Nile Red efflux assay, AcrB substrates are divided into two groups judging by their interacting sites: cave binders and groove binders.[67] Both sites are located in the binding pocket. This allows the pump to accommodate two kinds of substrates at the same time. Recently, the Bodipy-FL-maleimide

labeling assay was used to picture the complete substrate transportation pathway. AcrB substrates first entered from the lower cleft at TM8/TM9 groove and then bound to the deep binding pocket (Fig. 1.7).[68, 69]

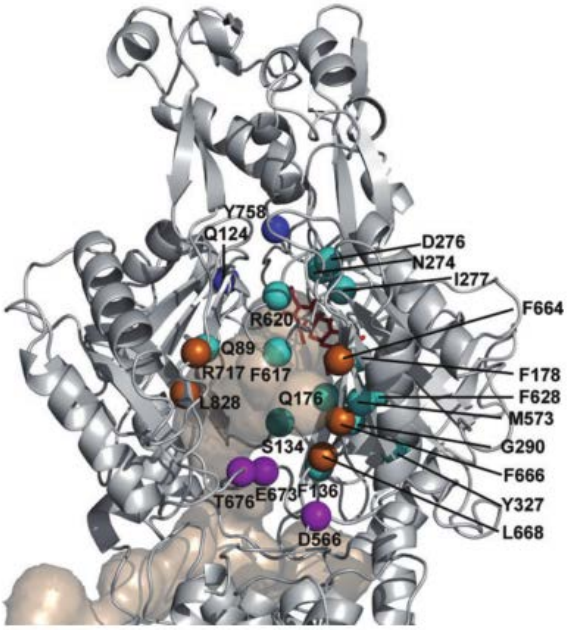

Figure 1.7 Substrate pathways in AcrB periplasmic loop. Residues showed positive results in Bodipy-FL-maleimide labeling or CPM/pyrene-maleimide assay were mapped in the AcrB protomer as spheres. Deep blue residues are at the exit gate of AcrB, while light blue residues are in the binding pocket. Orange and purple indicated residues are in the upper and lower region of cleft, respectively.[68] Reprinted from Molecular Microbiology, 78, 320-330 © 2010 by John Wiley and Sons

Due to the technical difficulty in crystallography, a complete crystallographic structure of the AcrAB-TolC complex has not been determined. The interactions between each subunit have been investigated by mutagenesis coupled with drug susceptibility assay, crosslinking, and computer modeling. An $AcrA_3$-$AcrB_3$-$TolC_3$ model has been proposed.[59] The tripartite complex

is 610,000 Da, 270 Å long, spanning across the entire cytoplasmic membrane and outer membrane. The α-hairpin of AcrA is docked with the coiled-coil helices in TolC. AcrA C-terminus (residue 315-397) is involved in interaction with AcrB. It is reported both AcrA and TolC could interact with AcrB independently with high affinity, which is not affected by the third component and substrates.[51, 59] However, it has been shown that addition of substrates could help stabilize the whole complex.[63]

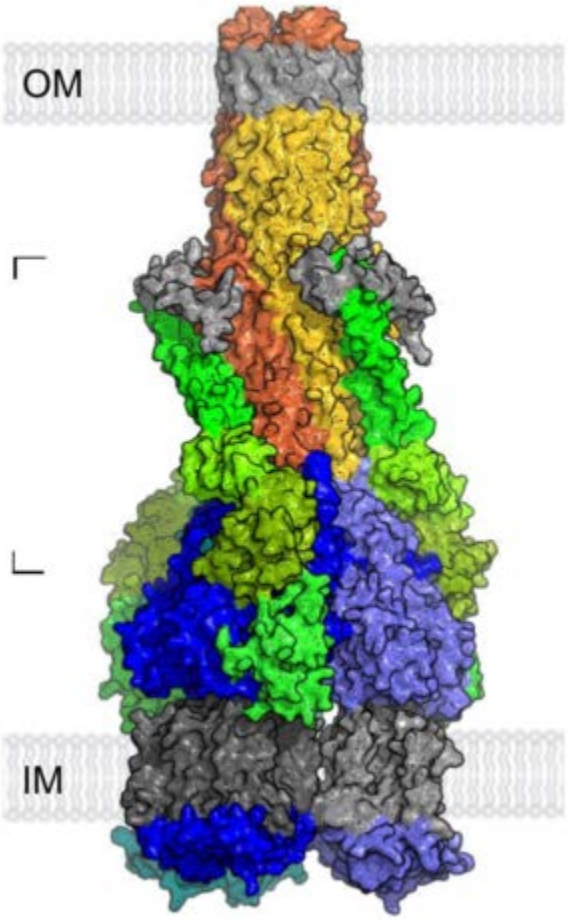

Figure 1. 8 Assembly of $TolC_3$-$AcrA_3$-$AcrB_3$ tripartite efflux pump by computer modeling.[59] Positions of outer membrane and inner membrane are indicated. Different colors were used to differentiate domains of TolC (Orange, yellow, and grey), AcrA (bright green), AcrB (blue, grey, and green). Figure adapted from Symmons, M. F., et al. The assembled structure of a complete

tripartite bacterial multidrug efflux pump. *Proc Natl Acad Sci U S A* **106**, 7173-8. Copy right (2009) National Academy of Sciences, USA.

1.7 Gram-negative Bacterial Outer Membrane Biogenesis

As mentioned in section 1.4, the outer membrane of Gram-negative bacteria offers a better shield against antibiotics comparing to Gram-positive bacteria. The outer membrane of Gram-negative bacteria is an asymmetric lipid bilayer with an outer leaflet made of lipopolysaccharide and an inner leaflet of phospholipid. Integral outer membrane proteins reside in this bilayer structure. More than sixty OMPs have been identified in Gram-negative bacteria, most of which form transportation channels called porins. All OM porins share a β-barrel structure motif formed by multiple β-strands. These β-strands form a hydrophilic pore in the center of the protein, which is main channel for the translocation of hydrophilic compounds. The hydrophilic pores are very narrow. For instance, the diameter of OmpF channel is approximately 10 Å. Only molecules smaller than 600 Da can diffuse across the outer membrane through porins.[70]

These integral OMPs are first synthesized in cytoplasm with N-terminal signal peptide. N-terminus signal sequence directs the unfolded OMP precursors to the Sec translocon in the plasma membrane. During or after the completion of the translocation, signal peptide is digested by signal peptidase.[71] Once the OMP precursors enter the periplasm, several chaperones help stabilize and transport the polypeptides to their final destination. Eventually, these nascent polypeptide chains fold into functional β-barrel proteins and insert themselves into the cell envelope.[72] Several periplasmic chaperones assist the folding and translocation process. For instance, DsbA and DsbC catalyze the disulfide bond formation and protein oxidation.[73] PPIase accelerates Proline cis-trans isomerization. Because of the high hydrophobicity of the OMP

polypeptides, several chaperones that could prevent the OMP polypeptides from aggregation in the hydrophilic environment of periplasm are recruited. SurA, Skp and DegP have been identified with this function.[74]

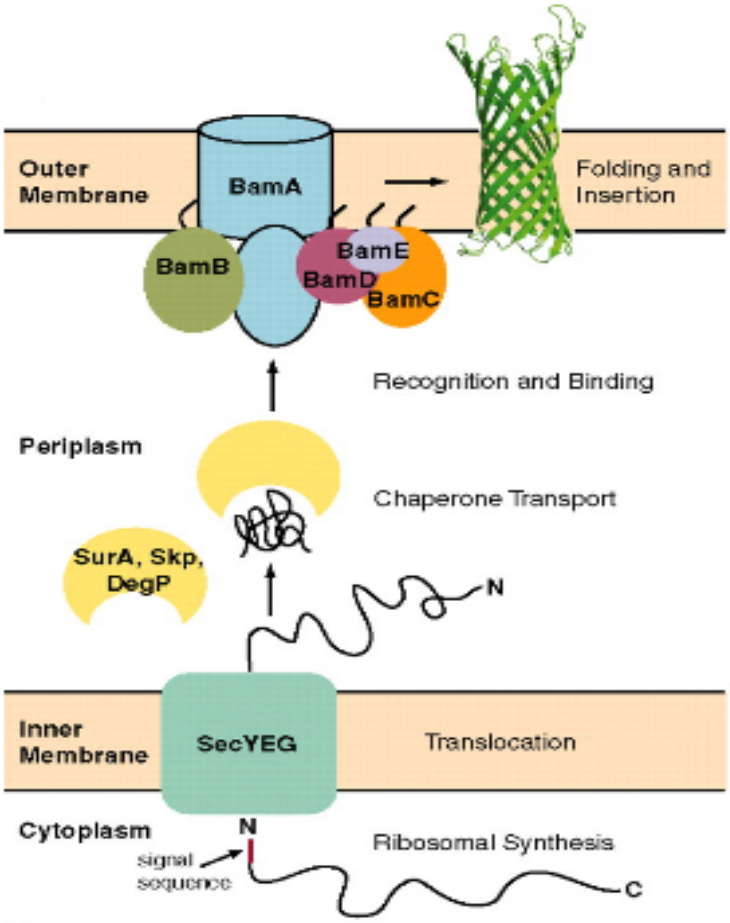

Figure 1.9 Translocation, folding and assembling of E. coli integral outer membrane protein in the assistants of periplasmic chaperones, Sec translocon and Bam complex.[75] Adapted from Hagan, C. L. et al. Reconstitution of outer membrane protein assembly from purified components. *Science* **328**, 890-2. Reprinted with permission from AAAS©2010

The exact roles of these chaperones in OMP biogenesis are still under investigation. One hypothesis is based on immunoprecipitation studies in SurA, Skp and DegP deficient strains.

SurA and Skp/DegP are two parallel pathways in assisting OMP biogenesis. SurA is the primary chaperone in helping the folding of the majority of OMPs. Those who fall off the SurA pathway are rescued by Skp and DegP.[76] Recently, another theory was proposed by Zhao et al. based on kinetic study of chaperone and unfolded OMP. It is believed SurA and Skp act at the early stage of the OMP folding while DegP serves as a final quality control role which helps the unfolded OMP precursors at a later stage.[77] DegP not only collaborates with Skp, but also with SurA which forms a SurA–OMP–DegP ternary complex.

1.8 Periplasmic molecular chaperone SurA

SurA was first identified as an essential gene in *Escherichia coli* for stationary phase survival. It is required for cells to tolerate the nutritional starvation phase. SurA is composed of 4 domains following a signal peptide: an amino terminus domain with the first 150 amino acids, two peptidylprolylisomerase domains of 100 residues each (P1 and P2 domain), and a carboxyl terminus domain. Crystallographic structure showed that the N, C-terminal domain and the first PPIase segment constitute a core module, while the second PPIase segment forms a satellite domain about 30 Å away in distance (Fig. 1.10).

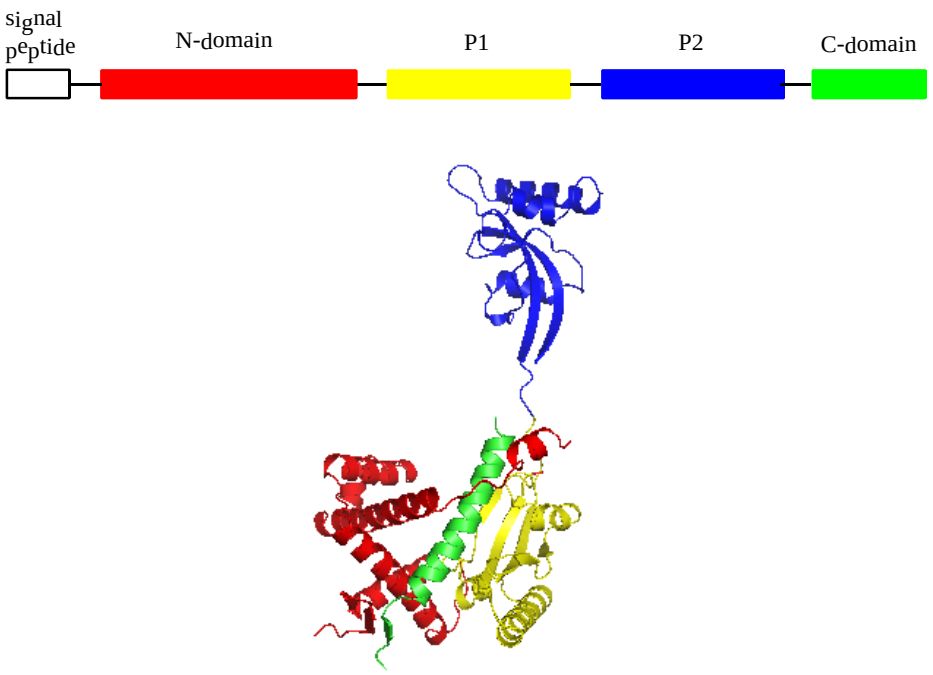

Figure 1.10 Structure of SurA. The sequence of SurA was color-coded as signal peptide (white), N-terminus domain (red), PPIase P1 domain (yellow), P2 domain (blue), C terminus domain (green). Protein structure was from protein data bank 1M5Y. Structure created using Pymol.

It has been proven that deletion of SurA in *E. coli* induces the cell stress factor σ^E. σ^E factor regulates the expression of OMPs.[78] Recently, in a thorough LC-MS/MS analysis of OMP abundance, only 8 of the 64 OMPs are negatively affected by SurA deletion. Decreasing levels of six of the eight OMPs are caused by suppressed mRNA level. Major OMPs such as OmpF is absent when SurA is knocked out. Expression level of LamB was reduced by 4- to 5- fold, while the level of OmpC and OmpA dropped by 2- to 3- fold. The abundances of some OMPs, such as, TolC and BamA, were elevated in the absence of SurA. Surprisingly, although only a small subset of OMPs has been affected, the overall OM density of the cell is drastically reduced. This is likely due to the high abundance of OmpF, OmpA, and LamB, which account for a large fraction of the OM. The LC-MS/MS study further elucidated the role of SurA in outer membrane

biogenesis. SurA is important to the folding and assembling of the majority of the OMPs. Most OMPs interact with SurA, DegP and Skp, depending on their availability. But OMPs like LptD and FhuA can only go through the SurA pathway in the periplasm. Another group of OMPs were down regulated by SurA *in vivo*, the mechanism of which remains unknown. [79]

SurA was first noticed for its sequence homology with the parvulin domain of PPIase. It was originally believed to assist protein folding mainly by mediating the cis-trans isomerization of proline. However, later experiments showed that the chaperone activity of SurA was independent from its PPIase domains.[80] Deletion of either P1 or P2 domain showed no effect on the ability of cell to survive in the presence of nobobiocin. SurA N-teminus and C-terminus domains (SurA N-C) are sufficient to restore membrane functionality and complete SurA activity *in vivo*.[81]

Substrate specificity of SurA has also been studied. Mckay et al. used phage display to identify several peptides that interact tightly with SurA.[82] Klappa and his group also selected multiple peptides by enzyme linked immunosorbent assay (ELISA) screening of cellulose-bound library peptides representing LamB, OmpF and OmpA.[81] All these peptides shared a similar sequence stereotype Ar-X-Ar. Ar stands for aromatic amino acids, while X can be any amino acids. Since the frequency of Ar-X-Ar was the highest in OMPs among all *E. coli* cell surface proteins, there is no doubt why SurA would preferentially bind with unfolded OMPs. Mckay and coworkers further studied the interaction of SurA and the two peptides WEYIPNV (pepN) and NFTLKFWDIFRK (pepC) using isothermal calorimeter (ITC).[83] Both peptides interacted with SurA with a binding affinity in μM range, which is the highest among all peptides tested. Also the peptides competed with unfolded OmpF and OmpG in binding to the core structural fragment of SurA. However, the co-crystallization of SurA-peptide showed pepN and pepC only interacted with the first PPIase segment. Deletion of P1 domain drastically increased the binding affinity

between SurA and peptide. Because PPIase domains are unrelated to SurA chaperone function, the peptides bound to P1 domain may not be native substrates of SurA. The competition between peptides and OMPs could be a result of the steric hindrance effect.

Later researches have linked SurA to different cellular activities. SurA, in collaboration with BamB, is involved in folding of outer membranes exported not only from Sec pathway, but also from twin arginine translocation (Tat) pathways.[84] The outer membrane biogenesis in different Gram-negative bacteria and mitochondria outer surface required SurA and its homologue.[85] Moreover, SurA is essential in helping outer membrane protein folding in reconstituted OMP assembling complex.[75] Despite of all these progresses in the understanding of the function of SurA, how SurA selects and interacts with its substrates remains unknown.

Immunoprecipitation studies revealed that SurA is highly related to the correct folding and assembling of outer membrane proteins. When *surA* gene is knocked out from *E. coli* genomic DNA, the cells are highly sensitive to hydrophobic drugs and membrane perturbants.[80] It is universally believed that this drug tolerance change caused by SurA deletion is affected by the OMP density. But there is no direct proof that may correlate the two observations. Elucidation of the relationship between SurA OM integrity and its role in cell permeability may offer a great target in fighting against drug resistance in Gram-negative bacteria.

1.9 Actions In Response To Slow Down the Spread of Multidrug Resistance

Microbes reproduce at an extreme fast speed, usually with generation times measured in minutes. This means that once drug resistance gene is generated, it can be transferred among the pathogen species very quickly. Therefore, effective treatments at the onset of the infection are extremely important in a clinical setting. The shortage of effective antimicrobials has raised significant

concerns and attracted comprehensive research interests. Measurements have been adopted from different aspects to address this global epidemic issue.

Several government agencies are sparing no effort on evoking awareness of the severe situation of infection caused by antibiotic resistant pathogens, especially in developing countries. One of the most straight forward approaches is to control the usage of antibiotics, not only in clinical treatment, but also in farming and aquaculture. Rational use of antibiotics limited the unnecessary exposure of microorganisms to antibiotics.[86] Another important issue is to improve the hygiene conditions in all affected areas. It has shown millions of dollars could be saved simply by practicing good hand hygiene by clinicians.

Currently, cases of drug resistance towards all commercially available antibiotics have been reported. Identification of new class of antibiotics is in urgent need. Historically, the majority of antibiotics came from natural products extracted from microbes. Because of the limitation of cultivation conditions, only 1% of bacteria have been studied. DNA samples from soil and marine habitats have been isolated and sequenced, which opens up great opportunities of discovering new antibiotics.[14] Another direction of genomic hunting is high throughput screening for essential genes for bacterial survival or targets in the crucial metabolic pathways.[14] For example, the key features in bacterium cell walls have been selected as targets. New antimicrobial peptides have been tested which bind with lipopolysaccharide (LPS) on the outer membrane to induce membrane distortion and increase permeability. However, this could only enhance the influx rate of hydrophobic drugs.[87] Furthermore, resistance in compliance with these antimicrobial peptides has been reported. OMPs are also a group of vital targets in drug penetration pathway. To increase the permeability of hydrophilic compounds, mutagenesis studies on OMP channels have been reported, but they are specific to structurally related drugs.[88]

In addition, it is impossible to mutate the OMP channels in the pathogen during the treatment. There is no effective strategy to deal with drug resistance from this perspective.

Vaccines against bacteria have also been developed.[89] The advantage of vaccines is there would not be the resistance problem. However, it is unlikely to have vaccines against all available disease related bacterial strains, not to mention the evolved second and third generation of existing microbes. And the effects of different vaccines are still under investigation. Phage therapy is also an alternative way to treat infection. But the method is relatively expensive since multiple bacteriophages may be required at the same time. Additionally, the treatment has to be monitored by physicians to ensure safety.[90]

As discussed above, my study in this thesis focuses on two proteins, a multidrug transporter and a periplasmic molecular chaperone. Efflux pump has been served as the target for the design of inhibitors. New efflux pump inhibitors have been tested as uptake enhancers to elongate the retention time of drugs within the cells. MC-207, 110 (Phe-Arg-β-naphthylamide, PaβN) is the first inhibitor of RND pump identified through the collaboration of Microcide Pharmaceuticals and Daiichi Pharmaceutical Co.[91] Because MC-207, 110 is a preferred substrate for the pump, it will compete with other substrates in interacting with the pump. Therefore, when high concentration of MC-207, 110 is used, the pump loses its extrusion ability to actively pump out other desired antibiotics. Derivatives of this compound haven been used as inhibitors to reverse drug resistance caused by mostly RND pumps, as well as particular efflux pumps in Gram-positive bacteria. Antisense DNA and siRNA provide are an alternative therapy in preventing mRNA translation and gene expression. Antisense phosphorothioate oligonucleotide encapsulated in novel anion liposome targeting AcrB has successfully restored antibiotic susceptibility in fluoroquinolone-resistant *E. coli*.[92] In OMP biogenesis, generally OMPs are

targeted in the fight against MDR. Still, little is known about how SurA and other chaperons affect cell permeability. As a result, there is no reported inhibitor for OMP biogenesis.

CHAPTER II. A REPORTER PLATFORM FOR THE MONITORING OF *IN VIVO* CONFORMATIONAL CHANGES IN ACRB

2.1 INTRODUCTION

Despite multiple drug resistant Gram-positive pathogens, such as Methicillin-resistant *Staphylococcus aureus* (MRSA), are in the media spotlight, the lack of new and effective antimicrobials against Gram-negative bacteria is the real concern.[93-96]One of the major mechanisms that confer intrinsic drug resistance to Gram-negative bacteria is the active pumping of drug efflux systems. Genetic modification of the drug efflux pump could change the drug susceptibility level of the bacteria.[97]Such an observation spurred the interest in searching for inhibitors that can block the function of efflux pumps.[98-102] A thorough understanding of the structure and function of this type of pumps is critical for such endeavors.

AcrB is one of the most extensively studied MDR efflux pumps.[103-115]Strains deficient in AcrB have been proven to be hyper-sensitive to antimicrobials. AcrB is the inner membrane component of the tripartite pump complex AcrAB-TolC. This complex spans the distance across the inner membrane, the outer membrane, and the periplasmic space in between. Crystal structures of both the apo-AcrB and AcrB-substrate complexes have been determined.[61, 62, 116] AcrB functions as a homo-trimer. The observation that the three promoters in the AcrB trimer have slightly different conformations prompts the proposal that this protein functions through a mechanism resembling that of a peristaltic pump. [117-120] Each subunit rotates through loose, tight and open conformations successively. One molecule of substrate is extruded per cycle. The translocation of protons from the periplasmic space provides the energy for the conformational change. This mechanism is supported by multiple mutational studies, through which the substrate binding sites and proton relay pathway have been identified. In addition, disulfide bonds

engineered at the interface of subdomains reduce protein flexibility and prevent each AcrB monomer from conformational changing, and consequently blocked the function of AcrB.[119]

The activity of AcrB can be monitored conveniently with a drug susceptibility assay. The *acrB* knockout strain is hyper-sensitive to many drugs that have been identified as AcrB substrates. This defect can be accommodated by the introduction of a plasmid encoding active AcrB. Therefore, the effect of mutations on the function of AcrB can be monitored by measuring the susceptibility to certain drugs using an AcrB-deficient *E. coli* strain expressing a plasmid-encoded AcrB mutant. Although the effect of a mutation that causes the loss of protein function is easy to identify, it is more difficult to attribute such changes to specific aspects of protein structure. A mutation may impair the function of AcrB from several different aspects, including the substrate binding site, disrupting the proton relay pathway, the interaction with AcrA and TolC, changing the conformation of the subunit (tertiary structure level) or the formation of an AcrB trimer (quaternary structure level). While extensive mutational studies have been focused on the first three aspects, there is not yet a convenient method that can identify if the impact of a detrimental mutation is on the tertiary or quaternary structure levels. In this study, I worked with Dr. Lu Wei and established a platform to examine the effect of mutations on protein tertiary structure (Figure 2.1). Briefly, double Cys mutations were introduced into AcrB at positions that can form disulfide bonds under the native conformation. These Cys pairs serve as reporter for the examination of the impact of further mutation on protein structure. A sophisticated blocking and labeling protocol was also developed to keep track of the disulfide bond versus free thiols in the protein. Although the analysis was performed after protein purification, the results actually reflected the conformation of AcrB when it was under the native condition in the inner membrane.

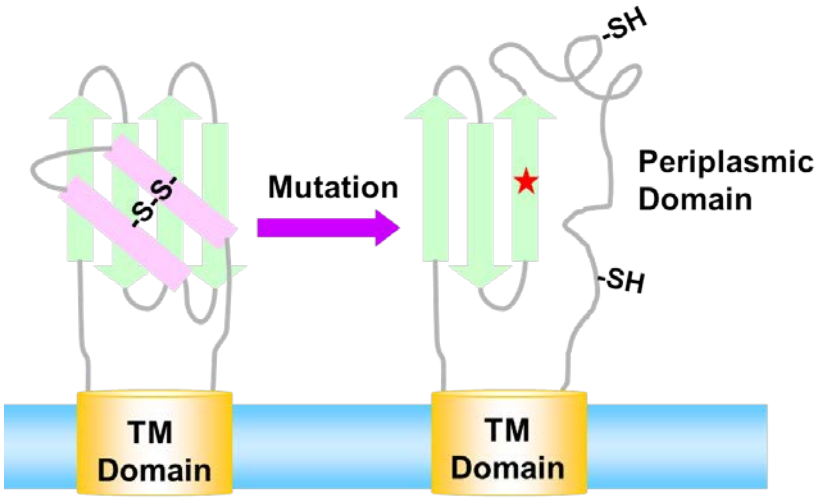

Figure 2.1 Concept of reporters for protein conformational change. Each AcrB reporter construct has a single pair of Cys in the periplasmic domain, which form a disulfide bond in the native conformation. If an additional mutation (red star) causes a change of local conformation, the extent of disulfide bond formation will be affected. The extent of disulfide bond formation can be monitored as a reporter for protein conformational change.

2.2 MATERIALS AND METHODS

Construction of plasmids

The DNA coding sequence of AcrB was amplified by PCR from *E. coli* genomic DNA and then digested with SphI and BamHI restriction endonucleases. The fragment was inserted in frame into the expression vector pQE70 between the restriction sites SphI and BglII to create plasmid pQE70-AcrB. A polyhistidine tag was introduced at the C-terminus to facilitate convenient protein purification. Plasmid pQE70-AcrB was then used as the template to construct the cysteine-less AcrB ($_{CL}$AcrB) using the Quick-change mutagenesis kit following the protocol provided by the manufacturer (Agilent, Santa Clara, CA). AcrB has two intrinsic Cys, Cys493 and Cys887. To prevent them from interfering with the reporter Cys pairs, these two Cys were

substituted by Ala to create $AcrB_{C493A/C887A}$, which was named $_{CL}AcrB$ in the rest of this study. The same protocol was also used to construct all the reporter pairs with $_{CL}AcrB$ as the template. In each reporter pair, a different pair of Cys was introduced to create $_{CL}AcrB_{V32C/I390C}$, $_{CL}AcrB_{T44C/T91C}$, $_{CL}AcrB_{M184C/V771C}$, $_{CL}AcrB_{T199C/T749C}$, $_{CL}AcrB_{I335C/A995C}$, $_{CL}AcrB_{Q726C/G812C}$, and $_{CL}AcrB_{A627C/T574C}$. To identify the performance of the disulfide trapping protocol developed in this study, four additional Cys-pair mutants were constructed with the same protocol to create $_{CL}AcrB_{A627C/G570C}$, $_{CL}AcrB_{A627C/F572C}$, $_{CL}AcrB_{A627C/V576C}$, and $_{CL}AcrB_{A627C/L578C}$. Protein coding sequences of all plasmids were confirmed by DNA sequencing.

Drug susceptibility assay

AcrB activity could be monitored conveniently by a drug susceptibility assay. The minimum inhibitory concentrations (MIC) of different stains were measured as described.[109] Briefly, an *acrB* deficient *E. coli* strain (BW25113*ΔacrB*) was used as the host cell. BW25113*ΔacrB*strain transformed with plasmid-encoded wild type AcrB ($_{WT}AcrB$) or pQE70 vector were used as the positive and negative controls, respectively. Plasmids encoding different AcrB mutants were transformed into BW25113*ΔacrB* as well. Freshly transformed cells were plated on LB-agarose plates containing 100 μg/mL ampicillin and 50 μg/mL kanamycin. The same ampicillin and kanamycin concentrations were used throughout the study when noted. A single colony was inoculated into a LB media supplemented with ampicillin and kanamycin. The exponential-phase cultures of different strains were diluted to an OD_{600nm} unit of 0.1 with LB broth. 5 μL of this culture was used to inoculate 1 mL LB media containing the indicated concentration of erythromycin or novobiocin. The cultures were incubated under shaking at 37^{o}C for overnight. The next morning, the OD_{600nm} of each culture was measured. This activity assay was conducted

under the basal AcrB expression condition, which was not supplemented with inducer. Each experiment was repeated at least three times.

Protein expression

To avoid potential contamination from genomic AcrB, all AcrB expression plasmids were transformed into BW25113Δ*acrB* for expression. A single colony from a freshly transformed plate was inoculated into 3 mL LB media supplemented with ampicillin and kanamycin and cultured overnight at 37°C. The overnight culture was used to inoculate 600 mL fresh LB media containing ampicillin and kanamycin. Then this culture was incubated with shaking at 37°C overnight. Cells were harvested the next morning by centrifuge. Protein was purified immediately without freezing the cell pellet.

Protein purification and blockage of free Cys

The cell pellet was suspended in a lysis buffer (30 mM iodoacetamide (IAM), 0.5 mM phenylmethanesulfonylfluoride (PMSF), 30 mM Tris, 0.5 M NaCl, pH 7.9) and sonicated for 15 minutes in ice/water bath with 5 s on/off intervals. The cell lysate was centrifuged at 15,317×g under 4^{o}C for 20 min. The pellet was then suspended again in a buffer containing 1.5% Triton, 10 mM IAM, 0.5 mM PMSF, 30 mM Tris, 0.5 M NaCl (pH 7.9) and sonicated gently at low amplitude for 10 minutes in ice/water bath with 5 s on/off intervals. The mixture was then incubated on ice and kept shaking for 2 hours, followed by centrifugation at 15,317×g under 4^{o}C for 20 minutes. The supernatant which contained the detergent solubilized AcrB was collected. Imidazole was added to a final concentration of 10 mM to reduce the non-specific binding during purification. The supernatant was mixed with Ni-NTA sepharose resin (Qiagen Inc., Valencia,

CA) for 40 minutes with rotation at 4°C. The suspension was packed into an empty column and subsequently washed with a wash buffer (0.5% Triton, 10 mM IAM, 50 mM imidazole, 30 mM Tris, 0.5 M NaCl, pH 7.9). The target protein was eluted with an elution buffer (0.5 M imidazole, 1% Triton, 10 mM IAM, 30 mM Tris, 0.5 M NaCl, pH 7.9). Compare with the AcrB purification protocols in literature, I omitted the step of purifying the membrane vesicles. I found that the additional step of purifying the membrane vesicle did not have a significant improvement on the purity of the sample under my experimental condition.

After elution, maleimide (MAL) and SDS were immediately added to protein samples to final concentrations of 50 mM and 4% (w/v), respectively. The high percentage of SDS denatured the protein and MAL was included to further block any residual free Cys. After incubated for 30 minutes at room temperature, proteins were precipitated using 15% trichloroacetic acid (TCA). After centrifugation, the precipitate was washed with cold acetone and then re-solubilized in a buffer containing 4% SDS and 50 mM Tris (pH 8.0). This precipitation and washing step were used to remove IAM and MAL from the sample. Protein concentration was determined by measuring the absorbance at 280 nm, with the re-solubilization buffer as blank.

Fluorescent labeling

The protein concentrations of different AcrB mutants were adjusted to the same level by measuring the absorbance at 280 nm. Labeling was performed as described bellow. First, dithiothreitol (DTT) was added to the samples to a final concentration of 50 mM. Then the samples were incubated at 37°C for 1 hour. Second, proteins in these samples were precipitated using 15% TCA. After centrifugation, the protein precipitate was washed with ice cold acetone. This step removed the extra DTT from the reduced proteins. Finally, a buffer containing 4% SDS,

50 mM Tris, pH 8.0, and 5 mM N-(5-fluoresceinyl) maleimide (F-MAL) was added immediately to the protein pellet to solubilize and label the freshly reduced free thiol groups. The pellet was resuspended with a pipette tip and incubated at room temperature for 30 minutes. After the incubation, 10 mM DTT was added to quench the labeling reaction.

The labeled samples were analyzed with SDS-polyacrylamide gel electrophoresis (SDS-PAGE) on 8% gels. After the extra fluorescence dye migrated out of the gel, the gel was collected and the fluorescence image was taken using the MiniVisionary gel documentation system (FOTODYNE Inc., Hartland, WI) under UV light. The same gel was stained with coomassie blue R250 and the image of the gel was then taken under normal white light.

Note: Construction of plasmids, protein purification, fluorescent labeling, protein expression level measurement were performed by WL (Dr. Wei Lu) and MZ (Meng Zhong), Drug susceptibility assay as performed by MZ

2.3 RESULTS AND DISCUSSION

2.3.1 Design and construction of double cysteine reporter pairs

Disulfide bond can not be formed in cytoplasmic proteins, due to the reducing environment in the bacterial cytosol. However, disulfide bonds are commonly found in periplasmic proteins, outer membrane proteins and the periplasmic domain of inner membrane proteins.[74, 121, 122] Taking advantage of the oxidative environment of periplasm, a series of reporter Cys pairs were introduced at different locations of the AcrB periplasmic domain. Based on the crystal structure of AcrB, I have selected seven locations where intra-subunit disulfide bond are likely to form. The criteria for the selection includes: 1) Residues to be changed need to be far away from crucial residues that are related to AcrB backbone and function. In other words, mutation and

formation of disulfide bond should not disturb the structure of AcrB or its function. 2) The distance between the two Cys residues of each pair should remain constant during the whole AcrB function cycle. AcrB functions through a rotary mechanism in which the three subunits rotate through three different stages.[61, 62, 119, 120] The distances between the two Cys of each reporter pair should stay similar in all three states, thus the formation of the disulfide bond is unlikely to affect function. After examining the three stages of AcrB structures, I selected seven regions to introduce the reporter pairs that meet the above criteria. Their positions are highlighted in Figure 2.2 by black circles, T199-T749 (1), Q726-G812 (2), M184-V771 (3), T574-A627 (4), T44-T91 (5), V32-I390 (6), and I335-A995 (7). All of the reporter residues exist in the the periplasm, the oxidative environment of which will enable the formation of disulfide bonds under the natural condition. [119]

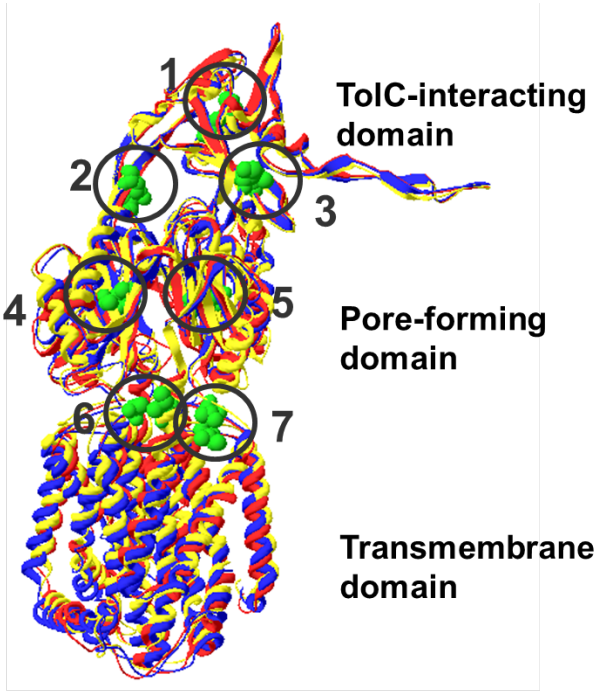

Figure 2.2 Superposition of the three states of AcrB, open (blue), tight (red) and loose (yellow). Positions of the reporter pairs were highlighted by green space-filled models with circles. The three domains of AcrB were labeled on the right.

Seven reporters were constructed, each containing a Cys pair at the indicated locations on a $_{CL}$AcrB background. Plasmids encoding the reporter AcrB constructs were transformed into BW25113Δ*acrB* for protein expression as described in the materials and methods section. All experiments were performed under a basal expression condition without induction. The expression levels of the reporters were comparable to the wild type AcrB, which were confirmed by Western blot analysis of membrane vesicles extracted from BW25113Δ*acrB* transformed with plasmids encoding different AcrB mutants (Figure 2.3).

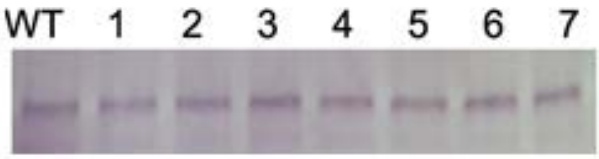

Figure 2.3 Western blot analysis revealed that the reporter constructs had similar expression levels as the wild type AcrB. The same numbering system as in Figure 2.1 was used to label the lanes. Wild type AcrB (WT) was used as a control.

2.3.2 Drug susceptibility assay of AcrB reporters

To meet the criteria as a structural reporter, the mutation to Cys and subsequent formation of disulfide bonds should not affect the structure and function of AcrB. Plasmids encoding the reporter genes were transformed into BW25113Δ*acrB*, and the drug susceptibilities of the strains to erythromycin and novobiocin were examined (Table 2.1). Five of the seven reporters were fully active. The MICs of two reporters, $_{CL}$AcrB$_{V32C/I390C}$ and $_{CL}$AcrB$_{I335C/A995C}$, were half of the value compared with other AcrB constructs. This slightly decreased activity is possibly because of the limited flexibility caused by the formation of the disulfide bonds.

Table 2.1 MIC of BW25113Δ*acrB* expressing plasmid encoded *acrB* mutants.

Plasmid or mutant	MIC (μg/ml)	
	Erythromycin	Novobiocin
Plasmid		
pQE70	4	4
pQE70AcrB	128	128
Mutation*		
Cysless	128	128
V32C/I390C	64	64
T44C/T91C	128	128
I335C/A995C	64	64
M184C/V771C	128	128
T199C/T749C	128	128
T574C/A627C	128	128
Q726C/G812C	128	128

*All mutations were constructed using $_{CL}$AcrB as the background.

The drug transporter activity of $_{CL}$AcrB was examined with a MIC assay as described in the materials and methods section. As shown in Table 1, plasmid encoded $_{CL}$AcrB fully restored the drug resistance of an *acrB* knockout strain, indicating that the replacement of these two Cys did not impair the function of AcrB, which is also consistent with results previously reported in literature.[119]

2.3.3 Fluorescein maleimide label and purification of AcrB reporters

$_{CL}$AcrB and $_{WT}$AcrB were used as negative controls for the disulfide trapping experiment. The protocol was derived from a procedure published for soluble proteins. [123] Several important modifications were described in the materials and methods section, which were critical to make it useful for membrane proteins. In the first lane, no IAM and MAL were added to block free Cys (Figure 2.4A). After purification, DTT was added to reduce the eluted protein samples. After the reduction, any Cys in a protein, either free or existed in a disulfide bond, would become reduced form and react with F-MAL during the labeling step to generate a bright fluorescent band. In the second lane, IAM was added during the protein purification procedure to block free Cys (Figure 2.4B). No reduction step was performed afterward. Therefore, no fluorescent labeling was expected to occur since there would be no free Cys in the protein. Finally, for samples in the third lane, protein was purified in the presence of IAM to block free Cys (Figure 2.4C). After purification, the extra IAM and MAL were removed, and the sample was reduced with DTT. If there was disulfide bond in the protein, the incubation with DTT would generate freshly reduced free Cys, which would be labeled and yield fluorescent band. In the case of $_{WT}$AcrB, the pattern of the three lanes was bright, dark, and dark, indicating the presence of free Cys but no disulfide bond in this protein, which is consistent with the known structure of AcrB (Figure 2.4D). The $_{CL}$AcrB was used as a negative control. None of the three bands were fluorescent in this case indicating the absence of Cys in this protein as expected.

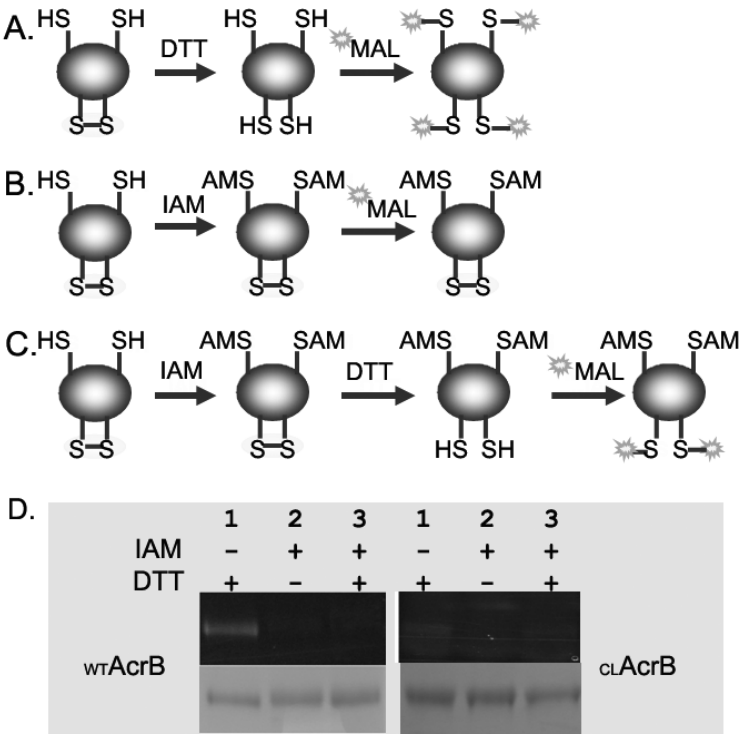

Figure 2.4 Controls for the disulfide trapping experiment. A. Purified protein was first incubated with DTT, and then labeled using F-MAL. All Cys residues in the protein would be labeled. B. Protein was purified in the presence of IAM, and then labeled using F-MAL. None of the Cys could be labeled. C. Protein was purified in the presence of IAM, and then reduced using DTT and labeled. Free Cys could not be labeled, while Cys protected by a disulfide bond during the IAM treatment could be labeled. D. $_{WT}$AcrB and $_{CL}$AcrB treated according to the procedures described in A (lane 1), B (lane 2), or C (lane 3). $_{WT}$AcrB contains two free Cys, while $_{CL}$AcrB contains no Cys. The same amount of protein was loaded in each lane as revealed by Commassie blue stain.

After expression, the protein purification procedure was performed as descried in materials and methods section. As shown in Figure 2.5, all reporters formed disulfide bonds was revealed by the bright, dark, and bright pattern. Samples in lane 1 and lane 2 were served as internal positive and negative controls in the quantification of the percentage disulfide formation. The

fluorescence intensities of lane 1 and lane 2 were designated as 100% and 0, respectively. The intensity of lane 3 was converted to percentage labeling using equation:

$$labeling\% = \frac{F3 - F2}{F1 - F2} \times 100$$

Where F1, F2 and F3 were fluorescence intensities of the band in lane 1, 2, and 3, respectively. The calculated percentage labeling for each reporter pair was shown in table 2.2.

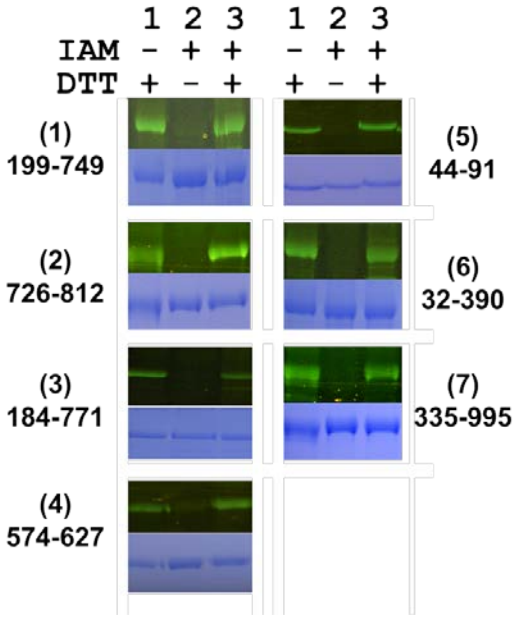

Figure 2.5 Labeling results of the Cys pair reporters. Samples in different lanes were treated similarly as those in Figure 2D. The similar protein amount was loaded in each lane as revealed by the Commassie blue stain.

Table 2.2 Percentage disulfide formation in the reporter Cys pairs as revealed by the percentage of fluorescence labeling.

Reporter construct	Disulfide bond%
V32C/I390C	82.5±6.8
T44C/T91C	100.7±3.0
M184C/V771C	76.2±4.9
T199C/T749C	82.7±2.9
I335C/A995C	51.7±0.8
T574C/A627C	102.9±6.8
Q726C/G812C	97.7±5.0

The extents of disulfide bond formation for different reporter pairs were different. Three pairs existed as complete disulfide bond, including $_{CL}AcrB_{T44C/T91C}$, $_{CL}AcrB_{T574C/A627C}$, and $_{CL}AcrB_{Q726C/G812C}$. Another three pairs, including $_{CL}AcrB_{V32C/I390C}$, $_{CL}AcrB_{M184C/V771C}$, and $_{CL}AcrB_{T199C/T749C}$, existed approximately 80% in the form of disulfide bond and 20% as free Cys. The last pair, $_{CL}AcrB_{I335C/A995C}$, existed with 50% in the form of disulfide bond.

2.3.4 Correlation between fluorescence intensity and the extents of labeling

To figure out the correlation between the fluorescence intensity and extent of labeling while using the current protocol, the different extent of labeling was mimicked by mixing purified $_{WT}AcrB$ and $_{CL}AcrB$. The purified $_{WT}AcrB$ and $_{CL}AcrB$ samples were adjusted to the same protein concentration and then mixed with different ratios to generate samples containing 100%, 90%, 80%, 60%, 40%, 20%, 10%, and 0% $_{WT}AcrB$. In the next step, the samples were reduced

with DTT and then labeled using F-MAL as described in the materials and methods section. After labeling, samples were analyzed with SDS-PAGE (Figure 2.6). Fluorescent intensities of different bands were quantified using software ImageJ[124, 125] and plotted against the percentage of $_{WT}$AcrB in the samples. As shown in Figure 2.5, the fluorescence intensities correlated very well with the percentages of $_{WT}$AcrB, indicting that the fluorescent intensity did reflect the extent of labeling, which correlated with the quantity of reactive thiols in the labeling step.

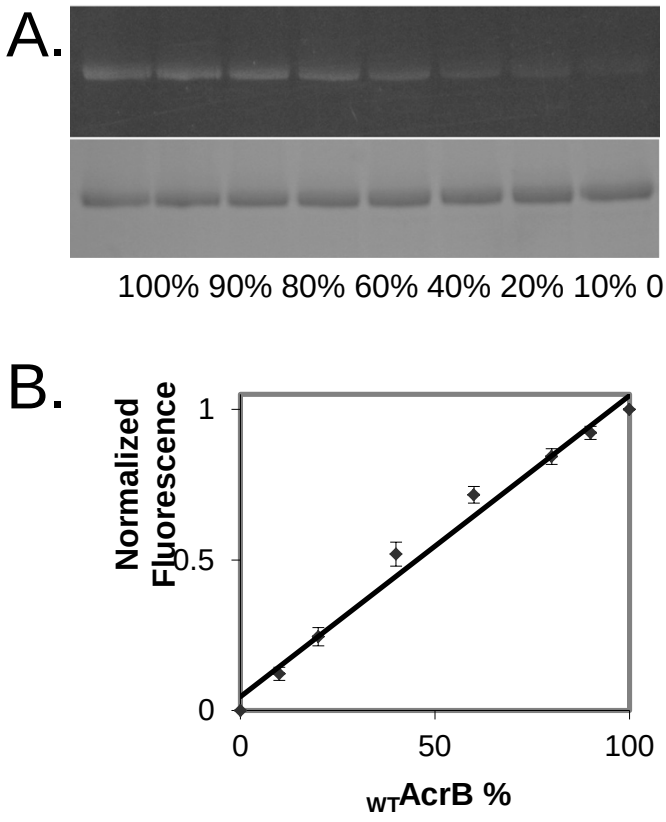

Figure 2.6 A. SDS-PAGE analysis of fluorescent labeling results of samples containing the indicated percentage of $_{WT}$AcrB. B. The fluorescent intensities of each band were plotted against the percentages of $_{WT}$AcrB. The experiment was performed three times. The average intensities and standard deviations were shown in the plot.

These results indicated that all reporter Cys pairs could form disulfide bond, and five out of the seven pairs did not significantly affect the transport activity of AcrB. These five pairs, which existed at different locations in the periplasmic domain of AcrB, could be used to monitor local conformational changes. Purified membrane proteins exist in detergent micelles. Limited by the size of the protein and bound detergent, in most cases NMR could not be used to study structures of membrane proteins. If the conformational change in the protein is drastic enough to cause a change of the secondary structure content or overall stability, then circular dichroism (CD) spectroscopy and limited protease digestion can be used to monitor the changes. However, more subtle changes are difficult to identify. The method described in this study has the following advantages: first, the combined usage of different reporters together could reveal a more detailed profile of AcrB conformational changes. Second, while most protein structure characterization methods can only tell information about purified proteins, the current method actually reveals the conformation of the protein while it is under the native environment *in vivo*. The presence of IAM throughout the protein purification process blocked all free Cys and maintained the profile of different Cys pairs at their native conditions.

The major concern of this study was the potential oxidation of free Cys in the protein purification process, as it would yield false positive result indicating higher disulfide bond percentage than the actual number. To keep the percentage of disulfide bond unchanged during the protein purification process, IAM was added throughout the purification process. IAM is a small molecule thiol modifier that can penetrate into protein hydrophobic core and react with membrane proteins.[123] In addition, proteins from freshly cultured cell is purifed, to avoid the possibility that free Cys might form disulfide bond during the freezing and subsequent storage

period. After sample was eluted from the affinity purification column, SDS and MAL immediately added into the protein samples. High concentration of SDS denatured AcrB to prepare it for fluorescent labeling, while MAL further eliminated any residual free Cys that might survive through the blocking process.

2.3.5 Study of distance sensitivity of the reporters

It is known that the formation of disulfide bond is very sensitive to the distance between the two Cys residues involved. Such sensitivity was served as the foundation for the reporter platform described in this study. The distances between the Cα of the involved Cys pairs in 171 disulfide bonds from 28 randomly chosen protein structures from the protein data bank were measured(Figure 2.7). According to Figure 2.7, disulfide bond has been observed to occur between two residues with Cαs less than 7.5 Å apart. While the distances ranging from approximately 4 to 7.5 Å, the majority clustered at 5 to 6.5 Å. This number is consistent with values reported in literature, which indicates disulfide bond may form between a pair of residues that possess a α-carbon to α-carbon distance ranges from 4 to8 Å.[126-128]

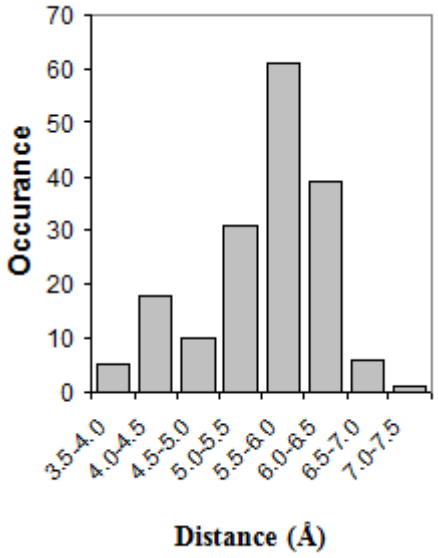

Figure 2.7 Summary of the distance between the Cα of two Cys in 171 disulfide bonds found in protein structures randomly chosen from the protein data bank.

To further verify the disulfide trapping protocol, the correlation between the extent of fluorescent labeling and the the real distance between the involved Cys was examined. Four additional Cys pairs were created. According to the crystal structure of AcrB, T574 and A627 locate in the middle of a pair of anti-parellel β-strands that exists in PC1 subdomain (Figure 2.8). Taking advantage of this intrinsic "ruler", the extent of disulfide bond formation between A627C, which located in the center of one strand, with five residues were measured. These five residues scattered on the other strand, including L578C, V576C, T574C, F572C and G570C. The distances between the Cα of A627 and the Cα of the five residues on the other strand are summarized in Table 2.3. These distances were obtained by measuring the corresponding distances in all independent AcrB crystal structures currently available, including 1IWG, 1OY6, 1T9T, 2HQC, 2GIF, 2DHH, 2RDD, and 3B5D. The average distances and standard deviations were also listed. The distance between the Cα of T574 and A627 is in the optimum range to form disulfide bond (which is one of the seven reporters created), while the distance between the Cα of A627 and F572 or V576 are slightly beyond the disulfide bonding distance. The distances between the Cα of A627 and G570 or L578 are too long to form the disulfide bond.

Table 2.3 Summary of the measured Cα distances and percentage of fluorescence intensity.

Res. 1	Res. 2	C	□ dist	Fluorescence %
A627C	T574C	5.4 ± 0.22		100
A627C	G570C	14.3 ± 0.38		7.7 ± 3.4
A627C	F572C	8.9 ± 0.25		12.5 ±6.0
A627C	V576C	8.1 ± 0.26		65.1 ± 10.4
A627C	L578C	14.5 ± 0.28		3.0 ± 2.7

The extents of disulfide bond formation of these five pairs were compared. After overnight expression, proteins were purified in the presence of IAM, and then reduced with DTT before labeled using F-Mal. As shown in Figure 2.8B, $_{CL}AcrB_{A627C/T574C}$ formed strong disulfide bond. Assuming the extent of disulfide bond formation in $_{CL}AcrB_{A627C/T574C}$ was 100%, the percentages of disulfide bond formation in the other four mutants were calculated through comparing their fluorescent intensities with that of $_{CL}AcrB_{A627C/T574C}$ in Figure 2.8B (Table 2.3). Two interesting observations were obtained. First, although the measured distances between the Cα in C627-C572 and C627-C576 are both longer than the distance normally observed in existing disulfide bonds, there were still significant levels of disulfide bond formation in both cases. Second, while the measured Cα distances in C627-C572 and C627-C576 were similar, the extent of disulfide bond formation was quite different. These observations may indicate that AcrB structure has a certain degree of flexibility, which involves a slight shift of the relative position between the two β-strands. The breathing effect of the structure may have temporarily brought the side chains of C627 and C572 or C576 within the disulfide bond forming distance. In addition, this movement

is asymmetric relative to the location of A627, which favored the formation of C627-C576 disulfide bond to a greater extent.

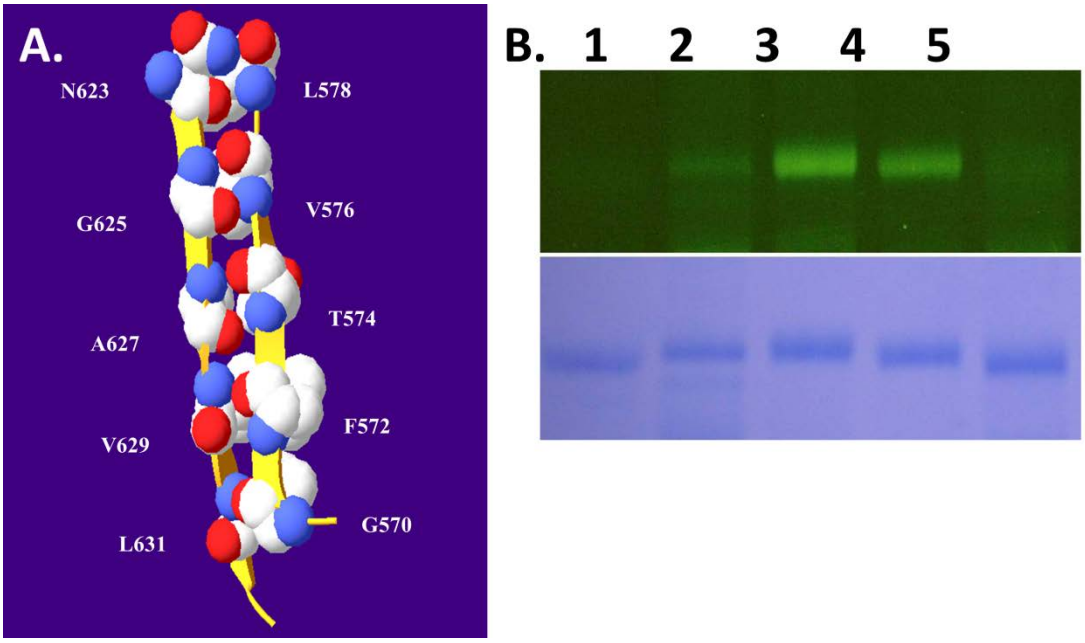

Figure 2.8 A. Side chains of 5 pairs of residues that within the β-strands were shown in space-filled model with labels on the side. B. Labeling results of Cys pairs, $_{CL}AcrB_{G570C/A627C}$ (lane 1), $_{CL}AcrB_{F572C/A627C}$ (lane 2), $_{CL}AcrB_{T574C/A627C}$ (lane 3), $_{CL}AcrB_{V576C/A627C}$ (lane 4), and $_{CL}AcrB_{L578C/A627C}$ (lane 5). Protein purification was carried in the presence of IAM, and then reduced with DTT and labeled using F-MAL. As revealed by the Commassie blue stain, the protein loading amount in each lane was the same.

To verify if the extent of fluorescent labeling reflects the distance in the reporter Cys pair under the native condition, the extent of disulfide bond formation of five Cys pairs separated by different distances was compared. These five Cys pairs locate in two closely spaced anti-parallel β-strands in AcrB PC1 subdomain. The results not only confirmed that the fluorescent labeling approach can faithfully reflect the distance between the involved Cys pairs, but also suggested

that there was certain degree of structural motion in the related region of AcrB. This motion may reflect the intrinsic structural flexibility of AcrB. However, it should not be critical for the function of AcrB, as the cross-linking between A627C and one of the other Cys did not affect the activity of the efflux pump.

Finally, the activity assay for these mutants was performed to confirm that these mutations did not cause a drastic change of AcrB structure (Table 2.4). $_{CL}AcrB_{T574C/A627C}$ had been shown to be fully active in earlier experiment. The MICs of the rest four pairs were also similar to that of the wild type AcrB. The mutations to Cys and formation of disulfide bonds had no negative effect on the activity of the protein.

Table 2.4 Drug susceptibility of four cysteine pair reporters for distance sensitivity measurement

Plasmid or mutant	MIC (μg/ml)	
	Erythromycin	Novobiocin
Wild type	128	128
G570C/A627C	128	128
F572C/A627C	128	128
V576C/A627C	128	128
L578 C/A627C	128	128

The disulfide trapping method is an established technique that has been applied successfully in the detection of conformational change in membrane proteins.[126-133] Usually Cys pairs introduced at strategic positions in the protein are first induced to form disulfide bond with a chemical catalyst, and then various methods are used to determine the formation of disulfide bond. The most commonly method used to detect the presence of disulfide bond is SDS-PAGE.[134] Under

reducing or non-reducing conditions, proteins containing disulfide bond may migrate differently in the gel. Nevertheless, the presence of intra-molecular disulfide bond may not always generate a detectable shift in migration. Another popular method in the detection and quantification of disulfide bond and free cysteine is mass spectrometry.[135]This method is more accurate, but is also more time consuming, expensive, and requires specific instrumentation. An alternative method is to use sulfhydryl-specific labeling reagents, including biotin, fluorescence dye, and radioactive probes.[123, 135] These labeling reagents can react with free thiols. However, cysteine in the form of free thiol may suffer from oxidation by ambient oxygen during the protein purification process, which may cause artifact in the estimation of the percentage of free cysteine in the protein. The procedure developed here is more reliable because all cyeteine in the protein were first blocked to prevent the formation of new disulfide bond during the detergent extraction and protein purification process. After purification, the protein was denatured in the presence of the blocking reagent, which could further eliminate residual free thiols that might not be accessible by the blocking reagent under native state. Finally, disulfide bond that presented in the protein before the purification process was reduced and immediately labeled with a thiol-reactive fluorescent probe. The experimental design included internal positive and negative controls, which could compensate for potential differences in chemical reactivity of Cys placed at different regions of the protein sequence. Through comparing the fluorescence intensity of the sample with those of the negative and positive controls, I could estimate the percentage labeling of the sample, which reflected the portion of the Cys pair that existed in the form of disulfide bond in the protein. The experimental results were highly reproducible due to these proactive experimental designs.

The establishment of multiple reporter Cys pairs in the AcrB periplasmic domain has set the stage for the investigation of AcrB conformational changes under various experimental conditions. For example, while the effect of detrimental mutations that disrupt know mechanisms such as substrate binding or proton relay are easy to interpret, mutations that disrupt AcrB function through interfering protein structure or folding are more difficult to pin down. Now the structural impact of such mutations can be assessed by the reporter constructs.

2.4 CONCLUSION

AcrB and its homologues are major players in conferring multidrug resistance to Gram-negative pathogens. Its structure is strongly connected to its function as an efflux pump. Study of AcrB conformational changes helps understand which residues are important to the protein activity and identify potential inhibitors as drugs for clinical treatment. Herein, a disulfide-trapping based reporter system was developed. Cysteine pair reporters can be labeled by fluorescein maleide to different extents which is highly related to its distance and local environment. These reporters could be used as a fast, convenient and sensitive method to probe local conformational changes in AcrB. Later this method has been used by my group to detect subtle conformational difference upon further mutagenesis studies. I expect that such a design might be applicable to other membrane proteins as well.

CHAPTER III. STUDY OF ACRB FOLDING AND TRIMERIZATION

3.1 INTRODUCTION

Oligomerization is a common feature in protein structure. The majority of oligomers are homo-oligomers.[136-140] Obligate oligomers exist and function exclusively in one oligomeric state. The assembly of obligate oligomers is an interesting and yet poorly understood process. Studies with soluble oligomeric proteins indicated that oligomerization may occur via a two-stage or a three-stage pathway.[141-144] In the two-stage pathway individual monomers remain unfolded in the absence of oligomerization, while in the three-stage pathway individual monomers fold into an independently folded structure, which may be different from the final conformation in the oligomer.[145]

It is not well defined how proteins oligomerize in the plasma membrane of a cell. Of all the proteins encoded in sequenced genomes, approximately 20-30% are predicted to be membrane proteins, many of which function as oligomers.[146] However, the mechanism of the oligomer assembly in the cell membrane of integral membrane proteins is still not clear, mainly due to the difficulty of characterizing protein tertiary and quaternary structures separately in the cell membrane under native condition. The anchoring of the subunits in the membrane restricts the movement of the subunits to two dimensions, which may increase local concentrations of the subunits and therefore the chance of encountering among them. Thus, the oligomerization of membrane-associated proteins may occur more efficiently.

In the case of obligate oligomers, it is not well defined how each subunit exist before they assemble into the final oligomeric state. In Gram-negative bacteria, the membrane insertion of inner membrane proteins occurs co-translationally. It is still unclear to what extent each individual subunit folds before the onset of the assembly. It still remains elusive whether it

occurs through a two-stage or three-stage pathway. The assemblies of heteropentameric membrane proteins have been shown to be sequential by several studies. For example, Green and Claudio studied the sequential folding and assembly of the heteropentameric Acetylcholine receptor (AChR).[147] Taking advantage of the temperature sensitive assembly of Torpedo AchR subunits in the mouse cell line, they first expressed the subunits at 37^{o}C, and then triggered the assembly by lower down the temperature to 20^{o}C. With this method, they found that within first few minutes the αβγ trimer was assembled, followed by the sequential addition of a δ, and finally a second α subunit. The authors concluded that the subunit folding events contribute to subunit recognition site formation during assembly. One factor that was not addressed in their study is, how close are the structure of each individual subunit to their final structure in the functional heteroligomer.

In this study, the relation between the subunit folding and oligomer assembly in a trimeric membrane protein, AcrB, was investigated. The rationale is, since the major difference between the two-stage and three-stage pathway is the existence of well folded, independent monomers under native condition, the observation of well folded monomeric AcrB in the cell membrane would support the three-stage pathway. To make this research possible, it is crucial to have a method to probe the structure of AcrB in the membrane under the native condition, as detergent extraction and purification may affect the conformation and oligomeric state of AcrB. For this purpose, a folding reporter platform has been constructed that can be used as a research tool to reveal the tertiary structure of individual subunits in the cell membrane.[148] In the current study, a well-folded monomeric AcrB mutant, $AcrB_{\Delta loop}$, was created. Part of a protruding loop was deleted in $AcrB_{\Delta loop}$ (Figure 3.1). Since AcrB is a structural and functional obligate trimer, monomeric AcrB has not been found in the cell membrane before. $AcrB_{\Delta loop}$ existed in the cell

membrane in a folded conformation highly similar to that of the final structure in the obligate trimer. In other words, the folding of each individual subunit does not need assistance from neighboring subunits. These results indicated that the trimerization of AcrB may occur through a three-stage pathway.

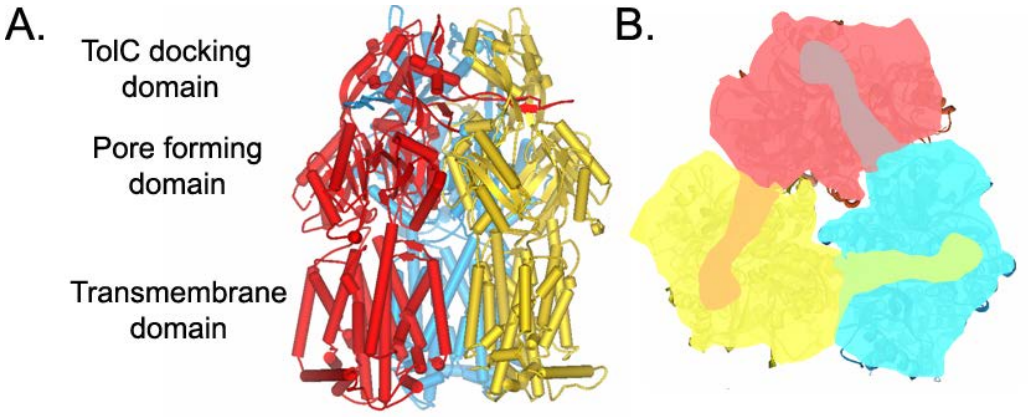

Figure 3.1 A. Side view of an AcrB trimer. Different domains were marked. The position of the inner membrane was marked between the grey bars. **B**. Head view of an AcrB trimer. The contour of each subunit was highlighted using a transparent envelope to illustrate the protruding loop.

3.2 MATERIALS AND METHODS

Cloning, expression and purification of AcrB and its mutants

The pQE70-AcrB plasmid was used as the template to construct the $AcrB_{\Delta loop}$ Mutant. (13) In this mutant the N211-G227 was deleted and the Quikchange mutagenesis kit (Agilent Technologies, Santa Clara, CA) was used to generate this deletion mutation (Figure 3.2).

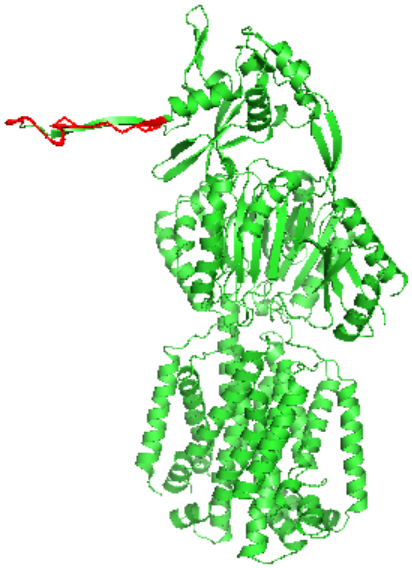

Figure 3.2 Structure of a single AcrB subunit. The part of the protruding loop that was removed in this study was highlighted in green. The structure was created using pdb file 2DHH.

Complementary primers used to construct of $AcrB_{\Delta loop}$ are as follows: 5'-CATTACCGCCATCAAAGCGCAGCAACAGCTTAACGCCTCTATTATTGC-3' and 5'-GCAATAATAGAGGCGTTAAGCTGTTGCTGCGCTTTGATGGCGGTAATG-3'.

With the same method, loop deletion mutation was also introduced into AcrB reporter constructs $_{CL}$AcrB, 32-390-AcrB, 44-91-AcrB, 184-771-AcrB, 199-749-AcrB and 726-812-AcrB. The coding sequences of all plasmids used in this study were confirmed by DNA sequencing. AcrB and all the mutants were expressed in an *E. coli* strain deficient in gene *acrB* (BW25113*ΔacrB*) and purified as described.[148]

Drug susceptibility assay of $AcrB_{\Delta loop}$ mutant

AcrB activity could be measured with a drug resistance assay. The minimum inhibitory concentrations (MIC) of different strains were measured using the protocol described

previously.[148] Briefly, *E. coli* strain deficient in gene *acrB* (BW25113*ΔacrB*) was used as the host cell. The plasmid encoding wild type AcrB ($_{WT}$AcrB) or empty pQE70 vector was transformed into the BW25113Δ*acrB* strain separately. These two transformed strains were used as the positive and negative controls, respectively. Plasmids encoding different AcrB mutants were also transformed into BW25113Δ*acrB* strain. Freshly transformed cells were plated on LB-agarose plates containing 100 μg/mL ampicillin and 50 μg/mL kanamycin. The same ampicillin and kanamycin concentrations were used throughout the study. A single colony was inoculated into a LB media containing ampicillin and kanamycin. The strains were cultured to the exponential-phase and then were diluted to an OD_{600nm} unit of 0.1 using LB broth. 5 μL of this culture was used to inoculate 1 mL LB media containing the indicated concentration of erythromycin or novobiocin. The cultures were incubated with shaking under 37^{o}C for overnight. The OD_{600nm} of each sample was measured the next morning. The activity assay was conducted under the basal expression condition. Each experiment was repeated in triplicates.

Expression, purification, and labeling of AcrB and its mutants

Labeling of AcrB reporters was performed as described in Chapter II. (13) Briefly, AcrB reporter mutants freshly expressed in BW25113*ΔacrB* was treated with iodoacetamide (IAM) and purified with Ni-Sepharose. IAM could block free thiols in the protein but it would not affect disulfide bonds. After purification, dithiothreitol (DTT) was added into the protein samples to reduce disulfide bonds and generate free thiols. These freshly generated thoils were immediately labeled with 5-Maleimido-fluorescein (Flu-MAL) and analyzed by SDS-PAGE. With this method, disulfide bonds existing in the protein can be quantified.

Blue Native PAGE analysis of wild type AcrB and AcrB$_{\Delta loop}$

BN-PAGE was performed as previously described.[149, 150] Briefly, purified protein samples were mixed with blue native loading buffer to reach a final concentration of 0.1M 6-aminoocaproic acid, 6% sucrose, 10mM 2-[bis(2-hydroxyethyl)amino-2-(hydroxymethyl) propane-1,3-diol-HCl, 1% Coomassie brilliant blue G-250, pH 7.0. Protein samples were load to a 4–20% gradient polyacrylamide gel . The electrophoresis was performed at 60 V in the 4°C refrigerator for 5 hours using a running buffer (25 mM Tris-HCl, 192 mM glycine, 0.01% Coomassie brilliant blue G-250, pH 8.3) . Then Coomassie Blue stain was used to visualize the protein bands. Band intensity was quantified with the software ImageJ. (44)

Limited Trypsin digestion of WT-AcrB and AcrB$_{\Delta loop}$

Purifed AcrB samples were dialyzed with a reaction buffer containing 20 mM phosphate buffer, 0.1M NaCl, 0.03% n-dodecyl-β-maltoside, 10% glycerol. Then trypsin was added into each sample at a molar ratio of 1:200. The samples were incubated at room temperature for the indicated period of time before phenylmethylsulfonyl fluoride (PMSF) (final concentration was 2 mM) and SDS-loading buffer (final concentration was 1X) was added to quench the digestion reaction. The samples were then heated at 95ºC for 2 minutes and analyzed using SDS-PAGE.

Analysis of expression levels of wild type AcrB and AcrB$_{\Delta loop}$ by immunoblotting

Freshly transformed colonies of BW25113*ΔacrB* strain containing plasmid-encoded wild type AcrB or AcrBDloop were inoculated into LB medium containing ampicillin and kanamycin. After overnight culture at 37°C, cells were harvested, resuspended in 10 mM HEPES-KOH buffer (pH 7.5) to an OD600 of 15. Then the cells were ruptured with French Press in the

presence of PMSF. Unbroken cells of the sonicated suspensions were removed by low-speed centrifugation and the membrane vesicle was collected by ultracentrifugation at 150,000 g for 1 hour under 4°C. The pellet was resuspended in 10 mM HEPES-KOH (pH 7.5) buffer containing 2% (wt/vol) SDS to solubilize the inner membrane proteins. The solubilization was enhanced by sonication and then incubated at 37°C for 2 hours. Then SDS-Loading buffer was added and the samples were separated on 8% SDS-PAGE and transferred to a nitrocellulose membrane (Millipore, Bedford, MA) for Western blot analysis with polyclonal rabbit anti-AcrB as primary antibody and an alkaline phosphatase-conjugated anti-rabbit (Abcam, Cambridge, MA) as secondary antibody. Then the protein-antibody conjugates were visualized with nitroblue tetrazolium chloride and 5-bromo-4-chloro-3'-indoyl phosphate p-toluidine. (Sigma-Aldrich, St. Louis, MO).

CD analysis of the structure and heat stability of WT-AcrB and AcrB$_{\Delta loop}$

CD analysis was performed on a JASCO J-810 spectrometer (JASCO, United Kingdom) with 1 nm bandwidth. Protein samples were dialyzed overnight against a low salt buffer (10 mM sodium-phosphate, 50 mM NaCl, 10% glycerol, 0.05% DDM, pH 7.5) before the CD measurement. Blank scans were performed with the exterior dialysis buffer. For far-UV CD spectra of secondary structure, samples in 1 mm path length cuvettes were scanned in the wavelength range 250–190 nm. Spectra were then corrected for background by subtraction of a blank curve obtained from the dialysis buffer. For the near-UV CD analysis, the scanning was performed in the wavelength range 350-250 nm using a 1cm path-length cuvette. Protein concentrations were determined with Bradford assay.

Chemical crosslinking

The WT-AcrB and $AcrB_{\Delta loop}$ were freshly expressed in BW25112Δ*acrB* strain and the bacteria cells were harvested and lysed by sonication in a buffer containing 50 mM phosphate, 0.15M NaCl and 0.5 mM PMSF (pH 7.5). After sonication the suspensions were centrifuged and the cell pellets were collected and re-suspended in a buffer containing 50mM phosphate, 0.15M NaCl, 0.5mM DSP (pH=7.5). The suspension was incubated under 37°C for 40 minutes. Tris-HCl (pH 8.0) was added to a final concentration of 50 mM to quench the crosslinking reaction. Then TritonX-100 was added to a final concentration of 1% to extract the inner membrane proteins and AcrB was purified as described above.

Purified WT-AcrB and $AcrB_{\Delta loop}$ samples were analyzed by non-reducing SDS-PAGE. Later, western blot analysis was performed with polyclonal rabbit anti-AcrB primary antibody and alkaline phosphatase-conjugated anti-rabbit secondary antibody.

Note: Cloning, expression and purification of AcrB mutants, fluorescence labeling, limited protease digestion, blue native analysis, CD analysis were performed by Dr. Wei Lu and Meng Zhong. Drug susceptibility was performed by MZ. Chemical crosslinking was performed by WL.

3. 3 RESULTS AND DISCUSSION

3. 3. 1 Construction of pQE70-$AcrB_{\Delta loop}$

The goal of this study is to determine if monomeric AcrB mutant can exist in the cell membrane, and if so, how does the structure of this mutant compare with that of wild type AcrB. The answer of this question may shed light on the oligomerization pathway of AcrB. The capability of AcrB monomer to fold independent from the neighboring subunits in the cell membrane would suggest

a three-stage oligomerization pathway, which involves well-folded monomer intermediate state. AcrB is an obligate trimer. No monomeric or dimeric AcrB has ever been observed in cell membrane. After extracted from the membrane using detergent, AcrB predominantly exists as a trimer. [61-63] Change of the sample buffer condition or prolonged storage may cause AcrB trimers to dissociate into monomer, but no evidence has been reported concerning if these monomers could re-assemble into trimer.[151]

To create monomeric AcrB in the cell membrane, we predict that the inter-subunit interface between neighboring subunits would be interrupted while at the same time the intra-subunit interactions should not be interrupted. Through examination of the AcrB structure, we speculated that mutations in the protruding loop as revealed in Figure 3.1 might generate monomeric AcrB mutant. It is far away from the bulk of the protein structure and is not expected to be important for the overall tertiary structure packing. While at the same time, it should be critical for the inter-subunit interactions. With the site directed mutagenesis kit, 17 residues were deleted in the loop which corresponds to half of the overall length of the loop. The loop deletion mutation was also introduced into five of the AcrB reporters described in Chapter II. The disulfide trapping method was used to investigate how loop deletion would affect AcrB conformation.

3. 3. 2 Drug susceptibility of $AcrB_{\Delta loop}$

The activity of $AcrB_{\Delta loop}$ was measured by a drug susceptibility assay. Plasmids encoding wild type AcrB or $AcrB_{\Delta loop}$ were transformed into BW25112*ΔacrB* strain. In parallel, vector pQE70 was also transformed into BW25112*ΔacrB*to serve as a negative control. Minimum inhibitory concentrations of these strains were measured for two established AcrB substrates, erythromycin and SDS (Table 3.1). The MIC of the strain containing plasmid-encoded $AcrB_{\Delta loop}$ was much

lower than the plasmid-encoded wild type AcrB, and was similar to the MIC of the same strain with the empty pQE70 vector. This result indicated that the mutant was completely non-functional, as it could not increase the resistance level of the host strain to those AcrB substrates.

Table 3.1 MICs of BW25113ΔacrB expressing plasmid encoded *acrB* gene

Plasmid or mutant	MIC (μg/ml)	
	Erythromycin	Novobiocin
BW25113Δ*acrB*	4	4
pQE70	4	4
pQE70AcrB$_{\Delta loop}$	4	4
pQE70AcrB	128	128

Normally, the drug efflux ability of AcrB can be disrupted by disrupting the substrate binding or proton relay pathway, the folding of each subunit, the assembly of a functional AcrB trimer, or the interaction between AcrB and its functional partners AcrA and TolC. Since the site of mutation is distant from the substrate binding, proton relay, and AcrA/TolC docking interface, the lack of function is more likely to be a result of disrupting subunit folding or trimerization.[59, 104, 107, 109, 110, 112, 113, 152]

3. 3. 3 Expression levels of AcrB$_{\Delta loop}$ and wild type AcrB

To evaluate how the truncation of the protruding loop will affect the overall structure and stability of the protein, the expression level of the mutant was examined. If a mutation dramatically reduced the overall stability of a protein, it could cause the mutant protein to fail the

quality control mechanism of the cell and result in a drastic decrease of the protein abundance. In this case, BW25113Δ*acrB* was used to express wild type AcrB and $AcrB_{\Delta loop}$ to prevent the interference from intrinsic AcrB expression. Membrane vesicles were extracted and then analyzed by immunoblot. The same samples were diluted 10 and 100 fold to further compare the expression levels of the two proteins in the cell (Figure 3.3). The densities of the blotting bands were very similar for both proteins, indicating AcrB expression levels in two strains are fairly close.

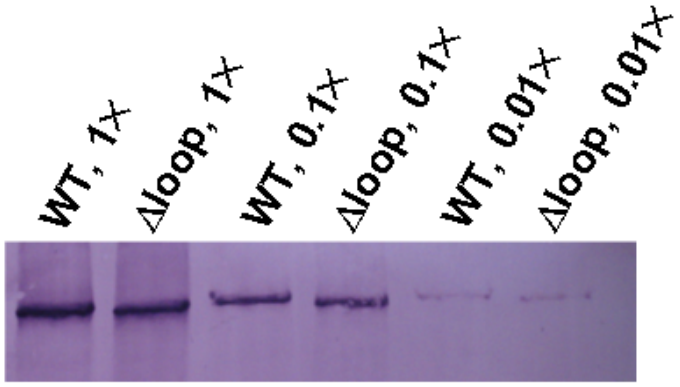

Figure 3.3 Comparison of the expression levels of wild type AcrB and $AcrB_{\Delta loop}$. **A.** Western blot analysis of membrane vesicles extracted from BW25113Δ*acrB* expressing the wild type AcrB or $AcrB_{\Delta loop}$. Each sample was diluted 1, 10 and 100 fold.

3.3.4 Structural study of $AcrB_{\Delta loop}$ by circular dichroism

Next, circular dichroism was used to characterize $AcrB_{\Delta loop}$ and wild type AcrB structures in detail. $AcrB_{\Delta loop}$ and wild type AcrB were first purified by Ni-NTA beads. The mutant protein can be purified following the same protocol as the wild type AcrB with comparable yield (Figure 3.4).

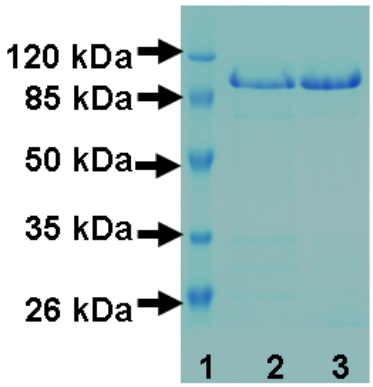

Figure 3. 4 SDS-PAGE of purified wild type AcrB (lane 2) and $AcrB_{\Delta loop}$ (lane 3) samples. Both proteins can be purified to near homogeneity. The positions of protein molecular weight markers were marked respectively.

Far UV CD spectroscopy provides valuable information about protein secondary structure. The "far UV" region in the CD spectra (190nm-250nm) of the two proteins superimposed well, suggesting deletion of the protruding loop did not change protein secondary structure. Both proteins showed two distinct peaks of α-helices (Figure 3.5A).

Thermal stability of the proteins was also compared. When protein is heated to certain temperature, it would slowly lose its secondary structure. In this case, the changes in α-helix signal were monitored. The wavelength was set at 222 nm with the increase of temperature from 4 to 98 °C (Figure 3. 5B).

If the truncation of the loop does affect the folding and internal packing of the AcrB subunit, then most likely there would be a change in the melting temperature. The change in the ellipticity at 222nm reflected the change in protein secondary structure upon heat denaturation. Residual helical structure maintained even when the proteins were heated to 98 $^{\circ}$C, which is consistent with previous observations that helices in helical membrane proteins are very stable and a

portion of them exist even in the unfolded stage.[153] The melting curves of the two proteins almost overlap, indicating a lack of significant difference in the thermal stability between $AcrB_{\Delta loop}$ and wild type AcrB.

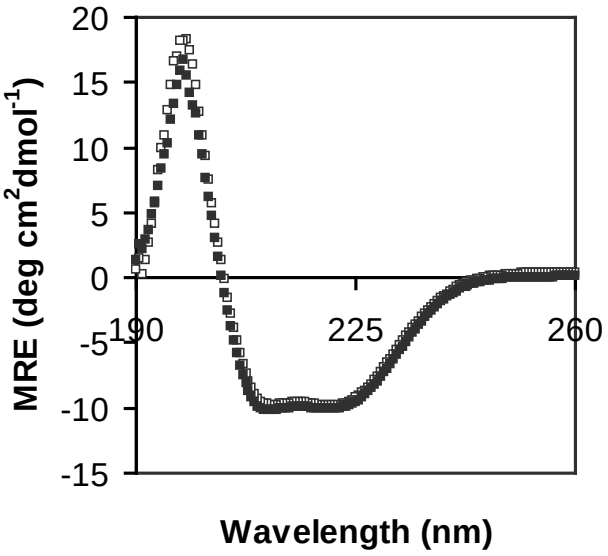

A)

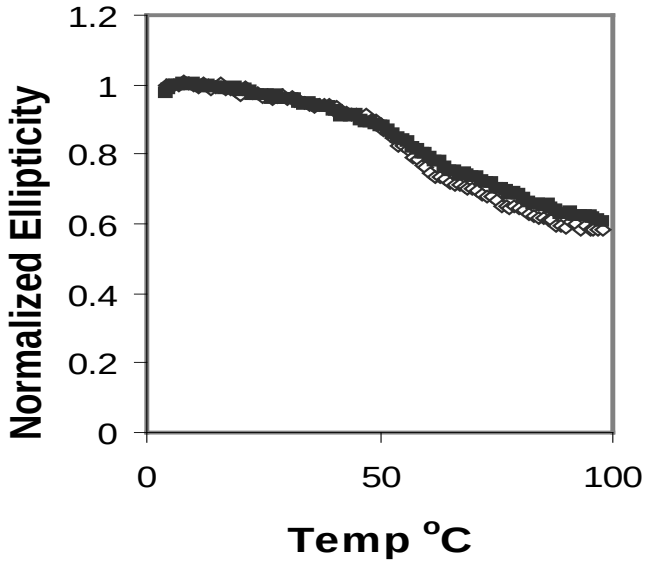

B)

Figure 3.5 A. Far UV CD spectra of wild type AcrB (open squares) and $AcrB_{\square loop}$ (filled squares) superimpose well onto each other, indicating the two proteins had similar secondary structure contents. **B**. Temperature denaturation curves of wild type AcrB (open diamond) and $AcrB_{\Delta loop}$ (filled squares). The ellipticity values monitored at 222 nm against the temperature was normalized to the reading at 4 ^{o}C. The thermal stabilities of the two proteins were very similar.

The near UV CD spectrum (260-350 nm) of both proteins was collected (Figure 3.6). The signal of near UV CD comes from aromatic residues including tryptophan, tyrosine, and phenylanine, which is related to protein's tertiary and quaternary structure. When protein confirmation changes, there is likely to be a change in the microenvironment of these aromatic residues, which will affect their UV absorption and the CD spectrum. Also, the near UV CD is sensitive to the intramolecular and intermolecular interaction of oligomeric proteins. The spectrums of the wild type and mutant proteins were different, proving there is a difference in the local structure of these residues (Fig. 3.6). This change may be at the tertiary structure or the quaternary structure level, as both may potentially change the microenvironment of the residues.

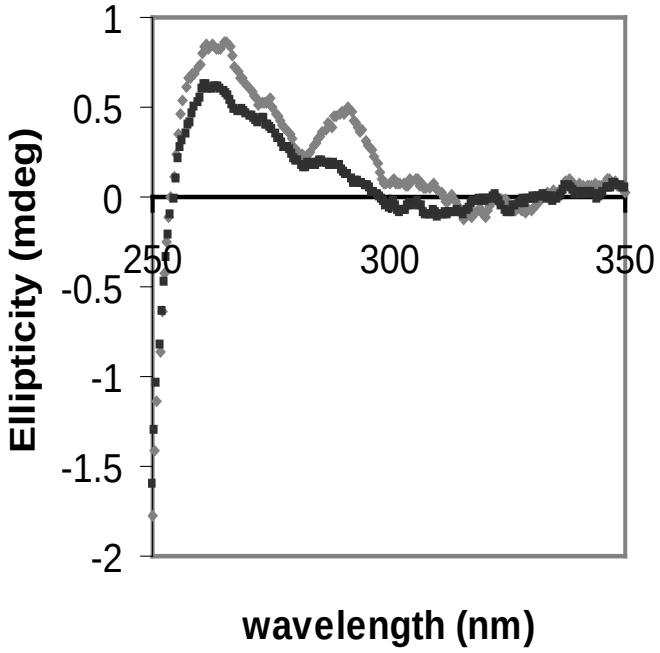

Figure 3.6 Near UV CD spectra of wild type AcrB (grey diamonds) and $AcrB_{\square loop}$ (black squares).

3. 3. 5 Structural study of $AcrB_{\Delta loop}$ by limited protease digestion

Limited protease digestion is another well established method that has been used extensively to probe a protein's structure.[154-158] A well folded protein is more resistant to protease digestion than a poorly folded one. The pattern of the resultant peptide fragments may also reveal the disordered portion of a protein. I compared the digestion results of $AcrB_{\Delta loop}$ and wild type AcrB at different time points of trypsin treatment. As shown in Figure 3. 7. After 15 min of incubation, 90% of full length AcrB was preserved. Under the same experimental condition, $AcrB_{\Delta loop}$ was digested much faster. A clear decrease of the full length protein was obvious within 5 min into digestion, and at 15 min a large portion of the protein was digested into smaller fragments. This result showed wild type AcrB was more resistant to trypsin digestion. This difference, again, can

be explained by the structural differences of wild type AcrB and $AcrB_{\Delta loop}$ at the tertiary and/or quaternary structure level. Difference in trypsin digestion rates elucidated the difference in the accessibility of Lys and Arg to the enzyme. Two factors might cause the observed difference in trypsin digestion rate: First, $AcrB_{\Delta loop}$ is a monomer. The inter-subunit interface in the trimeric wild type AcrB provides better protection to potential trypsin recognition site from digestion. Second, the tertiary structure of $AcrB_{\Delta loop}$ is different from that of wild type AcrB. Since $AcrB_{\Delta loop}$ was digested faster, its tertiary packing might be "looser" than the tertiary structure packing in wild type AcrB.

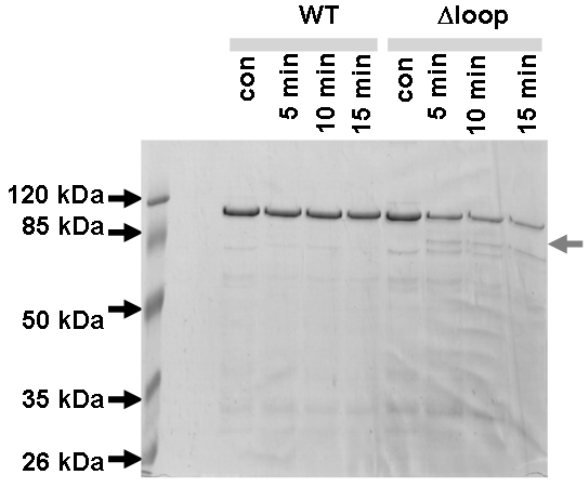

Figure 3.7 Limited trypsin digestion of purified wild type AcrB and $AcrB_{\Delta loop}$. Under the current experimental condition, wild type AcrB is highly resistant to the digestion. No apparent degradation could be observed. $AcrB_{\Delta loop}$ is much more sensitive to digestion. Degradation of the full length protein was apparent after 5 min of incubation. The grey arrow on the right pointed out a compact fragment resulted from trypsin digestion of $AcrB_{\Delta loop}$. Molecular weight marker was on the right of the gel.

3.3.6 Structural study of $AcrB_{\Delta loop}$ by cysteine pair reporters

To determine which factor is the cause of the digestion difference, the thiol trapping method described in chapter II was used to examine protein tertiary structure under the native condition. Most current protein structure characterization methods, such as CD spectroscopy and protease digestion discussed above, require the extraction of the target membrane protein from the cell membrane followed by purification. The sample preparation process may cause protein oligomers to dissociate, thus cannot present protein native state *in vivo*. Substitution of the two intrinsic Cys in AcrB with Ala has been shown to have no impact on AcrB activity.[115] Seven reporter cysteine pairs were introduced in the cysless AcrB ($_{CL}$AcrB). All seven pairs formed disulfide bond, and none of them affect the drug efflux activity of AcrB. The extent of disulfide bond formation in the protein under native condition, that is, before the cell membrane was disrupted, was probed using a blocking-reducing-labeling scheme as described in the materials and methods section. Although the protein was eventually purified and analyzed using SDS-PAGE, the blocking step helped to capture the state of the protein before it suffered from the stress of protein purification.

First, loop deletion was introduced into the cysless AcrB ($_{CL}$AcrB), the results were similar to what had been observed in wild type AcrB. Later, 5 reporter Cys pairs were introduced in the periplasmic domain of AcrB$_{\Delta loop.}$ If the protein tertiary or quanternary structure changed, the distance between cysteine pairs would be affected and the change in disulfide bond formation can be detected by the fluorescence labeling method. The extents of disulfide bond formation in five reporter pairs were used to reflect potential structural change in AcrB$_{\Delta loop}$. The profile of disulfide bond formation in these reporter pairs with the AcrB$_{\Delta loop}$ mutation was shown in Figure 3.8.

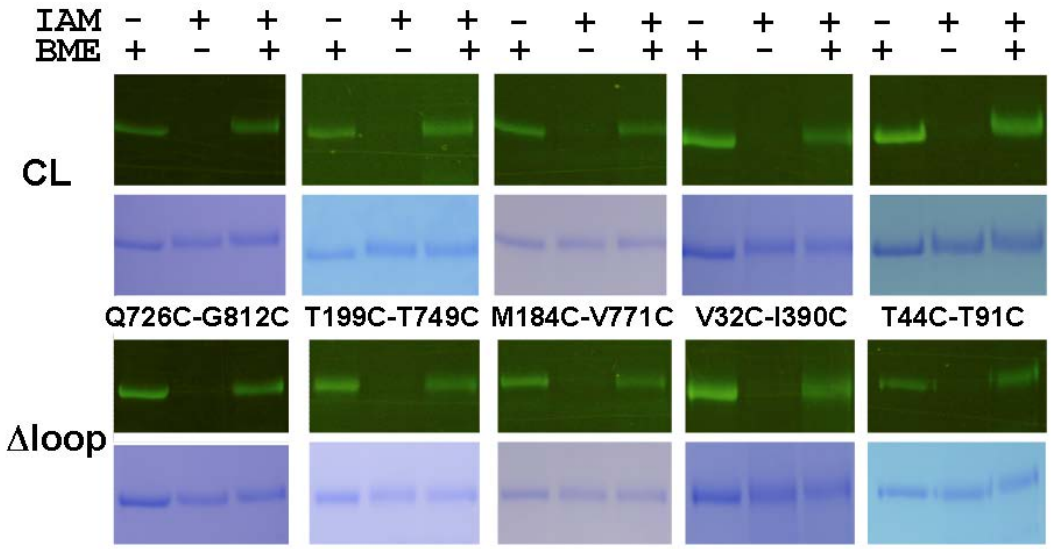

Figure 3.8 Disulfide bond formations in conformation reporters. The extents of sidulfide bond formation were very similar in $AcrB_{\Delta loop}$ as compared to the wild type AcrB. Therefore, the overall conformation, or tertiary structure, of $AcrB_{\Delta loop}$ is very close to that of the wild type AcrB.

The truncation of the protruding loop had no significant effect on the extents of labeling for all reporter pairs, suggesting that the tertiary structure of AcrB in the cell membrane was not affected by this mutation.

3.3.7 $AcrB_{\Delta loop}$ exists as a well-folded monomer

Finally, to investigate how the deletion of the loop eliminated transport activity, the oligomeric state of AcrB was examined using blue native PAGE (BN-PAGE). BN-PAGE is a method widely used in the determination of membrane protein oligomeric states and has been used to confirm that wild type AcrB is a trimer.[149, 150] The results of the BN-PAGE showed that $AcrB_{\Delta loop}$ migrated as a monomer. also It has been confirmed that under the same experimental

conditions wild type AcrB migrated as atrimer, consistent with the result in literature (Figure 3. 9).

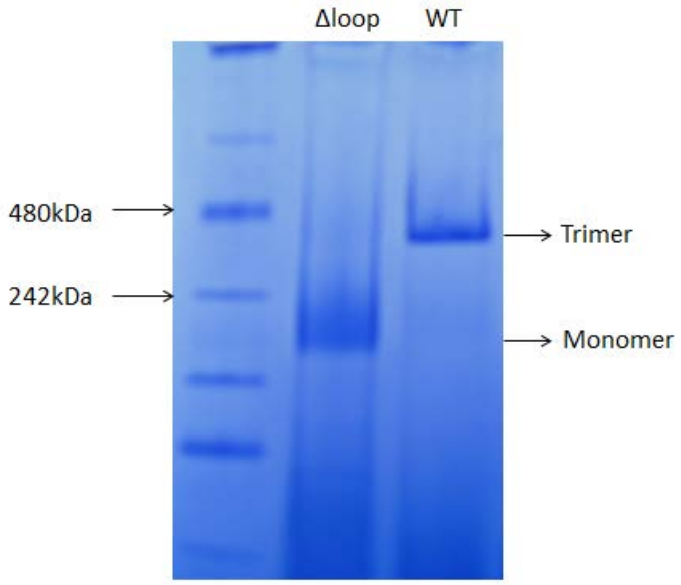

Figure 3.9 After detergent purification, freshly prepared wild type AcrB samples migrated as a trimer in the BN-PAGE. Under the same condition, purified $AcrB_{\Delta loop}$ migrated as a monomer.

The observation that $AcrB_{\Delta loop}$ migrated as a monomer in BN-PAGE after purification does not completely rule out the possibility that the protein may associate weakly as a dimer or trimer in the cell membrane, but dissociate during the process of purification and electrophoresis analysis. To further investigate the impact of the mutation on the quaternary structure of the protein, cross-linking experiments were conducted using membrane vesicles and di(N-succinimidyl) 3,3′-dithiodipropionate (DSP) as the crosslinker. DSP cross-links two $-NH_2$ groups. Crosslinking was performed using membrane vesicles extracted from BW25113Δ*acrB* cells expressing wild type AcrB or $AcrB_{\Delta loop}$. Immunoblotting with an anti-AcrB antibody was used to detect the protein bands after SDS-PAGE analysis. As shown in Figure 3. 10, the wild type AcrB trimer was

clearly visible, while $AcrB_{\Delta loop}$ only migrated as a monomer. Some wild type AcrB monomers were also visible, presumably due to the incompleteness of the cross-linking reaction. In the absence of cross-linking, wild type AcrB also migrated only as a monomer under the same experimental conditions. This result further confirms that $AcrB_{\Delta loop}$ exists as a monomer in the inner membrane of *E. coli*.

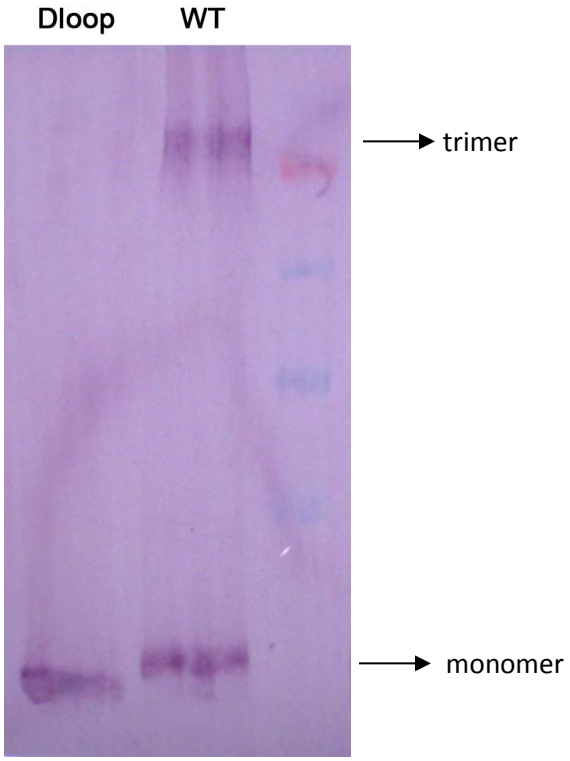

Figure 3.10 Western blot analysis of membrane vesicles extracted from BW25113Δ*acrB* expressing the wild type AcrB or $AcrB_{\Delta loop}$ after chemical cross-linking.

3.3.8 Impact of expressing $AcrB_{\Delta loop}$ in a wild type *E. coli* strain on AcrB activity

To examine if the expression of $AcrB_{\Delta loop}$ interferes with the wild type AcrB subunit, I transformed plasmid encoded $AcrB_{\Delta loop}$ into a wild type AcrB strain and examined the drug susceptibility level of the resultant strain. Earlier study has shown that when another functionless AcrB mutant, $AcrB_{D408A}$, was overexpressed in a wild type *E. coli* strain, the drug susceptibility

level of the strain is drastically reduced.[111] D407 and D408 in AcrB are two highly conserved acidic residues in the transmembrane domain that are critical for proton relay, which provides the energy to drive the protein conformational change critical for the function of AcrB. The crystal structure of $AcrB_{D407A}$ has been determined, which forms a trimer similarly as the wild type AcrB.[159] The exact reason that causes the observed dominant negative effect when $AcrB_{D408A}$ is expressed in the wild type *E. coli* strain remains elusive. $AcrB_{D408A}$ could potentially interrupt the normal function of genomic AcrB in the wild type strain through competing for binding with AcrA and TolC, or co-assembling with the genomic AcrB. In order for AcrB to function properly all three subunits in an AcrB trimer need to be active.

The MIC of the wild type strain BW25113 transformed with plasmids encoding wild type AcrB or $AcrB_{\Delta loop}$ were shown in Table 3.2. BW25113 transformed with the empty vector pQE70 was used as a control. Other than several established AcrB substrates, a non-AcrB substrate kanamycin was also included as a control for nonspecific effect. Expression of membrane proteins may cause stress in the cell and lead to a non-specific reduction of MIC. The MIC for kanamycin was monitored as a control for this non-AcrB specific effect. The expression of $AcrB_{\Delta loop}$ causes a small change of MIC at 2 folds or less for all substrates and kanamycin. This result indicates that the expression of $AcrB_{\Delta loop}$ does not specifically affect the function of the genomic AcrB.

Table 3.2 Minimum inhibitory concentration of BW25113 expressing plasmid encoded *acrB* mutant genes.

Plasmids	MIC (μg/ml)	
	Erythromycin	Novobiocin
pQE70	128	128
pQE70AcrB$_{\Delta loop}$	64	64
pQE70AcrB	128	128

Folding of membrane proteins is an intriguing and yet poorly understood biological process.[160] In terms of α-helical membrane proteins, the research community has acquired a decent understanding of the identification of transmembrane helices and the prediction of their topology in the membrane. However, how membrane proteins achieve their tertiary and quaternary structures remains largely elusive. Here, we demonstrated, using AcrB as an example, that for proteins in which a soluble domain contributes significantly to inter-subunit interactions, a three stage oligomerization pathway is more likely to be the case, as recognition between folded domains is required prior to oligomerization. For proteins containing only transmembrane domains, folding and oligomerization may happen co-translationally with membrane insertion following a two-stage model.

3.4 CONCLUSION

AcrB and its homologues are major players in the efflux of antimicrobials out of Gram-negative bacteria. The structural and functional unit of AcrB is a homotrimer. The assembly process of obligate membrane protein oligomers, including AcrB, remains elusive. It is not clear if an individual subunit folds into a monomeric form first followed by association (three-stage pathway), or if association occurs simultaneously with subunit folding (two-stage pathway). To

answer this question, the feasibility of creating folded monomeric AcrB mutant was investigated. The existence of folded monomers in the cell membrane itself would be an evidence of a three step pathway. A monomeric AcrB mutant, $AcrB_{\Delta loop}$, was created through the truncation of a protruding loop that appeared to contribute to the stability of AcrB trimer. $AcrB_{\Delta loop}$ expressed at a similar level as wild type AcrB. The secondary structure content and tertiary conformation of $AcrB_{\Delta loop}$ were very similar to that of the wild type AcrB. However, when expressed in an *acrB* deficient strain, $AcrB_{\Delta loop}$ failed to complement its defect in drug efflux. Results from Blue native polyacrylamide gel electrophoresis (BN-PAGE) and cross-linking experiments indicated that $AcrB_{\Delta loop}$ existed as a monomer. The expression of this monomeric mutant in a wild type *E. coli* strain did not have a dominant negative effect, suggesting the mutant could not efficiently co-assemble with genomic AcrB. $AcrB_{\Delta loop}$ is the first monomeric mutant reported for the intrinsically trimeric AcrB. The structural characterization results of this mutant suggest the oligomerization of AcrB might occur through a three-stage pathway involving folded monomers.

CHAPTER IV. INVESTIGATION OF MUTATIONS THAT RESTORE P223G ACRB ACTIVITY

4. 1 INTRODUCTION

AcrB and its homologues are the inner membrane component of the Resistance-Nodulation-Division (RND) family transporters in Gram-negative bacteria. AcrB forms a tripartite pump system with membrane fusion protein AcrA and outer membrane TolC.[161] In the AcrAB-TolC complex, AcrB plays a dominant role in determining substrate specificity and drives the operation of the complex.[61, 62, 162] A broad range of structurally unrelated antibiotics, detergents, organic solvents and dyes are substrates of the AcrAB-TolC pump.[161] Hence, the pump plays a major role in Gram negative bacterial drug resistance. The energy necessary to drive the active transport of substrates against their concentration gradient by AcrAB-TolC efflux pump comes from the proton motive force. Protons flow across the cytoplasmic membrane through a pathway in the transmembrane domain of AcrB, which drives the conformational rotation that enables the uptake of substrates from the outer leaflet of cytoplasmic membrane or periplasm and the subsequent efflux of these substrates through TolC.[163] In the process of substrate efflux, each AcrB monomer rotates through three comformations, access, binding, and extrusion.[62, 119]

Several groups have successfully solved the AcrB crystal structure.[61, 62, 108, 119] AcrB consists of 12 transmembrane (TM) domain and two large periplasmic loops which spans 70 Å in the periplasm. Mutations at the TM domains, D407A, D408A, K940A, and T978A disrupted the electrostatic network and disabled the pump.[163, 164] It was believed the TM domains were only responsible for the proton translocation.[162] The two loops served as the linkers between TM helix 1 and TM helix 2 and TM helix 7 and TM helix 8, repesctively. Based on the structure and functionality, the periplasmic region is divided in to a porter domain and a TolC-docking

domain.[165] (Figure 4.1) Exchange of AcrB and AcrD periplasmic loops altered the substrate preference of the proteins, suggesting that residues important for substrate specificity determination reside in the porter domain.[65] Further mutational studies and AcrB-ligands cocrystallization identified a deep binding pocket.[66, 117, 166, 167] Depending on where they interact, substrates were divided into two groups: groove binder and cave binder.[67, 168] Using the Bodipy-FL-maleimide labeling method, Nikaido et al. elucidated the full substrate pathway *in vivo*.[68, 69] Substrates first bind to the lower entrance of the cleft region, then go through the hydrophobic binding pocket, finally to the AcrB funnel. Because the top part of the protein fits with the periplasmic tip of TolC, this region of the protein is widely believed to be the TolC docking domain. In each of the AcrB monomer, a hairpin like loop inserts into the neighboring chain helps stabilize the whole trimer structure.[58, 169]

My group has studied the role of protruding hairpin loop extensively.[170] AcrB is only functional at its trimeric state. Deletion of the loop led to stability and activity loss of trimeric AcrB. Further characterization showed mutation of proline 223 to glycine had the biggest impact on drug tolerance. $AcrB_{P223G}$ existed as a weakly associated trimer *in vivo*.[170] Here we conducted random mutagenesis studies on $AcrB_{P223G}$ and identified nine mutants with restored protein activity. The mutants were characterized from four aspects: protein expression level, trimer stability, AcrA/TolC-AcrB interaction, and substrate binding.

4. 2 MATERIALS AND METHODS

Cloning, expression and purification of $AcrB_{P223G}$ and its mutants

Plasmid pQE70-AcrB was used as the template in the construction of $AcrB_{P223G.}$[170] The Quick Change mutagenesis kit (Agilent Technologies, Santa Clara, CA) was used to create $AcrB_{P223G}$.

Complementary primers used for the construction of $AcrB_{P223G}$ are as follows: 5'-CTCGGTGGTACGGGGCCGGTGAAAGGCCAAC-3' and 5'-GTTGGCCTTTCACCGGCCCCGTACCACCGAG-3'. Additional site-directed mutations were created using the same method with primers accordingly. Protein coding sequences in all plasmids used in this study were confirmed by DNA sequencing. (Eurofins MWG Operon, AL) AcrB and its mutants were expressed in an *E. coli* strain deficient in gene *acrB* (BW25113*ΔacrB*) and purified as described.[21]

Drug susceptibility assay of AcrB mutants

AcrB activities were studied by a drug resistance assay. The minimum inhibitory concentrations (MIC) of different strains were measured as described.[115] Briefly, *E. coli* strain deficient in gene *acrB* (BW25113*ΔacrB*) was used as the host cell. Plasmids encoding different AcrB mutants were used to transform BW25113Δ*acrB* as well. Freshly transformed cells were plated on LB-agarose plates containing 100 μg/mL ampicillin and 50 μg/mL kanamycin. The same ampicillin and kanamycin concentrations were used throughout the study when noted. A single colony was used to inoculate a LB media supplemented with ampicillin and kanamycin. The exponential-phase cultures of different strains were diluted to an OD_{600nm} unit of 0.1 using LB broth. 2 μL of this culture was added to LB-agar plate containing the indicated concentration of antibiotics. The plates were incubated with shaking at 37^{o}C overnight and the MICs were recorded the next morningBW25113Δ*acrB* strains transformed with plasmid-encoded wild type AcrB ($_{WT}$AcrB) or $AcrB_{P223G}$ were used as the positive and negative controls, respectively. Each experiment was repeated at least three times.

Random mutagenesis of AcrB and mutants screening

Random mutagenesis of AcrB was achieved by two methods, hydroxylamine hydrochloride treatment and error-prone PCR. Chemical mutagenesis by hydroxylamine hydrochloride was performed as described with some modifications.[171] Plasmid pQE70-acrB$_{P223G}$ was incubated in 44 mM potassium phosphate buffer (pH 6.0), 5 mM EDTA and 0.46 M hydroxylamine hydrochloride at 70°C for 40 mins. To quench the reaction, Tris-HCl (pH 8.0) and EDTA were added to the mixture to final concentrations of 90 mM and 9 mM, respectively. DNA was purified by gel extraction kit (Qiagen, CA) and later used for transformation.

Error prone PCR was carried out using GeneMorph II EZClone domain mutagenesis kit (Agilent, CA). First, 500 ng of pQE-AcrB$_{P223G}$ was amplified by Mutazyme II DNA polymerase with two pairs of primers. Primer RM1 (5'-ATGCCTAATTTCTTTATCGATCGC-3') and primer RM2 (5'-AACGGCGTGGTGTCGTATGG-3') were used to generate mutations in the first periplasmic loop of AcrB. Primer RM3 (5'-CGTTGATCCTGACTCCAGCTC-3') and RM4 (5'-ATCGACCAGCTCTCGTACAG-3') were used for the second periplasmic region of AcrB. PCR products were separated and quantified using agarose gel, purified by gel extraction kit. Next, 500ng PCR products were used as mega-primers to amplify AcrB$_{P223G}$ using EZClone reaction. DpnI was added to digest DNA template at 37ºC for 1 hour. PCR products from the second step were purified by gel extraction kit.

E. coli BW25113Δ*acrB* was electroporated with purified hydroxylamine mutagenesis and error-prone PCR mutagenesis of plasmids pQE70-AcrB$_{P223G}$. 1 mL LB broth was added, and the culture was shaken at 37ºC for 1 hr without addition of selective antibiotics. Then the electroporated cells were plated on LB agar plates containing 100 µg/mL ampicillin, 50 µg/mL kanamycin, and 16-32 µg/mL erythromycin. Plasmids were extracted from colonies that were

able to grow on the erythromycin plates and retransformed into BW25113Δ*acrB* strain. Drug susceptibility of each mutant was tested. Those who showed both increased activity were sent to DNA sequencing (Eurofins MWG Operon, AL).

Blue Native PAGE analysis of AcrB mutants

BN-PAGE was performed as described.[149] Briefly, purified protein samples were mixed with blue native loading buffer to reach a final concentration of 0.02M 6-aminoocaproic acid, 1% dodecylmaltoside, 5% glycerol, 0.1% Coomassie brilliant blue G-250, pH 7.0. Protein samples were loaded to a 4-15% polyacrylamide gradient gel (Bio-rad, CA). The electrophoresis was performed using a running buffer (50mM Tricine, 7.5mM imidazole, 0.02% Coomassie brilliant blue G-250, pH 7.0) at 150mA, in the 4°C refrigerator for 4 hours. The protein bands were visualized after Coomassie Blue stain. Band intensity was quantified using the software ImageJ.

AcrA-AcrB, TolC-AcrB interaction assay

pQE70 histidine-tagged AcrB and its mutations were engineered into BW25113Δ*acrB* strain to study *in vivo* interaction of AcrB, AcrA and TolC. Co-purified AcrA and TolC after crosslinking with AcrB-His on Ni-NTA beads were quantified by immunoblot. DSP crosslinking and co-purification were performed as described with modifications.[172] Briefly, BW25113Δ*acrB* harboring pQE70-acrB-his and mutant plasmids were cultured overnight in 100 mL LB supplemented with ampicillin and kanamycin. Cells were harvested, washed with 5 mL 50 mM Na-phosphate buffer (pH 7.2) twice. The pellet was resuspended in 5 mL Na-phosphate buffer containing 4 mM cross-linking agent Dithiobis(succinimidylpropionate) (DSP) (Pierce), and incubated at 37ºC for 30 mins. Tris was added to a final concentration of 50 mM to quench the

reaction. Cell membrane vesicles was collected and extracted with 25 mM Tris buffer, 0.2M NaCl, 2% Triton X-100 (pH=8.0) for 2 hrs on ice. Soluble fractions were incubated with Ni-NTA resins for 45 mins on ice. 10 bed volumes of 10 mM and 50 mM imidazole were used to wash impurities off the resin. Bound AcrB-His were then eluted with 25 mM Tris buffer, 0.2 M NaCl, 0.03% DDM, 0.5 M imidazole (pH 8.0). Dithiothreitol (DTT) was added to a final concentration of 50 mM to the samples in order to break crosslinks. Finally, the samples were analyzed by SDS-PAGE and immunoblotted with AcrA antibody and TolC antibody.

Analysis of expression levels of AcrB mutants by immunobloting

Freshly transformed colonies of BW25113*ΔacrB* strain containing plasmid-encoded wild type AcrB, $AcrB_{P223G}$ and mutants were used to inoculate LB medium containing ampicillin and kanamycin. Cells were harvested after overnight culture and ruptured using French Press in 10 mM HEPES-KOH buffer (pH 7.5) and 0.5 mM PMSF. Unbroken cells were removed by low-speed centrifugation and the membrane vesicle was collected after ultracentrifugation at 150,000 g for 1 hour at 4°C. The pellet was resuspended in 10 mM K-HEPES (pH 7.5) buffer containing 2% (wt/vol) SDS for solubilization of inner membrane proteins. Then after adding SDS-Loading buffer the samples were separated on 8% SDS-PAGE and immunoblotted using polyclonal rabbit anti-AcrB antibody.

Fluorescent labeling

Bodipy-FL-maleimide labeling was conducted following the published method.[68] Briefly, BW25113*ΔacrB* cells harboring plasmids encoded AcrB mutants were cultured overnight at 37ºC. 10 mL culture were harvested by centrifugation at 4,000×g for 5 min, washed twice using

10 ml of buffer A (50 mM potassium phosphate, 0.5 mM $MgCl_2$, pH 7.0), and finally resuspended in 5 mL of the same buffer containing 0.4% glucose and 6 μM Biodipy-FL-maleimide. Final cell density was adjusted to OD_{660} of 3.5. The mixture was shaken at room temperature for 1 hr. Next, Cells were harvested by centrifuge, washed with 5 ml buffer A with 0.4% glucose, and then washed again with 5 ml buffer A. AcrB was then purified following as described with some modifications. Cells were lysed by sonication and centrifuged at 16,000×g for 15 minutes. Buffer B (50 mM sodium phosphate, 0.2 M NaCl, pH 8.0) containing 10 mM imidazole 2% DDM was used to solubilize the pellets for 2 hours on ice. The samples were then collected by centrifugation at 16,000×g for 20 minutes. The supernatant was incubated with Ni-NTA beads at 4°C for 2 hrs. Resins were then washed with buffer B containing 50 mM imidazole, and 0.03% DDM. Finally the protein was eluted with buffer B containing 500 mM imidazole, and 0.03% DDM (pH 8.0).

Samples after purification were resolved by SDS-PAGE. Fluorescence signal were collected by Typhoon Phosphorimager at the excitation wavelength of 488 nm. The gel was then stained with Coomassie blue stain and imaged under white light. Bands from both gels were quantified by ImageJ and relative labeling content was calculated.

4.3 RESULTS AND DISCUSSION

4. 3. 1 Random mutagenesis screening of repressor mutants that can restore $AcrB_{P223G}$ activity

P223G mutation decreases AcrB oligomer stability and compromises efflux activity.[170] In this study, random mutagenesis and positive screening were used to identify mutations that recover AcrB activity caused by P223G mutation. This could potentially help us identify residues and

regions which are important for AcrB oligomerization and improve our understanding about the mechanism of the AcrAB-TolC pump.

We used LB agar plate containing erythromycin to screen for high activity colonies. The reason erythromycin was used as the screening substrate was that the difference of MIC between WT AcrB and $AcrB_{P223G}$ is significant. MIC of erythromycin of $AcrB_{P223G}$ was 8 μg/mL. The erythromycin concentrations in our screenings were 16 μg/mL and 32 μg/mL.

Here, we used two methods to introduce random mutations into the gene of $AcrB_{P223G}$, chemical mutagenesis and error-prone PCR. Using hydroxylamine hydrochloride chemical mutation, we were only able to identify two mutations, T199M and D256N, which showed higher antimicrobial resistance. Error-prone PCR was also used to achieve uniform spectrum of mutation with equivalent mutational rates. Two pairs of primers, RM1/RM2 and RM3/RM4 were designed, so that we could confine the random mutations to two periplasmic regions: residue 30 to 332 and residue 494 to 889. We focused our mutation studies in the periplasmic region, since it is likely that the periplasmic domain play a more important role in substrate binding, trimerization, and interacting with AcrA/TolC.

Two random mutagenesis methods were used to search for mutations that could restore $AcrB_{P223G}$ activity. Hydroxylamine hydrochloride treatment showed a low mutational rate. The reason was that the method is biased, as it would only result in transition from C to T and G to A.[173] In this way, the method itself limited the possibilities of some codon transition. Compare to chemical mutation, error-prone PCR has several advantages. First, the method largely reduced mutational bias. Second, mutational rate can be controlled by modification of buffer condition. Third, primer design could help us control the mutational sites. Despite all the advantages, due to the limitations of codon similarities, the method still wasn't completely random. With this design,

we identified nine mutants in AcrB periplasmic loop region with increased susceptibility to erythromycin, T199M, A209V, D256N, G257V, M662I, Q737L, D788K, P800S, and E810K.

To ensure that the increased activity did not come from bacterial strain evolution or mutations in the plasmid vector, all mutations were constructed by site-directed mutation, retransformed into BW25113Δ*acrB* strains. Five AcrAB-TolC pump substrates were tested to confirm the mutants drug susceptibilities, erythromycin, novobiocin, tetracycline, tetraphenylphosphonium, and rhodamine 6G. MICs of the nine mutants were shown in Table 4. 1. All of the mutants showed increased MIC comparing to $AcrB_{P223G}$ for all five AcrB substrates. Locations of these mutations were mapped onto AcrB structure. (Figure. 4.1)

Table 4.2 showed the conservations of these nine residues in AcrB and 13 homologues. Although overall the sequence of AcrB is highly conserved in Gram-negative bacteria, only three residues here were conserved. This is a reasonable observation since mutation of highly conserved sites might by itself cause function loss. Highly conserved residues are likely to be structural or functional related.

Table 4. 1 Conservation in inner membrane component of RND type efflux pump of amino acid residues who restored $AcrB_{P223G}$ activity.

Organism	Protein	199	209	256	257	662	737	788	800	810
E.coli	AcrB	T	A	D	G	M	Q	D	P	E
E.coli	AcrD	T	S	D	G	V	I	Y	S	G
E.coli	AcrF	T	V	D	G	V	A	I	F	Y
P. Aeruginosa	MexB	T	A	D	G	M	A	W	F	Y
H. pylori	AcrB	D	V	I	G	V	Q	E	R	P
Y. pestis	AcrB	T	I	D	G	V	A	W	F	Y
V. cholera	AcrB	T	E	N	G	V	A	W	F	Y
K. pneumonia	AcrB	T	A	D	G	V	A	W	F	Y
A.baumannii	AdeB	L	R	T	N	P	D	G	Q	R
A. tumefaciens	AmeB	T	Q	G	A	I	D	N	S	S
P. Putita	TtgB	T	A	D	G	M	Q	D	P	E
C. jejuni	CmeB	G	V	N	E	G	M	N	T	V
B. pseudomallei	AmrB	A	H	G	G	N	M	E	K	I
N. gonorrhoeae	MtrD	A	N	S	N	V	G	V	T	T

To figure out by which means these mutations increase $AcrB_{P223G}$ activity, we characterized the mutants from four aspects: 1) protein expression level; 2) oligomer stability; 3) AcrA/TolC interaction; 4) drug binding.

Table 4. 2 MIC (μg/mL) of BW25113Δ*acrB* harboring the corresponding plasmids. Drugs tested were Erythromycin (Ery), Novobiocin (Nov), Rhodamine 6G (R6G), Tetraphenylphosphonium (TPP), and Tetracycline (Tet).

plasmids	MIC (μg/mL)				
	Ery	Nov	Tet	TPP	R6G
pQE70-AcrB	128	320	2.56	320-640	>640
pQE70-AcrB$_{P223G}$	8	40-80	0.64	20-40	40-80
pQE70-AcrB$_{P223G/T199M}$	128	160	2.56	320-640	>640
pQE70-AcrB$_{P223G/A209V}$	64	80	1.28	40-80	>640
pQE70-AcrB$_{P223G/D256N}$	32-64	160-320	2.56	320	>640
pQE70-AcrB$_{P223G/G257V}$	64	160	2.56	80-160	>640
pQE70-AcrB$_{P223G/M662I}$	64-128	80	1.28	160	160
pQE70-AcrB$_{P223G/Q737L}$	64	160	2.56	160-320	>640
pQE70-AcrB$_{P223G/D788K}$	128	160	2.56	160-320	160-320
pQE70-AcrB$_{P223G/P800S}$	64	80	1.28	40-80	>640
pQE70-AcrB$_{P223G/E810K}$	128	160	2.56	160-320	>640

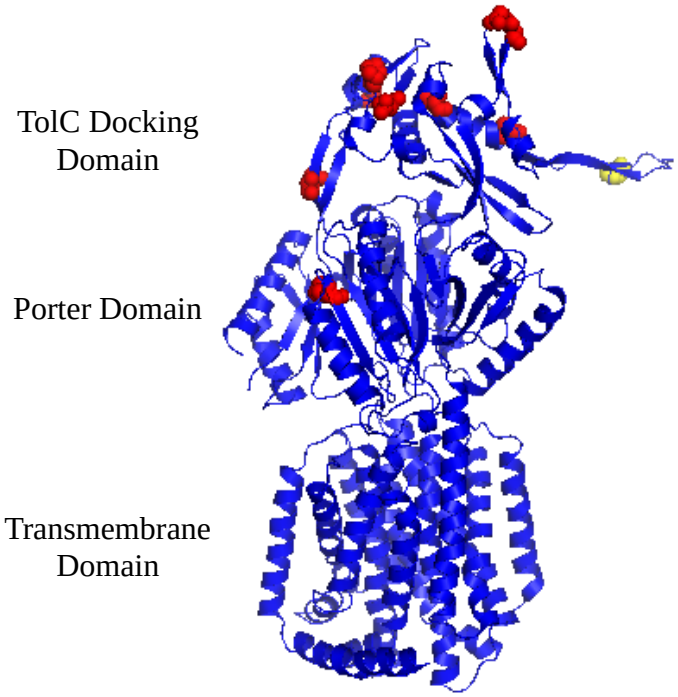

Figure 4. 1 Structure of AcrB (created using protein data bank file 1IWG by Pymol). Proline 223 at the protruding loop was marked in yellow. Mutations were marked in red.

4. 3. 2 Expression Levels Of $AcrB_{P223G}$ Mutants

To determine the effects of additional mutations on $AcrB_{P223G}$ expression level, we extracted membrane vesicles from BW25113Δacrb expressing AcrB mutants, and analyzed with quantitative western blot. (Figure. 4. 2)

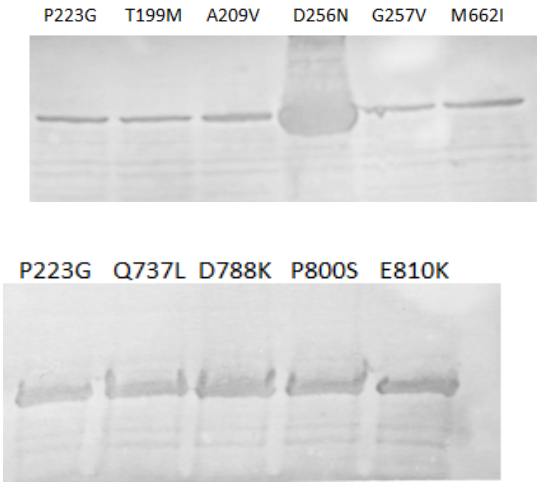

Figure 4.2 Western blot analysis of membrane vesicle extracted from BW25113ΔacrB expressing $AcrB_{P223G}$ and mutants.

Eight of the nine mutations, T199M, A209V, G257V, M662I, Q737L, D788K, P800S, E810K showed no significant difference in expression level when comparing to $AcrB_{P223G}$. Interestingly, one of the mutations, D256N drastically increased AcrB level, approximately by 20 fold. Also, as revealed in figure 4.3, cells expressing $AcrB_{P223G/D256N}$ grow much slower than $AcrB_{P223G}$. The growth rates of all other mutants were similar to that of WT AcrB and $AcrB_{P223G}$. Previous result has shown that the expression level of $AcrB_{P223G}$ is comparable with that of WT AcrB. However, the trimer stability of $AcrB_{P223G}$ in *vivo* was much lower than WT AcrB. Introduction of D256N increase the overall amount AcrB number, therefore more active form of AcrB trimer could have provided more efficient drug extrusion and increased pump activity. D256N is the only mutation that increased AcrB expression level drastically. Gene expression is related to several global cellular parameters, such as gene and plasmid copy number, abundance of tRNA and ribosomes, and growth rate.[174] Our group has shown that when expressing in a low copy number plasmid pBAD, AcrB expression level could be raised by three fold. In this case, we speculate the growth

differences between mutants are due to the tRNA abundance. The relative content of tRNA of amino acid Asp is twice as high as that of Asn. The real-time codon frequency of "GAT" (Asp) is three times higher than "AAT" (Asn).[175] The lower abundance of tRNA may contribute to the lower growth rate of $AcrB_{P223G/D256N}$ and higher expression level. This observation has also been verified by Rand et al. using medium with iron, glucose, and nitrogen limitations.[176] The up-regulation of AcrB is inversely proportional to cell growth rate. Additionally, the feedback mechanism induced cell's self-defense system could also stimulate AcrB expression and promotes higher drug resistance.[174]

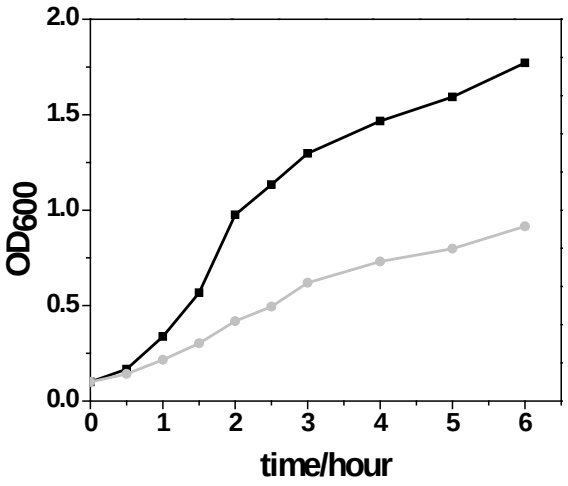

Figure 4.3 Cell density OD_{600} of $AcrB_{P223G}$ (black) and $AcrB_{P223G/D256N}$ (Grey) in five hours. The start culture cell density for both strains was 0.100.

4. 3. 3 BN-PAGE Analysis Of AcrB Mutant Oligomerization States

To evaluate the impacts of the mutations on AcrB oliogomerization states, we used BN-PAGE to study AcrB mutant trimer stability. BN-PAGE is a widely used technique in characterizing protein complex from biological membrane, homogenates of cell and tissue, and studying protein-protein interaction. The technique has been used extensively in studies of MDR

transporter oligomerization.[177, 178] Freshly purified AcrB mutants were separated by BN-PAGE. (Figure 4. 4 A & B) Protein band intensities in the gel were quantified using ImageJ and trimer percentage was calculated using the following equation:

$$\text{Trimer\%} = = \frac{I_T}{I_T + I_M}$$

I_T = intensity of trimer band, I_M = intensity of monomer band

Both gels used $AcrB_{P223G}$ as a control. After the calculation, trimer percentage of all mutants were normalized by that of $AcrB_{P223G}$ and showed in Figure 4. 4C.

A)

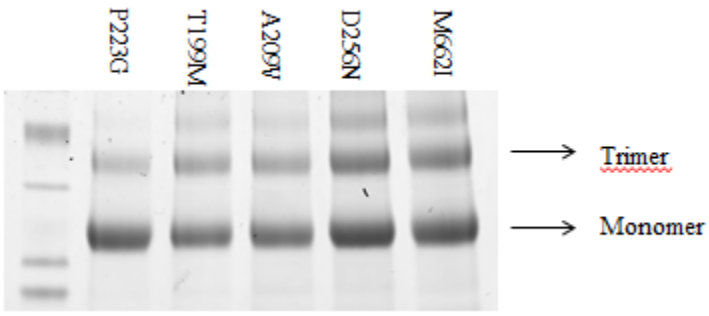

B)

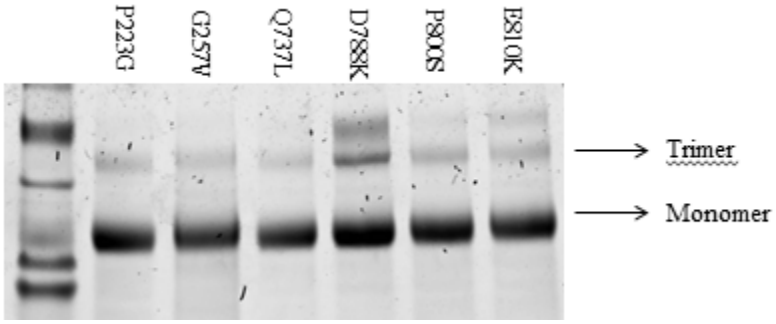

C)

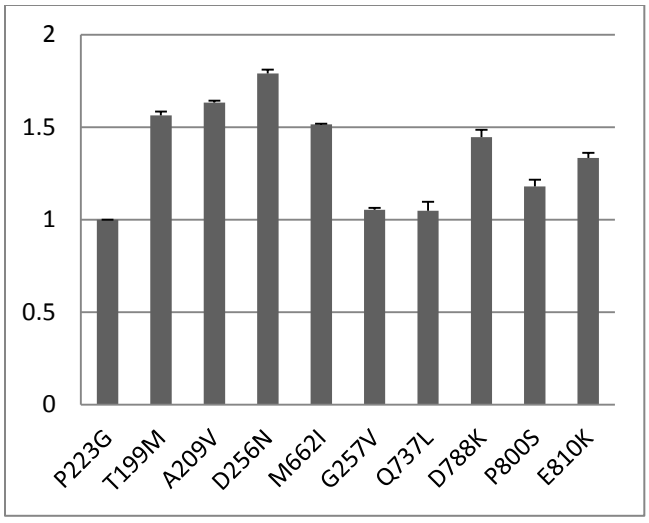

Figure 4. 4 A) & B) BN-PAGE analysis of purified AcrB constructs. Positions of monomer and trimer bands were marked. $AcrB_{P223G}$ was loaded into both gels as control for quantification. C) Trimer percentage of mutants normalized by trimer percentage of $AcrB_{P223G}$. The experiment was repeated three times, average value and standard deviation were shown.

The majority of $AcrB_{P223G}$ existed as monomer which makes it incompetent to perform AcrB function. In five of the mutants, $AcrB_{P223G/T199M}$, $AcrB_{P223G/A209V}$, $AcrB_{P223G/D256N}$, $AcrB_{P223G/M662I}$, $AcrB_{P223G/D788K}$ showed approximately 1.5 to 2 fold increase in trimer percentage. The trimer percentage of $AcrB_{P223G/E810K}$ was increased by 1.3 fold.

4. 3. 4 *In Vivo* AcrA-AcrB Interaction

The majority of mutations occurred at the TolC docking domain of AcrB. To verify if these mutations have any impact on AcrA/TolC-AcrB interaction, DSP crosslinking and copurification were performed. Images of Western blot membrane and gel after Coomassie blue staining were showed in Figure 4. 5. Coomassie blue gels were used to quantify AcrB. Ratio of intensity of AcrA or TolC bands to AcrB bands were compared between WT AcrB, $AcrB_{P223G}$, and mutants.

In each case, BW25113Δ*acrB* transformed with pQE70 vector were used as a negative control to confirm that the signal was not from non-specific interaction of AcrA and TolC with Ni-NTA resin. No signal could be visualized for negative control, suggesting AcrA and TolC could not retain on Ni-NTA resin without cross-linked with AcrB. $AcrB_{P223G/T199M}$ and $AcrB_{P223G/G257V,}$ and $AcrB_{P223G/P800S}$ showed higher AcrA signal than $AcrB_{P223G}$. It is possible that these mutations improved AcrA/AcrB interaction, which could help stabilize the AcrAB-TolC tripartite complex.

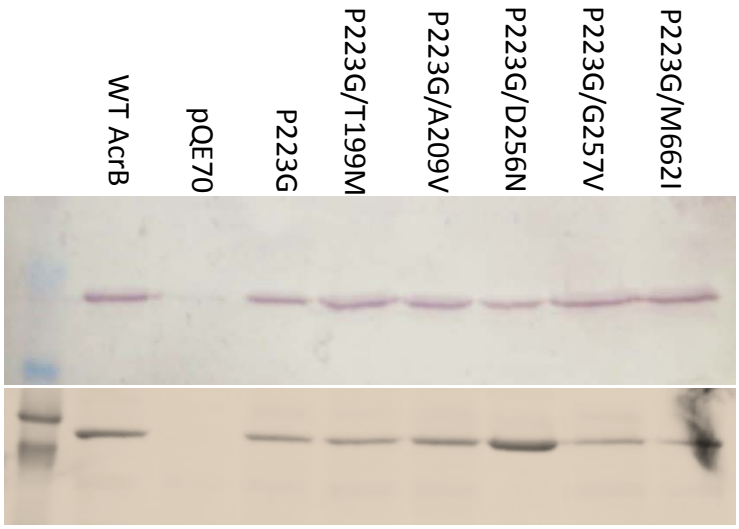

A)

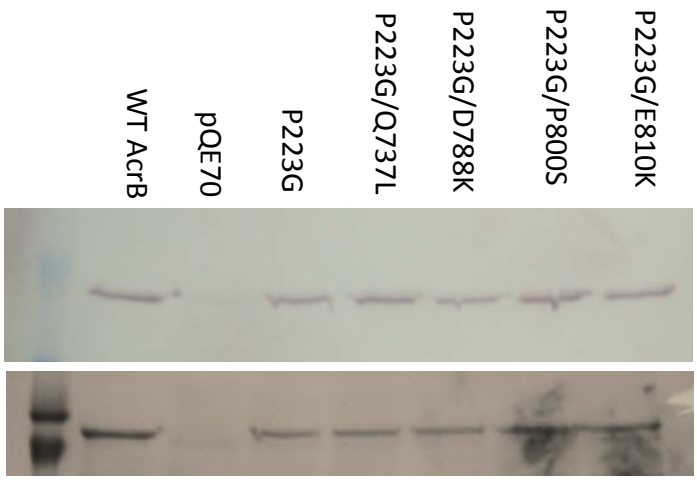

B)

Figure 4.5 A) Top: Western blot analysis of co-purified AcrA after DSP crosslinking from BW25113Δ*acrB* expressing WT AcrB, pQE70, $AcrB_{P223G}$, $AcrB_{P223G/T199M}$, $AcrB_{P223G/A209V}$, $AcrB_{P223G/D256N}$, $AcrB_{P223G/G257V}$, and $AcrB_{P223G/M662I}$. Bottom: Coomassie blue staining of co-purification samples after DSP crosslinking. Each lane is in accordance to AcrA western blot membrane. B) Top: Western blot analysis of co-purified AcrA after DSP crosslinking from BW25113Δ*acrB* expressing WT AcrB, pQE70, $AcrB_{P223G}$, $AcrB_{P223G/Q737L}$, $AcrB_{P223G/D788K}$, $AcrB_{P223G/P800S}$, and $AcrB_{P223G/E810K}$. Bottom: Coomassie blue staining of co-purification samples after DSP crosslinking. Each lane is in accordance to AcrA western blot membrane.

To examine if these mutations affect AcrB interaction with other components in the pump, DSP crosslinking was used to study the interaction between AcrA and AcrB *in vivo*. First, much less AcrA was copurified with $AcrB_{\Delta loop}$ than with WT AcrB (data not shown), suggesting AcrA prefers interacting with trimeric AcrB. However, there was no difference between the level of AcrA copurified with WT AcrB and $AcrB_{P223G}$. This, along with MIC test, further proved that instead of existing as monomer *in vivo*, $AcrB_{P223G}$ existed as a loose trimer which is partially active. Four of the mutants, T199M, A209V, G257V, and P800S, lead to higher AcrA co-purification than $AcrB_{P223G}$. AcrA existed as an oligomer *in vivo*.[105] These results indicate that oligomeric AcrA has a higher affinity towards these mutants. The interaction with AcrA may help strengthen AcrB trimer.

4. Bodipy-FL-maleimide labeling of $AcrB_{P223G/M662I}$

Of all mutations, $AcrB_{P223G/M662I}$ is especially interesting. This is the only mutant that resides in AcrB porter domain. It is unlikely that this mutation could have any effect on AcrA or TolC

interaction. Studies have shown that conversion of Phe664 and Phe666 to alanine drastically decreased MICs.[66] Nikaido and coworkers have used Bodipy-FL-maleimide labeling method to prove that Phe664 and Phe666 were at the substrate pathway.[61] Therefore, we speculate that Met 662 was involved in substrate binding. To prove the hypothesis, we introduced a cysteine as Met 662, and did Bodipy-FL-maleimide labeling. (Figure 4. 6) There were two cysteines in WT AcrB, none of which is in substrate binding pocket. Thus, WT AcrB was used as negative control, while $AcrB_{F664C}$ was used as positive control. $AcrB_{M662C}$ could be labeled by Bodipy-FL-maleimid, suggesting Met662 is accessible to AcrB substrate. It is likely that Met662 is in the drug extrusion pathway. However, $AcrB_{M662C}$ stained less strongly than $AcrB_{F664C}$, which may indicate substrate interaction at this site is much weaker.

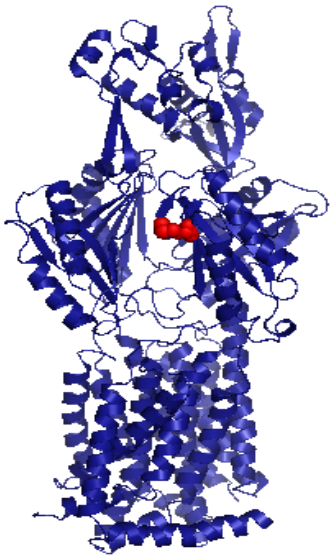

A)

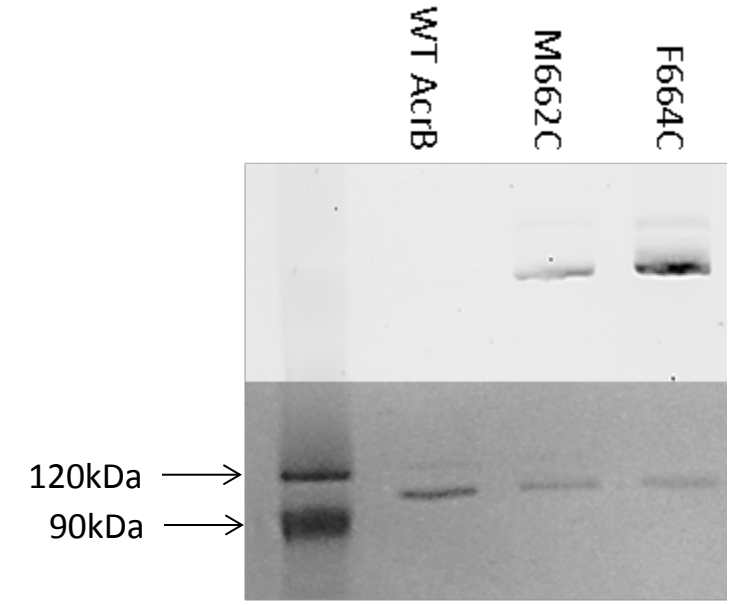

B)

Figure 4. 6 A) Structure of AcrB from a different angle (created using protein data bank file 1IWG). Met 662 was highlighted in red. B) Top: covalent label of WT AcrB, $AcrB_{M662C}$, and $AcrB_{F664C}$ by 6 μM Bodipy-FL-maleimide. Bottom: Coomassie blue staining of the corresponding gel after Bodiphy-FL-maleimide labeling.

Only one mutation, M662I, happened at AcrB substrate binding pocket. As we know, the drug binding site of AcrB is highly phenylalanine rich.[66] Drugs mainly interact with the protein through hydrophobic interaction. Conversion from Met to Ile increased the hydrophobicity, which may increase the mutants-ligand affinity.[179] Also, AcrB is more stable in its trimeric states with this mutation, suggesting that interaction with substrates could help hold the oligomer together. This ligand-induced oligomerization has been observed in several receptor proteins.[180, 181]

Three residues were identified at the inter-subunit interface in an AcrB trimer (Table 4). Ala209, Gln737, Glu810 and the residues within 6Å of each amino acid in the neighboring chain were

marked in Figure 6. Residues close to Ala 209 and Gln 737 were both hydrophobic. Thus, mutations to valine and leucine increase the hydrophobic interaction between chains and strengthen the trimer. Percentage interface assecible surface area (ASA) of Glu 810 is much lower than the other two residues. The mutation might have a minor impact on the association between chains of $AcrB_{E810K}$. However, Glu 810 is exposed, which makes it possible to be related to AcrA or TolC interaction.

Table 4.3 Interface property of Ala 209, Glu 737, and Gln 810. Interface between each AcrB subunit calculated using online server PROTORP

Residue Number	Residue Name	Interface ASA	% Interface ASA	Segment
209	ALA	31.24	1.15	5
737	GLN	43.94	1.61	17
810	GLU	9.53	0.35	20

A) 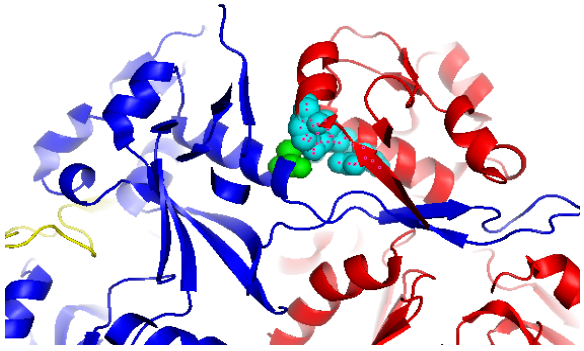

B)

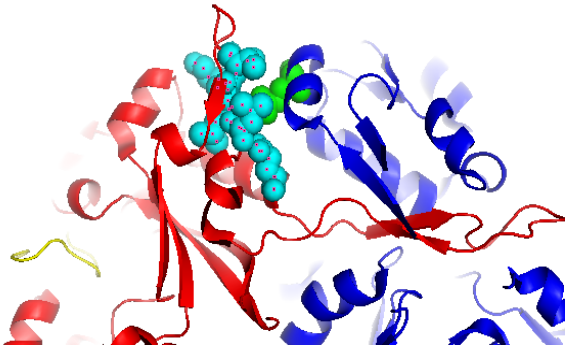

C)

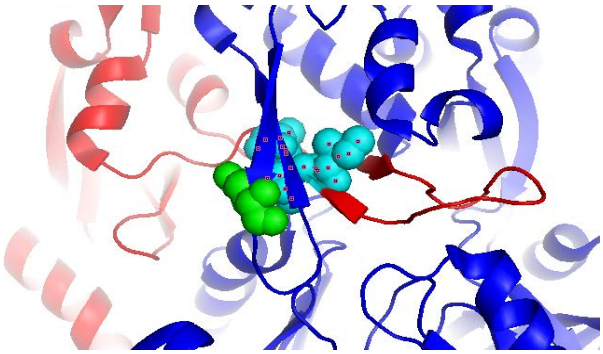

Figure 4. 7 Zoom in view of neighboring residues of amino acids Ala 209 (A), Gln 737 (B) and Glu 810 (C) at interface between AcrB monomers. The residues at the interface were shown in green, neighboring residues were marked in cyan. The three chains in AcrB trimer were marked in red, blue and yellow, respectively.

4. 4 CONCLUSION

AcrB and its homologous are the inner membrane components of the major multidrug transporter in Gram-negative bacteria. It assembles with AcrA and TolC to form a tripartite pump system. AcrB recognizes and exports a broad range of functionally and structurally unrelated substrates, and therefore decreases the drug susceptibility of the bacteria. AcrB harvests the proton motive force to drive the conformational change required by function and determines the substrate specificity of the pump. AcrB exists and operates as a homotrimer *in vivo*. Previous mutational studies showed when a Pro (P223) at the inter-subunit interface was replaced by a Gly, the trimer

stability was reduced, leading to drastically compromised protein activity. Using hydroxylamine treatment and error prone PCR, random mutagenesis was performed and nine mutants were identified that restored the activity loss in $AcrB_{P223G}$. The mechanism of activity restoration was analyzed based on current understanding of AcrB function. Nine mutants were identified with higher efflux activity. The mechanisms of restoration were evaluated and summarized from four aspects (Table 4.4). We found that while some mutations recover the function of $AcrB_{P223G}$ through directly increase the cellular abundance of AcrB trimer, others work indirectly through affecting substrate binding or AcrA-AcrB interaction.

Table 4.4 Summary of effects of mutations on protein expression, trimer stability, AcrA interaction, and substrate binding.

Mutation	T199M	A209V	D256N	G257V	M662I	Q737L	D788K	P800S	E810K
Expression level			✓						
Trimer percentage	✓	✓	✓		✓		✓	✓	✓
AcrA interaction	✓			✓				✓	
Substrate affinity					✓				

CHAPTER V. HETEROLOGOUS EXPRESSION OF *H. PYLORI* ACRB IN *E. COLI*

5. 1 INTRODUCTION

In 1982, *Helicobacter pylori* (*H. pylori*) was first identified from the stomach of patients with gastritis and peptic ulceration in Western Australia. It is a unipolar, spiral-shaped gram-negative bacterium, about 0.5-1.0 μm in width and 2.5-4.0 μm in length. At least 50% of the world's population is infected by H. pylori.[182] Infection by *H. pylori* causea chronic gastric inflammation, which slowly develops into peptic ulcer and duodenal ulcer.[183] Recently, it has been established that infection with *H. pylori* is associated with atrophic gastritis, leading to a higher occurrence of gastric cancer.[184]

Routine *H. pylori* diagnosis can be done by testing blood antibody, stool antigen, carbon urea breath, and endoscopy.[185-187] These tests do not need microbial culture. Because *H. pylori* culture is time consuming, labor intensive and expensive, it is not practical to be used as a diagnosis technique. However, it is sometimes required to culture the bacterium in research labs and for epidemiologic purpose. For instance, antibiotic susceptibility, bacterium metabolism, growth factor studies have to be performed in plate or broth culture. The growth of *H. pylori* requires a micro-aerobic environment with high humidity.[188] Normally, *H. pylori* is incubated in 30-37ºC CO_2-rich shaker. Subtle change in environment, such as addition of antibiotics, glucose and lipid, nutritional deficiency, pH change, abnormal temperature may induce the formation of coccoid.[189] Coccoid is a viable, metabolically active but non-cultivable form of *H. pylori*. To prevent coccoid growth, numerous efforts have been made to optimize *H. pylori* culture. It has been shown when particular supplements were added to medium, *H. pylori* growth can be improved and accelerated.[190] The supplements can be whole animal whole blood, serum, corn starch, egg yolk emulsion, and charcoal. Nevertheless, growth of *H. pylori* takes 3-5 days with the optimum

condition, which is much longer comparing to the growth of other bacterium species. Moreover, cultivation of *H. pylori* increases the risk of exposing the researcher to a pathogenic organism. Therefore, the alternative path involving heterologous expression has been widely employed in studies of *H. pylori* proteins.[191, 192]

Long before the discovery of *H. pylori*, H_2-receptor antagnoists has been successfully used to cure patients with ulcer gastritis.[193] Later, acid pump inhibitor has been used in clinical treatment.[194] Both drugs decrease gastric acid secretion of parietal cells in the stomach. However, due to the spread of multidrug resistance, it is becoming more and more difficult to eradicate *H. pylori* infection. Since 1990s, several antibiotics have been prescribed routinely for gastric disease treatment. Today, tetracycline, metronidazole, amoxicillin, clarithromycin, bismuth, and H^+/K^+-ATPase inhibitors are commonly used. Two or three antimicrobials are generally needed to completely eradicate the bacterium.[195] Unfortunately, an effective approach to cure *H. pylori* in all patients has not been developed. According to geographical distribution, drug resistance is usually caused by variable mechanisms.

Triple antimicrobial therapy (proton pump inhibitor, amoxicillin, and clarithromycin) are recommended for clinical eradication of *H. pylori* infection in many countries. When the cocktail therapy was first introduced in 1990s, the successful rate is over 80%.[196] However, in a recent summary, only 18% of the hospital reported over the 85% successful *H. pylori* eradication rate due to multidrug resistance. Several factors contributed to antibiotic resistance in *H. pylori*, including point mutation, enzyme inactivation, and drug efflux. Using RT-PCR, site-directed mutagenesis study, and efflux pump inhibitor, the link between RND efflux pump system and MDR in *H. pylori* is emerging.[197] However, so far, no other research group has explored the role of the AcrA-AcrB-TolC efflux system in *H. pylori*. Due to the restrictions in the growth

conditions, *H. pylori* is much more difficult to culture than *E. coli*. Hence, I tried to heterologously express *H. pylori* AcrB in *E. coli* system using recombinant DNA techniques. Different growth conditions and different vectors were evaluated.

5.2 MATERIALS AND METHODS

Construction of plasmids

The genes encoding *H. pylori* AcrB and AcrA were amplified from *Helicobacter pylori* 26695 genomic DNA (ATCC, VA). The primers used for the PCR reactions were listed in table 5.1.

Table 5.1 Primers used for the amplification of AcrB and AcrA from *H. pylori*

Primers	Sequence
HPacrBFW	5'-ATTCCATATGTATAAAACAGCGATTAATCGTCC-3'
HPacrBRV	5'-AACCCTCGAGAGTTTTTTGGTTTTGATAAAACC-3'
HPacrAFW	5'-AGCATATGATACGAAAAATTTTAATAG-3'
HPacrARV	5'-TGAAGCTTATTTCGTTTGGATAAACC-3'

After amplification, PCR product containing *H. pylori* AcrB gene was digested using NdeI and XhoI. Product containing *H. pylori* AcrA gene was treated with NdeI and HindIII. Digestion products were separated by agarose gel electrophoresis and extracted from gel extraction kit. Purified DNA fragments were inserted into pET-22b (New England Biolabs, MA) and pBAD-33 vector (Addgene, MA).

Preparation of competent cell

Three kinds of competent cells were prepared.[198] For *E. coli* BW25113Δ*acrB* preparation, first

E.coli BW25113ΔacrB was streaked on a LB plate containing 50 µg/mL kanamycin, and incubate at 37ºC overnight. A single colony was used to inoculate 3 mL LB medium and grow at 37ºC overnight. A 200 mL LB media culture inoculated with 2 mL overnight BW25113Δ*acrB* culture was shaken vigorously till OD600 gets to 0.4. No selection marker was added at this step. Cells was cooled and centrifuged at 3,000 rpm for 15 mins at 4ºC. The pellets were resuspended in 12 mL of cold 0.1 M $CaCl_2$, and incubate on ice for 45 mins. Cells were collected by centrifuge at 3,000 rpm for 15 mins. Supernatant was discarded and cells were resuspended in 3.2 mL cold 0.1M $CaCl_2$ containing 15% glycerol. Competent cells were aliquoted into cold Ependorff tubes, frozen in liquid nitrogen, and stored at -80ºC. *E. coli* BW25113Δ*acrB* harboring pBAD33-HPacrB or pET22-HPacrB competent cells were prepared the same way with addition of chloramphenicol and ampicillin to the LB agar plate, respectively.

Transformation, co-transformation and colony screening

1 µL 50 ng/µL plasmids was added to 60 µL competent cell, and incubate on ice for 30 mins. The plasmid-cell mixture was heat-shocked at 42ºC for 1 min, followed by immediate incubation on ice for 5 mins. 1 mL LB medium was added to the cell. The cells were incubated at 37ºC for 45 mins, and plated on LB agar plates containing antibiotics.

For co-transformation, pBAD33-HPacrB/pET22-HPacrA and pBAD33-HPacrA/pET22-HPacrB were each transformation into BW25113Δ*acrB* competent cells, respectively. Ampicillin, kanamycin and chloramphenicol were all added in the LB plates. In addition, 8 µg/mL novobiocin or erythromycin was added to the plates. The colonies that are able to grow in substrate containing plates were further analyzed.

Drug susceptibility assay

AcrB activity was monitored using a drug susceptibility assay as described in chapter 2.

Western blot analysis of AcrB expression in active colony

Western blot analysis was performed as described in chapter 2.

Plasmid loss

Active colonies were first cultured in LB media containing ampicillin, kanamycin and chloramphenicol overnight. 5 µL of overnight culture were used to inoculate 5 mL LB medium containing only kanamycin. The cultures were shaken at 37°C for 24-96 hours continuously. 1 mL culture were taken out at 24, 36, 48, 72, and 96 hrs, and diluted 10,000 times. 10 µL cultures were plated on LB agar plate with kanamycin and incubated overnight. 10 colonies were picked from each plate and cultured in LB medium with kanamycin. After the growth, each culture of the colonies was diluted with LB medium containing ampicillin and chloramphenicol. Colonies that failed to grow in the presence of ampicillin and chloramphenicol were studied.

5. 3 RESULTS AND DISCUSSION

5.3.1 Sequence Alignment Of AcrB From *H. pylori* and *E. coli*

AcrB is highly conserved in Gram-negative bacteria. Previously, Srikumar and co-workers showed when expressing in *E. coli* strain, MexB from *Pseudomonas aeruginosa* increased drug resistance of *E. coli* AcrB deficient strain.[199] This result indicates that AcrB from a different organism expresses and functions in *E. coli*. I used online server T-coffee to align amino acid sequences of AcrB from *H. pylori* and *E. coli*. The results demonstrated *H. pylori* AcrB was 86%

similar to *E. coli* AcrB (Figure 5. 1). The high similarity score offered potential for heterologous expression of *H. pylori* AcrB in *E. coli*.

```
Ecoli           MPNFFIDRPIFAWVIAIIIMLAGGLAILKLPVAQYPTIAPPAVTISASYP
Hpylori         MYKTAINRPITTLMFALAIVFFGVMGFKKLSVALFPKIDLPTVVVTTTYP
                * :  *:*** : ::*: *:: * :.: **.** :*.*  *:*.::::**

Ecoli           GADAKTVQDTVTQVIEQNMNGIDNLMYMSSNSDSTGTVQITLTFESGTDA
H
pylori         GASAEIIESKVTDKIEEAVMGIDGIKKVTSTSSKNVSI-VVIEFELEKPN
                **.*: ::..**: **: : ***.:  ::*.*... :: :.: **  .

Ecoli           DIAQVQVQNKLQLAMPLLPQEVQQQGVSVEKSSSSFLMVVGVINTDGTMT
Hpylori         EEALNDVMNKISSV-RF--DDSNIKKPSINKFDTDSQAIISLFVSSSSVP
                : *  :* **:. .  :  :: : :  *::* .:.   ::.:: :..::.

Ecoli           QEDISDYVAANMKDAISRTSGVGDVQLFGS-QYAMRIWMNPNELNKFQLT
Hpylori         ATTLNDYAKNTIKPMLQKINGVGGVQLNGFRERQIRIYADPTLMNKYNLT
                   :.**.  .:*  :.: .***.*** *  :  :**: :*. :**::**

Ecoli           PVDVITAIKAQNAQVAAGQLGGTPPVKGQQLNASIIAQTRLTSTEEFGKI
Hpylori         YADLFSTLKAENVEIDGGRIVN------SQRELSILINANSYSVADVEKI
                 .*:::::**:*.:: .*:: .      .* : **: ::.  *. :. **

Ecoli           LLKVNQDGSRVLLRDVAKIELGGENYDIIAEFNGQPASGLGIKLATGANA
Hpylori         -----QVGNHVRLGDIAKIEIGLEEDNTFASFKDKPGVILEIQKIAGANE
                     * *.:* * *:****:* *: : :*.*:.:*.  * *:  :***

Ecoli           LDTAAAIRAELAKMEPFFPSGLKIVYPYDTTPFVKISIHEVVKTLVEAII
Hpylori         IEIVDRVYEALKRIQAISPN-YEIRPFLDTTSYIRTSIEDVKFDLILGAI
                :: .  :   * :::.: *.  :*    ***.::: **.:*   *: . *

Ecoli           LVFLVMYLFLQNFRATLIPTIAVPVVLLGTFAVLAAFGFSINTLTMFGMV
Hpylori         LAVLVVFAFLRNGTITLVSAISIPISIMGTFALIQWMGFSLNMLTMVALT
                *..**:: **:*   **:.:*::*: ::****::  :***:* ***..:.

Ecoli           LAIGLLVDDAIVVVENVERVMAEEGLPPKEATRKSMGQIQGALVGIAMVL
Hpylori         LAIGIIIDDAIVVIENIHKKL-EMGMSKRKASYEGVREIGFALVAISAML
                ****:::******:**:.: : * *:. ::*: :.: :*  ***.*: :*

Ecoli           SAVFVPMAFFGGSTGAIYRQFSITIVSAMALSVLVALILTPALCATMLKP
Hpylori         LSVFVPIGNMKGIIGRFFQSFGITVALAIALSYVVVVTIIPMVSSVVVNP
                 :****:. : *  * ::: .*.**:. *:*** :*.: : * :.:.:::*

Ecoli           IAKGDHGEGKKGFFGWFNRMFEKSTHHYTDSVGGILRSTGRYLVLYLIIV
Hpylori         R--------HSRFYVWSEPFFKALESRYTKLLQWVLNHKLIIFIAVVLVF
                         :. *: * : :*:    :**. :  :*. .   ::  :::.

Ecoli           VGMAYLFVRLPSSFLPDEDQGVFMTMVQLPAGATQE-RTQKVLNEVTHYY
Hpylori         VGSLFVASKLGMEFMLKEDRGRFLVWLKAKPGVSIDYMTQKS--KIF---
                **  ::  :*  .*: .**:* *:. ::  .*.: :  ***   ::

Ecoli           LTKEKNNVESVFAVNGFGFAGRGQNT--GIAFVSLKDWADRPGEENKVEA
Hpylori         QKAIEKHAEVEFTTLQVGY-GTTQNPFRAKIFVQLKPLKERKKEHQLGQF
                 .  :::.*  *:.  .*: *  **.  .  **.**   :*  *.:  :
```

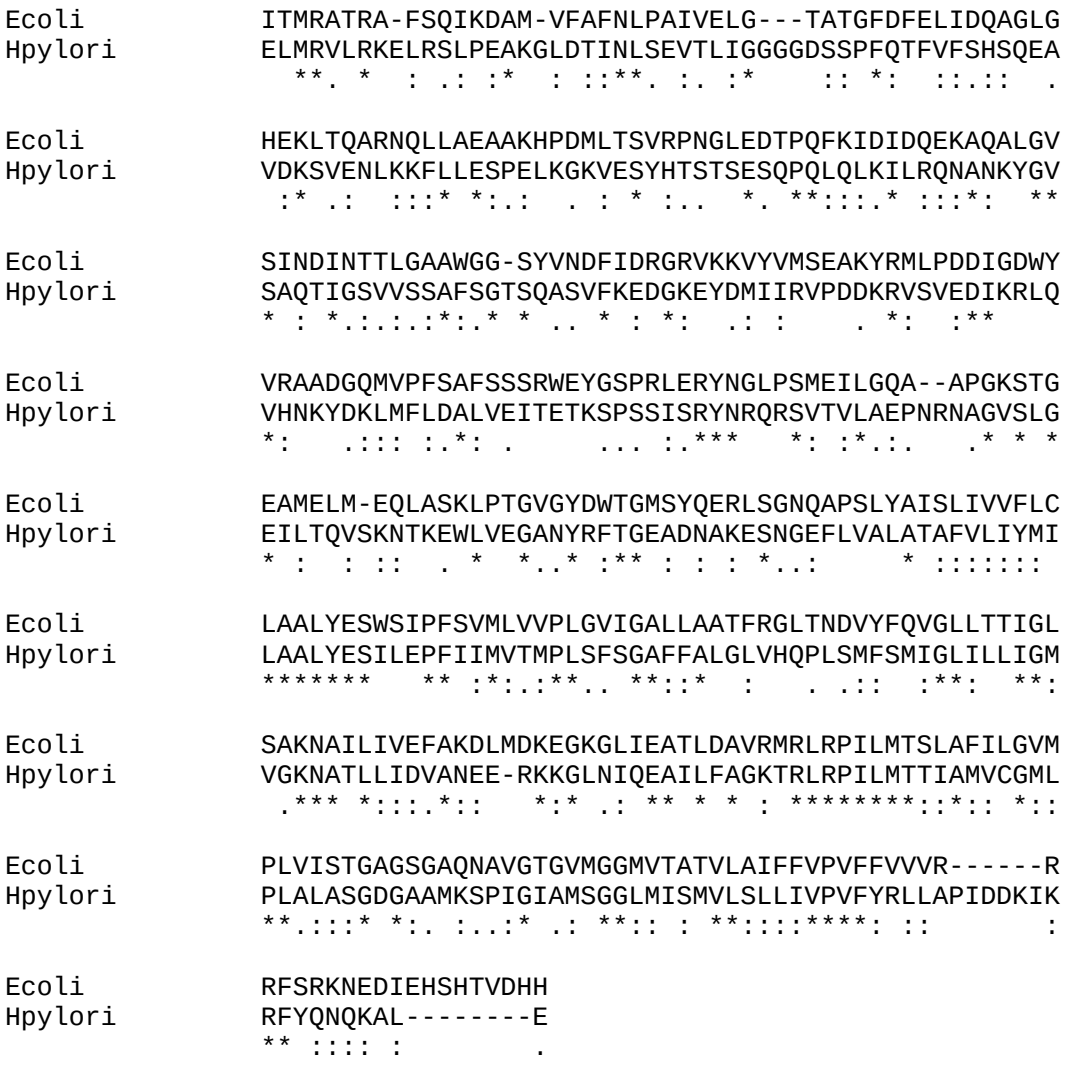

Figure 5.1 Sequence alignment of AcrB from *E.coli* and *H. pylori* using online alignment server T-COFFEE

5.3.2pMal-HP AcrB And pBAD33-HP Did Not Confer Drug Resistance To BW25113Δ*acrB*

Drug susceptibility test was conducted using BW25113Δ*acrB* strains transformed with pMal-HP acrB or pBAD33-HP acrB (Table 6.2). None of the strains showed increased activity for any drug tested comparing to negative control. This result indicated that either *H. pylori* AcrB cannot be expressed in *E. coli* or cannot functionally replace *E. coli* AcrB. Two vectors were tested here.

The main difference between pMal-pIII vector and pBAD 33 vector is the copy number. pMal-pIII is a high copy number vector generally leading to high protein expression yield. But some proteins, especially membrane proteins, are reported to be toxic when expressed at high level. An alternative low copy number vector pBAD33 was also used. However, neither high nor low copy number vectors yielded any colonies with increased drug resistance when transformed into BW25113Δ*acrB*.

5. 3. 3 Co-transformation Of *H. pylori* AcrB And AcrA Into BW25113ΔacrB Strain

The efflux pump required all three components, AcrB, AcrA and TolC, to properly assemble to be functional. AcrB from *H. pylori* might not be compatible with *E. coli* AcrA. The sequence similarity of *E. coli* AcrA and *H. pylori* AcrA was much lower than that of AcrB (Figure 5.2). I co-transformed both AcrB and AcrA from *H. pylori* into BW25113Δ*acrB*. This time I directly plated transformed cells on LB agar plates containing kanamycin, ampicillin, chloramphenicol and specific antibiotic substrates. Any colonies that could grow on these plates would harbor the high drug tolerance. Two colonies, HPA/B-1 and HPA/B-2, were able to grow on LB agar plates containing novobiocin after two days' incubation at 37ºC. These were the only two colonies that were ever obtained to grow on agar plates that contained both substrate and antibiotics. No other transformation effort was successful. I characterized these two colonies to determine the mechanism of increased drug resistance.

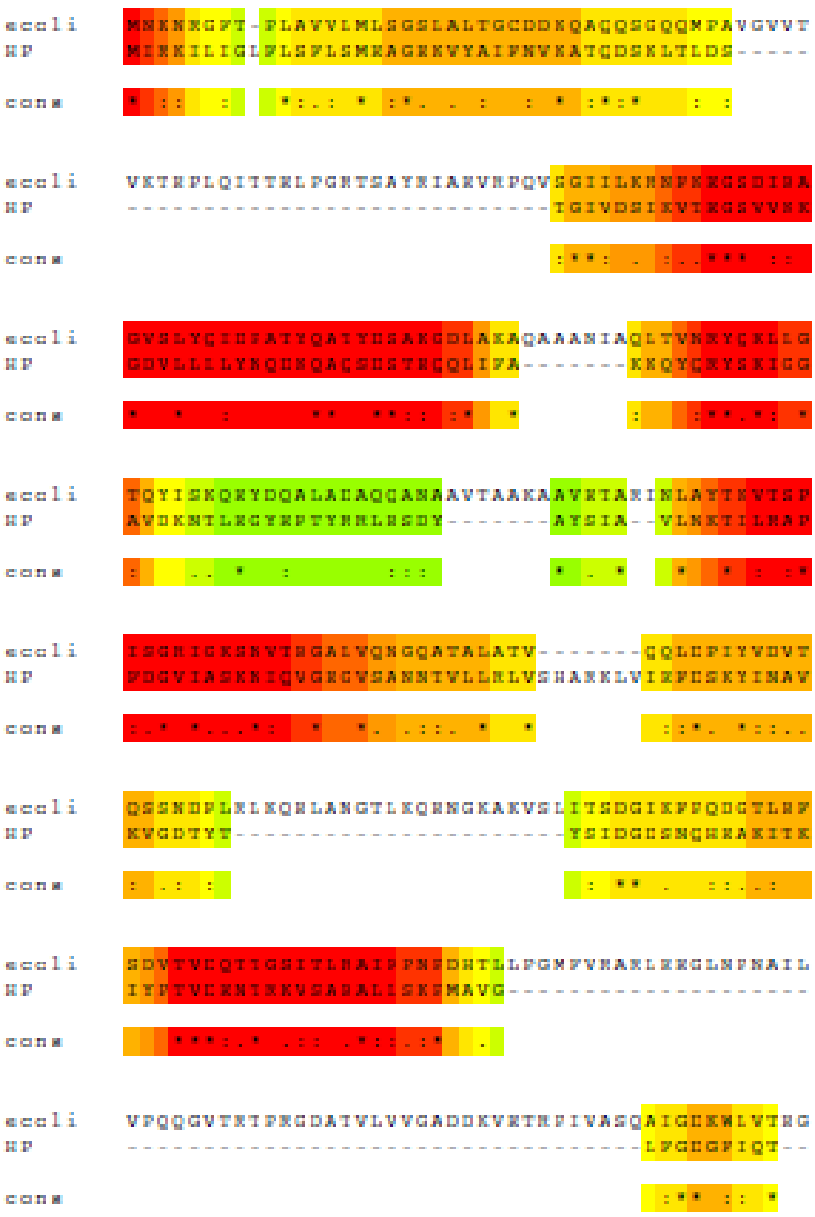

Figure 5.2 Sequence alignment of AcrA from *H. pylori* (HP) and *E. coli* (Ecoli) with online server T-COFFEE.

5. 3. 4 Restriction Enzyme Treatment Of HP A/B-1 And HP A/B-2

First, to clarify whether the resistance was from *H. pylori* AcrB expression, I used restriction enzyme digestion to verify the plasmids and Western blot analysis to examine AcrB expression.

Two vectors with ampicillin and chloramphenicol resistance gene, respectively, were used in this study. Thus, the plasmids extracted were a mixture of pBAD-HPacrB and pET22b-HPacrA Enzymatic digestion using NdeI/XhoI and NdeI/HindIII were used to verify the plasmids (Figure 5. 3).

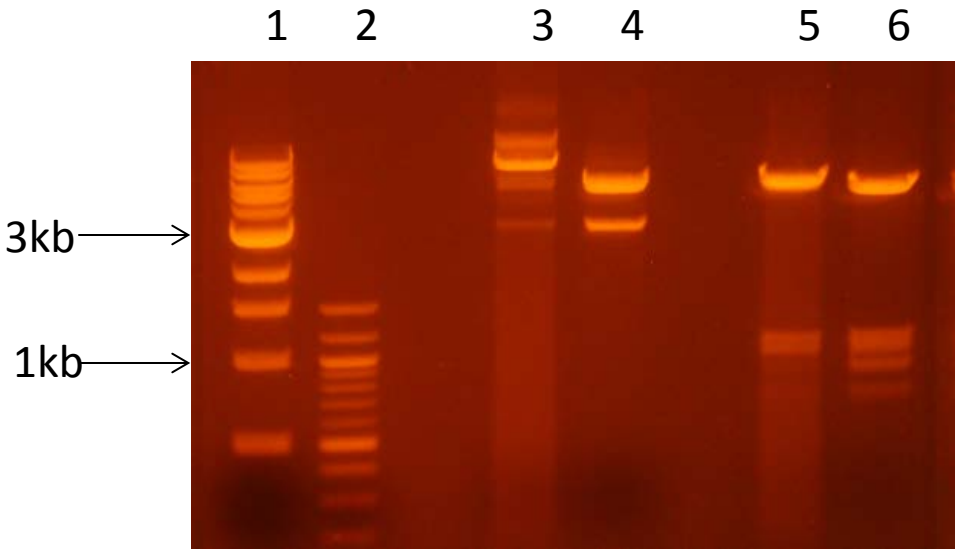

Figure 5.3 Restriction enzyme digestion of plasmids extracted from HPA/B-1 and HPA/B-2. From left to right: 1 kb protein ladder, 100 bp protein ladder (New England Biolabs, MA), HPA/B-1 digested with NdeI/XhoI, HPA/B-2 digested with NdeI/XhoI, HPA/B-1 digested with NdeI/HindIII, and HPA/B-2 digested with NdeI/HindIII. The positions of 3 kb and 1 kb bands were marked, respectively.

In both colonies, a band of approximately 3kb showed up when treated with NdeI/XhoI, which was in accordance to the size of *H. pylori* AcrB. When treating with NdeI/HindIII, the DNA was excised mainly into two fragments of approximately 5 kb and 1.2 kb in size. The 5 kb band was consistent with the vector size. The band around 1.2 kb was consistant with the size of *H. pylori* acrA gene. The difference in the intensity of the band was due to the efficacy of the treatment.

The restriction enzyme digestion results indicated that plasmids of *H.pylori* acrB and acrA did exist in both colonies.

5. 3. 5 Western Blot Analysis Of AcrB Expression In HPA/B-1 And HPA/B-2

Next, Western blot was used to examine the protein expression level of *H. pylori* AcrB in the membrane vesicle. Two kinds of *E. coli* AcrB antibodies were used, antibody one was raised against full sequence *E. coli* AcrB and antibody two recognizes the last 14 amino acids of *E. coli* AcrB. It was first used by Nikaido et al. and displayed a strong affinity to *E. coli* AcrB. According to the sequence alignment result, the 1032-1045th amino acids of *E. coli* and *H. pylori* AcrB are quite different (Figure 6.1). As a result, the peptide antibody was not expected to recognize *H. pylori* AcrB. Membrane vesicles from both colonies were extracted and immunoblotted (Figure 6.4). BW25113*ΔacrB* expressing *E. coli* AcrB, pMal-pIII HPacrB, pBAD33 HPacrB, both pET22b HPacrA and pBAD33 HPacrB (inactive colonies) were used as controls.

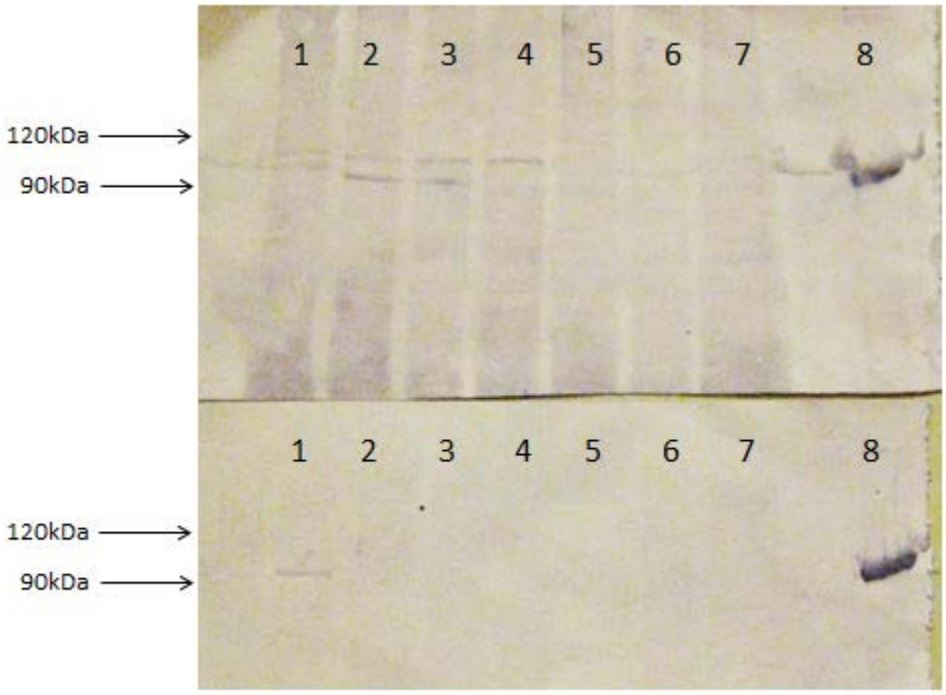

Figure 5. 4 Western blot analysis of membrane extract from different AcrB strains with AcrB antibody (top) and peptide antibody (bottom). From Left to right: 1) BW25113 strain; 2) HPA/B-1; 3) HPA/B-1 with 1 mM IPTG; 4) BW25113ΔacrB with HPacrA and HPacrB plasmids, inactive colonies; 5) BW25113ΔacrB with pBAD33 HPacrB 6) BW25113ΔacrB with pMal HPacrB; 7) BW25113ΔacrB with pBAD33 HPacrB in the presence of 3.2 μg/mL novobiocin; 8) purified *E. coli* AcrB.

Only in the active colonies, an extra band can be detected by *E. coli* AcrB antibody. In some of the Western blot results with full length antibody, two bands were detected. Only the lower band was proved to be related to AcrB (data not shown). No bands showed up in those colonies with low drug resistance. This implied the MIC difference between colonies was result from the extra bands. At the same time, this band cannot be recognized by peptide antibody, indicating this

band is not *E. coli* AcrB. MoreoverAcrB substrate novobiocin (3.2 µg/mL) was added to induce additional protein expression. However, no induction was observed.

In the original design of the gene, a poly-histidine tag was introduced at the end of *H. pylori* AcrB. Protein purification was attempted taking advantage of the tag. Unfortunately, no protein could be obtained. This suggested the band on the western blot membrane, which was previously assumed to be *H. pylori* AcrB was possibly some other proteins.

5. 3. 6 MIC Analysis Of HPA/B-1 And HPA/B-2 After Plasmids Loss

A plasmid loss method was used to probe the mechanism behind the observed decrease of drug susceptibility in the two colonies. First, the colonies were cultured for several days in the absence of selective markers to stimulate the growth of bacterial strains harboring no exogenous plasmids. Cultures were then plated onto LB agar plates containing only kanamycin. Single colony was picked to ensure the homogeneity of the culture. Colonies who cannot survive in chloramphenicol and ampicillin were selected. Next, drug susceptibility assay were performed for the colonies with no plasmid (Table 5.2). Since the substrate of *H. pylori* AcrB is still unknown, multiple antibiotics have been tested, including erythromycin, novobiocin, nalidixic acid, tetracycline, and neomycin. BW25113Δ*acrB* containing only *H. pylori* AcrA plasmid or AcrB plasmid were used as negative controls. The MIC of the colony without plasmids was the highest among all strains, suggesting the drug resistance of HP A/B-1 and HP A/B-2 was solely from the bacterial strains. During the culturing period, introduction of foreign antimicrobials stimulated the evolution of bacterial strains. However, HPA/B-1 and HPA/B-2 showed no enhanced drug tolerance to tetracycline, which is an *E. coli* AcrB substrate. The observation and

Western blot result confirmed that there was no *E. coli* AcrB contamination in HP A/B-1 and HPA/B-2. Furthermore, the neomycin MICs of HPA/B-1, HPA/B-2, and plasmid loss strain were increased to larger than 64 μg/mL, which greatly exceeded the reported MIC of *E. coli* straining expressing AcrD, 12 μg/mL. Therefore, I speculated that it was not AcrD that affected the drug resistance either. It was reported AcrF level was elevated by 80 folds in Δ*acrAB* strain [ref]. It is possible that the high drug susceptibility was the effect of the AcrF. Since tetracycline is substrate of AcrF. The result that the bacterial strain cannot extrude tetracycline proved that the AcrF was not the determine factor in HPA/B-1 and HPA/B-2. In conclusion, the reason caused enhanced susceptibility in HPA/B-1 and HPA/B-2 was still unknown. The Western blot analysis result using full length AcrB antibody suggested the higher drug tolerance might come from the elevated expression of another protein with a sequence similar to AcrB.

Table 5. 2 Drug susceptibility of BW25113ΔacrB expressing different plasmids.

Plasmids	nalidixic acid	erythromycin	novobiocin	tetracycline	neomycin
HPacrA	<1.25	<4	32	<1.25	>64
HPacrB	<1.25	32	16	<1.25	>64
HP A/B-1	10	128	>256	<1.25	>64
HP A/B-2	10	128	>256	<1.25	>64
No plasmid	10	128	>256	<1.25	>64
WT *E.coli* AcrB	5	128	>256	10	>64

5. 4 CONCLUSION

Due to the technical difficulties in culturing *H. pylori*, heterologous expression of proteins in a foreign host such as *E. coli* became a convenient approach in protein engineering. Expression of *H. pylori* AcrB and AcrA in *E. coli* was attempted. Under the conditions tested, AcrB from H. pylori failed to express in *E. coli*. In the two colonies with high drug tolerance, the increased drug susceptibility was resulted from induced evolution during long culturing time. Addition of antibiotics in the culture stimulated the expression of an unknown protein which is similar to AcrB in protein sequence. This protein was unlikely to be neither AcrD nor AcrF.

CHAPTER VI. SURA STRUCTURAL FLEXIBILITY AND ACTIVITY—INSIGHT INTO MECHANISM OF PERIPLASMIC MOLECULAR CHAPERONE FUNCTION

6.1 INTRODUCTION

Gram-negative bacteria cells have two layers of membranes. The outer membrane of the gram-negative bacteria consists of lipoproteins, lipopolysaccharides, phospholipids, and proteins. The outer membrane proteins (OMPs) family is large. There are more than sixty OMPs in Gram-negative bacteria. Most of these proteins form porins, mainly for transportations of substances in and out of cell.[200] All porins share a β-barrel structure assembled by multiple anti-parallel β-strands. The center of porins is a hydrophilic pore. As a result, in general porins serve as the major channels in the outer membrane for the translocation of small hydrophilic compounds. The size of the central pore in porins is normally quite small. In *E. coli* only moleculessmaller than 600 Da can pass through the channel.[201]

OMPs are first synthesized in the cell cytoplasm. Later the nascent protein is recognized by signal recognition particles and released from ribosome. After it is translocated through the inner membrane by the Sec machinery, the N-terminus signal peptide is digested by the N-signal peptidase.[202] Then the β-barrel protein presursors are delivered through the periplasmic space and finally inserted into the outer membrane. Due to the high hydrophobicity of the protein sequence, periplasmic molecular chaperones are required to assist the OMP folding process and prevent them from aggregation.[76]

So far, three major periplasmic molecular chaperones have been discovered in *Escherichia coli*. They are SurA, Skp, and DegP.[76] They share redundant chaperone activities in helping folding and maturing of OMPs. According to the current understanding, among the three chaperones, SurA is the primary chaperone that is involved in most OMPs' biogenesis. Those OMP

intermediates that fall off the SurA pathway are saved by Skp and DegP.[203] Recently Zhao and Coworkers studied the kinetics of OMPs interaction with the three chaperones. Their hypothesis is that because of the much faster kinetics of OMP interaction with SurA and Skp than with DegP, SurA and Skp may function at the early stage of OMP biogenesis, while DegP acts at a later time.[77] It has also been found that OMPs density dropped drastically in SurA deficient strain, while little has been affected in the Skp and DegP deficient strain.[80, 204, 205] Two potential explanations have been proposed for the drastic change of OMP density. First, in SurA deficient strain, σ^E transcription factor is induced, which subsequently down regulates mRNA level of several OMPs and leads to a decrease of OMP synthesis rate.[204-207] Second, without SurA, large amounts of nascent OMPs in the periplasm cannot be stabilized and thus aggregate.[80, 208] Furthermore, depletion of SurA leads to an increased sensitivity to hydrophobic drugs and detergents. However, no direct evidence has been discovered to show correlation between a change of OMP density and outer membrane permeability.[209, 210]

SurA was first identified as an essential gene in *Escherichia coli* for stationary phase survival.[207] Crystal structure of SurA showed four domains: an N- terminus domain with the first 150 amino acids, two peptidyl prolyl isomerase (PPIase) domains of approximately 100 residues each, and a C- terminus domain. The N, C-terminal domains and the first PPIase domain assemble into a core structure, with the second PPIase segment forms a satellite domain about 30 Å away.[82]Deletion of the two PPIase domains has been shown to have no impact on SurA chaperone activity. A truncated SurA construct containing only the N-terminal and C-terminal (NCt) domains is sufficient to restore SurA activity in a *surA* gene knockout strain *in vivo*.[209] The mechanism of interaction between SurA and OMPs has been the subject of many studies.[81-83,211,212] However, how SurA recognizes and binds to nascent OMPs still remains unclear. It is

generally acknowledged that peptides containing an A-X-A fragment would preferentially interact with SurA, in which A is an aromatic and X is a random residue. Such fragments appear in a high frequency in OMPs. Using phage display, Mckay and coworkers identified several peptides that showed strong affinity towards SurA. Through an isothermal calorimeter study, two of the peptides have been shown to compete with unfolded OMPs to bind with SurA. However, the co-crystallization of SurA and these peptides demonstrated that both peptides interacted with the first PPIase segment of SurA, which is known to be irrelevant to the chaperone function.[213] In terms of the SurA-OMP interaction, neither the binding site(s) nor potential structural rearrangement during the interaction has been elucidated. Herein, we conducted extensive mutagenesis studies to identify critical residues and site(s) on SurA for its activity. In addition, I limited the structural flexibility of SurA through the introduction of four individual disulfide bonds. I found that SurA was highly tolerant to mutations and not likely to undergo large scale conformational change while conducting its function cycles.

6. 2 MATERIALS AND METHOD

Cloning, Protein Expression and Purification.

SurA has been expressed in both periplasm and cytoplasm. For cytoplasmic SurA expression, *surA* gene lacking the signal peptide sequence was amplified from the genomic DNA of *E. coli* strain K-12 with primer csurAFW and csurARV and cloned into vector pET22b in frame between NdeI and XhoI sites. For periplasmic SurA, full length *surA* gene was amplified using primer psurAFW and psurARV and cloned into vector pMal-pIII in frame between NdeI and EcoRI sites. A polyhistidine tag was introduced into the C-terminus of both proteins to facilitate purification. pMal-pIII SurA N-C was amplified from constructed pMal-pIII SurA using

overlapping PCR. First, psurAFW and P2, P3 and psurARV were used to amplify SurA N- and C- domain, respectively. Later, psurAFW and P4 were used to add linker and poly-histidine tag to amplified SurA N-domain. Finally, psurAFW and psurARV were used to connect SurA N- and C- domains. Site directed mutagenesis was conducted following the manufacturer's manual using the QuikChange II XL Site-Directed Mutagenesis Kit (Agilent Technologies, USA). All primers used were listed in table 6.1. All sequences were confirmed by DNA sequencing (Operon, USA).

Table 6.1 DNA primers used for the construction of cytoplasmic SurA, periplasmic SurA and periplasmic SurA N-C.

Primer	Sequence
csurAFW	5'-TTAACATATGGCACCACAGGTAGTCGATAAAGTCG-3'
csurARV	5'-TTAACTCGAGGTTGCTCAGGATTTTAACGTAGG-3'
psurAFW	5'-TTAACATATGAAGAACTGGAAAACGCTGCTTC-3'
psurARV	5'-ATAGAATTCAGTGATGGTGGTGATGATGAGAACCACCGTTG-3'
P2	5'-ATGATGATGATGGCTTCCGTTCAGCTCAGTGCTG-3'
P3	5'-CACCACCATCACAGTGGT CGTAATGTCGATAAAACCGAC-3'
P4	5'-CGACCACTGTGATGGTGGTGATGATGATGATGGCTTCCGTTC-3'

For SurA expression, plasmids were used to transform *E. coli* BW25113Δ*surA* strain. Cells were grown at 37°C in LB medium supplemented with 100 μg/mL ampicillin and 50 μg/mL kanamycin to an OD_{600} of 0.6, and then induced with 1 mM isopropyl-D-thiogalactopyranoside (IPTG). Cytoplasmic SurA was purified as described.[212] For

periplasmicSurA, the periplasmic fraction was prepared by osmotic shock and later purified using metal affinity chromatography as described (pMal Protein Fusion and Purification System manual, Qiagen literature, Qiagen Inc., Chatsworth, CA). A phosphate buffer (25 mM Na-phosphate, 10% glycerol, 200 mM NaCl) supplemented with 20 or 250 mM imidazole was used in the washing and elution steps, respectively. Purified SurA was dialyzed against the phosphate buffer to remove excess imidazole. The same phosphate buffer was used throughout the study unless otherwise noted. Purified proteins were analyzed using SDS-PAGE with a 12% homogeneous polyacrylamide gel and visualized after Coomassie Blue stain. Protein concentrations were determined using the BCA protein assay.

OmpF gene was amplified from *E. coli* genome without N-terminus signal peptide by PCR. PCR product was digested with NdeI and HindIII, and inserted into pET22b vector. A poly-histidine tag was added at the C-terminus of the protein. The protein was expressed under IPTG (1mM) induction for 4 hours at 37ºC. Cells were harvested and lysed by sonication. The supernatant was discarded and the pellet was dissolved using 30 mM Tris buffer, 100 mM NaCl, 8 M urea (pH=8.0). The soluble part was incubated with urea pretreated Ni-NTA resin for 45 mins. Next, a buffer containing 30 mM Tris, 100 mM NaCl, and 8 M urea supplimented with 10mM or 40mM imidazole was used to wash the resin. Finally, a buffer containing 20 mM NaAc-HAc and 8 M urea buffer (pH=4.0) was used for protein elution. After elution, Tris was added immediately to adjust the pH to 8.0.

Expression level of SurA

Freshly transformed colonies of BW25113*ΔsurA* containing plasmid-encoded SurA were used to inoculate LB medium supplemented with ampicillin and kanamycin. After cultured at 37°C for 6 h, cells were harvested and subjected to osmosis shock as mentioned above in the purification of

periplasmic SurA. The supernatant containing periplasmic SurA was analyzed using SDS-PAGE on a 12% gel, and then transferred to a polyvinylidene difluoride membrane (Millipore, Bedford, MA) for Western blot analysis using a polyclonal rabbit anti-SurA primary antibody and analkaline phosphatase-conjugated anti-rabbit (Abcam, Cambridge, MA) secondary antibody, and then protein-antibody conjugates were visualized using nitroblue tetrazolium chloride and 5-bromo-4-chloro-3'-indoyl phosphate p-toluidine (Sigma-Aldrich, St. Louis, MO) as substrates.

SurA activity assay

surA gene knockout *E. coli* strain (BW25113*ΔsurA*) was used as the host cell. BW25113Δ*surA*strains harboring plasmids encoding wild type (WT) surA (pMal-SurA) or the empty vector pMal-pIII were used as the positive and negative controls, respectively. Plasmids encoding different SurA mutants were used to transform BW25113Δ*surA* as well. SurA activities in different strains were tested using two methods, a drug susceptibility assay and an OMP expression level assay.

Drug susceptibility assay

A single colony was used to inoculate a LB media supplemented with 100 μg/mL ampicillin and 50 μg/mL kanamycin. Exponential-phase cultures of different strains were diluted to OD600nm of 0.1 using LB broth. 10 μL of this culture was used to inoculate 1 mL LB media containing the indicated concentration of novobiocin. The cultures were incubated overnight at 37°C. The next morning, the minimum inhibitory concentration (MIC) was determined as the lowest concentration that inhibited the growth of the bacteria. Each experiment was repeated at least three times.

FimD and OmpA expression level assay

Different strains of *E. coli* cells were grown in LB media, at 37ºC to an OD600nm of 0.8. Outer membrane fractions were extracted as described with some modifications.[214] Briefly, cells were collected by centrifugation, lysed using French press, followed by ultracentrifugation at 100,000g for 1.5 h. The pellet was resuspended in buffer A (50 mM Na-phosphate, 100 mM NaCl, 1% N-lauryl sarcosinate, pH 7.5) and incubated at 4ºC for 1 h. The outer membrane fraction was then further isolated by ultracentrifugation at 100,000g for 1.5 h. The pellet was then resuspended in a denaturing buffer B (4 M urea, 2% SDS, 50 mM Na-phosphate, 100 mM NaCl, pH 7.5, 10 mM EDTA) and sonicated for 5 min. All samples were centrifuged for 5 min at 16,000*g* and the soluble component was analyzed using SDS-PAGE. Next, proteins on the gel were transferred to a polyvinylidene difluoride membrane and detected using Western blot as described above except that an anti-FimD antibody (a kind gift from Dr. Luis Angel Fernandez) was used as the primary antibody.

Circular Dichroism (CD) Spectroscopy

CD Spectra were collected using a JASCO J-810 spectrometer (JASCO, United Kingdom) with 1 nm bandwidth. Blank scans were performed using phosphate buffer. Spectra were then corrected for background by subtracting the blank scan.

Fluorescence Spectroscopy

Fluorescence emission spectra were collected using a Perkin Elmer LS-55 fluorescence spectrometer (PerkinElmer, Waltham, MA) at 4°C. Tryptophan emission of SurA was monitored

at an excitation wavelength of 280 nm. Blank scans were collected and subtracted from the spectra.

Protease Accessibility Assay

A trypsin to SurA molar ratio of 1:200 was used in the experiments. The reaction was performed in phosphate buffer at room temperature for the indicated period of time, and then phenylmethylsulfonyl fluoride (PMSF) was added to a final concentration of 2 mM to stop the reaction. SDS loading dye was then added and the samples were immediately heated at 95°C for 5 min before analyzed using SDS-PAGE.

Fluorescent labeling

SurA Cys pair mutants were freshly expressed in BW25113*ΔsurA* as described above. Cell was harvested by centrifuge at 4,000g for 20 min at 4^{o}C and then resuspended in ice cold Buffer A (30 mM Tris buffer, 20% sucrose, 1 mM EDTA). After incubated for 10 min on ice, cells were collected using centrifugation at 8,000g for 20 min at 4^{o}C. Cell pellet was resuspended again in ice cold water containing 5 mM $MgSO_4$ and 1 mM PMSF. 10 mM iodoacetamide (IAM) was added to block all the free thiol groups. Periplasmic extraction was then separate from the cell debris through centrifugation and applied to a Ni-NTA column. All subsequent wash and elution buffers contained 5 mM IAM. After purification, maleimide (MAL) and SDS were immediately added to protein samples to final concentrations of 50 mM and 4% (w/v), respectively. SurA and its mutants were then precipitated, reduced using DTT and labeled using a thiol specific fluorescence probe fluoroscein-maleimide (Sigma-Aldrich, St. Louis, MO) as described.[58]

Quantification of levels of disulfide bond formation

Extent of disulfide formation was quantified as described.[58] Briefly, I included IAM during the protein purification process to prevent the formation of disulfide bond during protein purification. After purification, Ireduced the disulfide bond in the sample using DTT and then labeled the sample using excess fluorescein-maleimide. To quantify the extent of disulfide bond formation, I included two internal control samples: for the positive control sample, I did not add IAM during protein purification. Therefore, all Cys in the protein was labeled after reduction (100% labeling). For the negative control, IAM was used during protein purification, but the sample was not reduced using DTT before labeling. Therefore, there should not be any labeling (0% labeling). The extent of disulfide bond formation could then be calculated as a ratio of $(I_{sam}-I_{neg})/(I_{pos}-I_{neg})$, in which I_{sam}, I_{neg}, and I_{pos} were band intensities of the sample, and negative and positive controls, respectively.

Fluorescence polarization study of SurA and OMPs interaction under macromolecular crowding condition

SurA was incubated with FITC with a ratio of 1:2 in 20 mM PBS buffer (pH=7.4) at room temperature for 1 hr. Tris-HCl was added to quench the reaction for 0.5 hr. Excessive dyes were dialyzed overnight. The concentration of the protein was determined by Bradford assay. Fluorescence polarization based titration was performed on a Perkin-Elmer LS-55 fluorescence spectrometer (Perkin-Elmer, Waltham, MA) at 20 ºC. FITC-SurA was first diluted into 400 µL Tris buffer to a final concentration of 2 µM. Purified OmpF was added into FITC-SurA, fluorescence polarized was recorded. The excitation and emission wavelengths of FITC-SurA were 479 and 515 nm, respectively.

6.3 RESULTS AND DISCUSSION

6.3.1 Identification of residues critical for SurA function

The aim of our research is to identify amino acids that are important to SurA chaperone function. Potential residues critical for function could be identified through sequence alignment. SurA is highly conserved in most Gram-negative bacteria.[213, 215-217] I aligned the sequence of SurA from *E. coli* with its homologues from six different organisms using the online sequence alignment tool T-coffee (Figure 6. 1).[218]

```
EC  25 VDKVAAVVNNGVVLESDVDGLMQ-SVKLNAAQARQQLPDDAT----LRHQIMERLIMDQIILQMGQK  86
PA     VDKVAAVVNNGVVLESDVDSMMS-TVKSQAKQAGQQLPDDKT----LRHQILEREIMDAIILQLGDK
PS     LDRVVAIVDNDVIMQSQLNQRMR-EVQQTIEKRGADAPPTDV----LQQQVLERLITENLQLQIGER
ZM     VHKATAIVNGTIITNTDIEQRFALILASAGGDVSRISEEDRN---MARLQILRNLIDETLEIQEAKA
VV     LDKVAVIVNDGVILQSDIDTATK-TLRANAKKSGQALPDADV----LNEQIVDKLIIDTLQTQEADR
NH     GQSALATVGGTEISTEQFRQIYNDRLQQIGRQFGRPLPPDQVRALGLDRQILQQVIAEAALDEDAQR
        . . . *..  :   :.       :     .                *:: . * :    : ..

EC  87 MGVKISDEQLDQAIANIAK--QNNMTLDQMRSRLAYDGLNYNTYRNQIRKEMIISEVRNNEVRRRI  150
PA     AGLQITDQQLDQAIQNIAA--QNRMSVDQLRSRLAYDGMNYNTYRAQIRKEMLISEVRNNEVRRRV
PS     SGIRISDEELNQAMGTIAQ--RNNMSLEQFREALARDGLSLETAREQIRREMVISRVRQRRVAERI
ZM     NDIIITPTELDQIFEHYAR--NMKKTPEAFSADLQAIGSSAKSVKRQVEADMAWRRLLGRRVEPFV
VV     IGVRIDDTRLNQAIEEIAR--NNNQTIDELSAAIASEGVSYAEFREQIRKEMAASEARNALVRRRI
NH     KGLKVSDEEIGRQIKSDPNFKGANNAFDAARFAGLIRQLGYT-------EQRYVAEQRNMALRRQI
        .: :   .:.: :   .     . : :           .          :    .     :   :

EC 391 AAQKDRAYRMLMNRKF-SEEAASWMQEQRAS-------AYVKIL-----SN  420
PA     AAQKERAYRMLFNRKF-AEEAQTWMQEQRAG-------AYVKILD--NNAQ
PS     QFREQQALSLLRNRKY-DEELQAWLRQIRDE-------AYVEV------KL
ZM     QPNFQQIHNQLQEDRV-NKRAIRYLRDLRRD-------AI-------IDYR
VV     SAMKNKAYRILFNRKF-NEEVGAWMQELRAG-------AFVEIINEEENDG
NH     ASDETKKLREGVQRGLSDEYIGQYIVKLEAEIGTKINQAAVAQITGASSNF
            :     :     :    :: . .        *
```

Figure 6.1 Sequence alignment of SurA from *E. coli* (EC) with homologues from *Pantoea ananatis* (PA), *Pseudomonas stutzeri* (PS), *Zymomonas mobilis* (ZM), *Vibrio vulnificus* (VV), and *Nitrobacter hamburgensis* (NH). The numbers indicate positions of the starting and ending residues in the sequence of *E. coli* SurA. Asterisks, colons and periods indicate identical, conserved and semi-conserved residues, respectively.

The majority of conserved amino acids resided in SurA N, P1, and C-terminal domains. Since SurA chaperone activities are proved to be independent from the PPIase domains, our mutations were focused on conserved residues in N- and C-terminal domains (NCt). In these two domains, 4 residues are invariable, and 48 residues are conserved, which is 26% of total amino acids in NCt module. All the the invariable and conserved residues were mappedonto the crystal structure of SurA. The focus of our study was SurA chaperone function. Residues that contributed to intra-molecular interactions and were mostly likely to be important for maintaining the structural integrity of SurA were eliminated from our mutational studies. Mymutation studies were focused on conserved residues that were exposed to the surface, whose side chain appeared not to be making critical intra-molecular interaction. Drug susceptibility assay of BW25113Δ*surA* containing plasmids encoding different SurA mutants was used as an initial tool to examine the effect of the mutations. The same strains containing plasmid encoded wild type (WT) SurA or the empty vector were used as the positive and negative controls, respectively. Twenty three residues were mutated individually, and only one mutation, Val-37 to Gly, showed a dramatic decrease of SurA activity (Table 6. 2).

Table 6.2 Novobiocin MIC of BW25113ΔsurA expressing plasmid encoded surA mutants**.**

Mutants	MIC (μg/mL)	Mutants	MIC (μg/mL)
BW25113	128	Y398A	128
pMal-pIII	16	N403A	128
V32G	64	K405A	128
V37G	16	E408A	64
D41K	128	W413G	128
V42C	128	Q415A	128
M114G	128	E416A	128
Y120A	128	R418G	128
Y125A	128	Y422A	128
Y128A	128	I425A	128
Q131G	128	M136G	128
I132G	128	Deletion of L153-Q163	128
E135G	128		

6.3.2 $SurA_{V37G}$ has decreased expression level and structural stability

To determine what caused the reduction of MIC level in $SurA_{V37G}$, I first examined the expression level of the mutant as compared to that of the WT SurA in BW25113Δ*SurA* (Figure 6. 2).

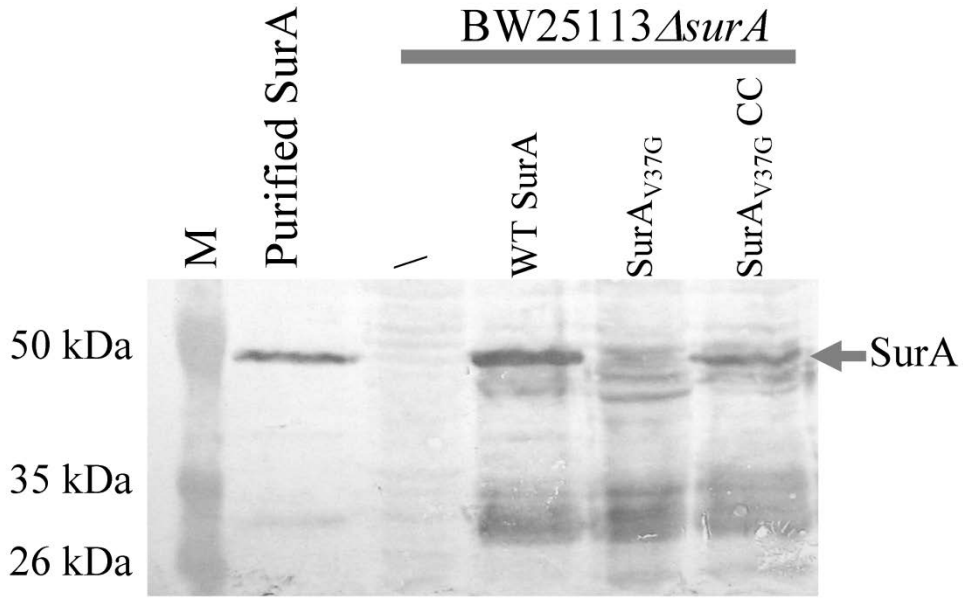

Figure 6.2 SurA expression levels in different strains. Western blot analysis of osmotic fluid from BW25113, BW25113*ΔsurA*, and BW25113*ΔsurA* containing plasmid-encoded WT SurA, $SurA_{V37G}$ and $SurA_{V37G/A30C/I425C}$ ($SurA_{V37G}$ CC). An anti-SurA antibody was used. The molecular masses of bands in the molecular mass marker were marked on the left of the gels.

It appeared that SurA was not stable *in vivo*, since a large amount of SurA degraded fragments could be observed. In the case of $SurA_{V37G}$, only fragments were observed. Full length SurA could barely been detected. It was likely that the mutation drastically decreased the stability of the protein, which led to insufficient amount of SurA in the periplasm to carry out the chaperone function.

To further compare the structure and stability of WT SurA and $SurA_{V37G}$, I characterized both proteins purified from the cytoplasm. Studies have shown that SurA purified from the cytoplasm has the same structure and function as those purified from the periplasm.[82]

I first examined the structure of $SurA_{V37G}$ and WT SurA by CD. Far-UV CD spectra of SurAV37G and WT SurA superimposed well, suggesting both proteins had similar secondary structure. Both proteins are approximately 50% alpha-helical, which is consistent with solved SurA crystal structure (Figure 6. 3A).

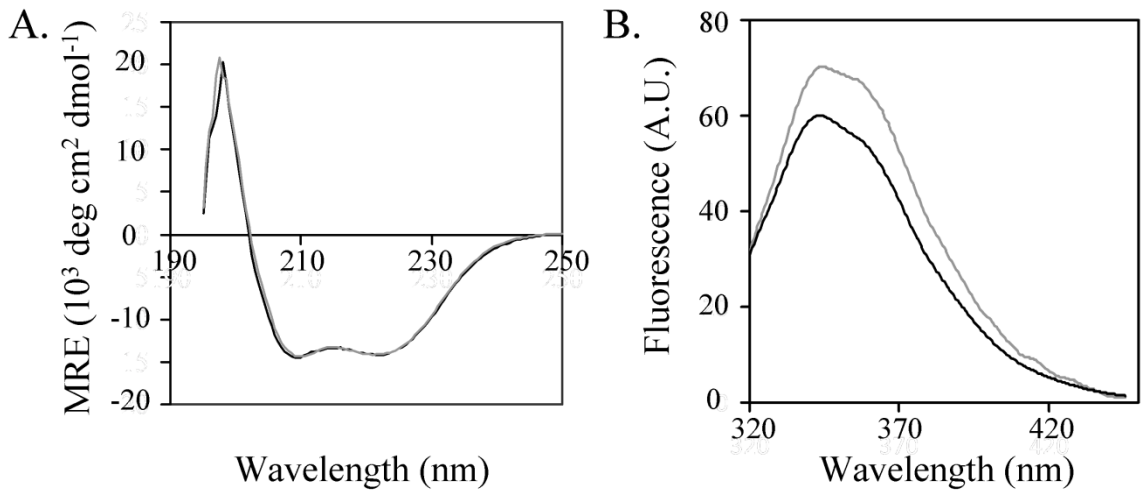

Figure 6.3 Characterization of $SurA_{V37G}$ (grey) and WT SurA (black). A) Far-UV CD spectra.B) Tryptophan emission spectra. Excitation wavelengths were 280 nm.

I also compared tryptophan fluorescence spectrum of WT SurA with that of the mutant (Figure 6. 3B). The fluorescence of $SurA_{V37G}$ was slightly higher than WT SurA, indicating that the local microenvironment was different, possibly a consequence of mutation. In summary, the data from CD and fluorescence spectroscopy indicated that while the secondary structure compositions of the two proteins were very similar, there was some change in the global structure as revealed by the fluorescence difference.

The low level of full length $SurA_{V37G}$*in vivo* suggested that the mutation affected SurA stability. To further examine protein stability, Iperformed limited trypsin digestion on both $SurA_{V37G}$ and WT SurA using purified proteins (Figure 6. 4). Protease digestion hasbeen used extensively in studies of protein stability and rigidity.[156-158] $SurA_{V37G}$ and WT SurA were treated with trypsin and the progress of digestion was monitored over time using gel electrophoresis. Approximately 90% of SurAV37G was digested within 5 min while 60% of WT SurA remained intact after 30 min of trypsin treatment. The mutation did decrease SurA stability drastically.

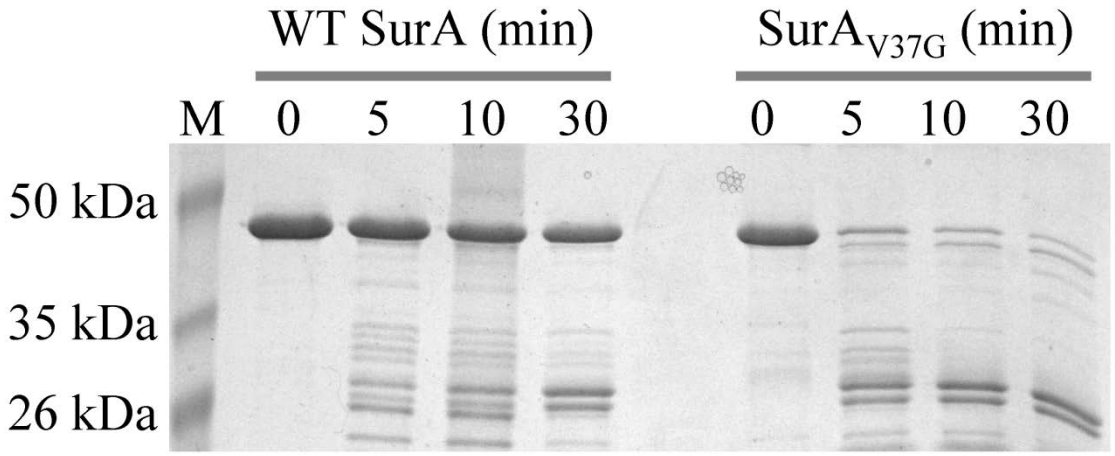

Figure 6.4 Limited trypsin digestion of purified WT SurA and SurA$_{V37G}$. Typsin and protein molar ratio is 1:200. Wild-type SurA was highly resistant to protease digestion, 63.3% remained after trypsin treatment for 30 min. SurA$_{V37G}$ was more sensitive to trypsin digestion, with less than 10% of SurA$_{V37G}$ left after 5 min. The molecular masses of bands in the molecular mass marker were marked on the left of the gel.

6.3.3 V37G mutation affects the anti-parallelβ-sheet network of the N- and C-termini

A close examination of SurA structure showed that Val-37 locates in an N-terminal β strand, which was involved in a three stranded anti-parallel β sheet involving the last few amino acids at the C-terminus (Figure 6. 5B). Our hypothesis is that the β-sheet locks the N- and C-termini together and thus plays an important role in stabilizing SurA tertiary structure. A mutation to Gly might have disrupted the formation of the β-strand and/or its interaction with the neighboring strands, and therefore destabilized the three-stranded β sheet. To examine if Val-37 to Gly affected the local structure of the β sheet, I introduced a pair of Cys to monitor the formation of disulfide bond (Figure 6. 5C).

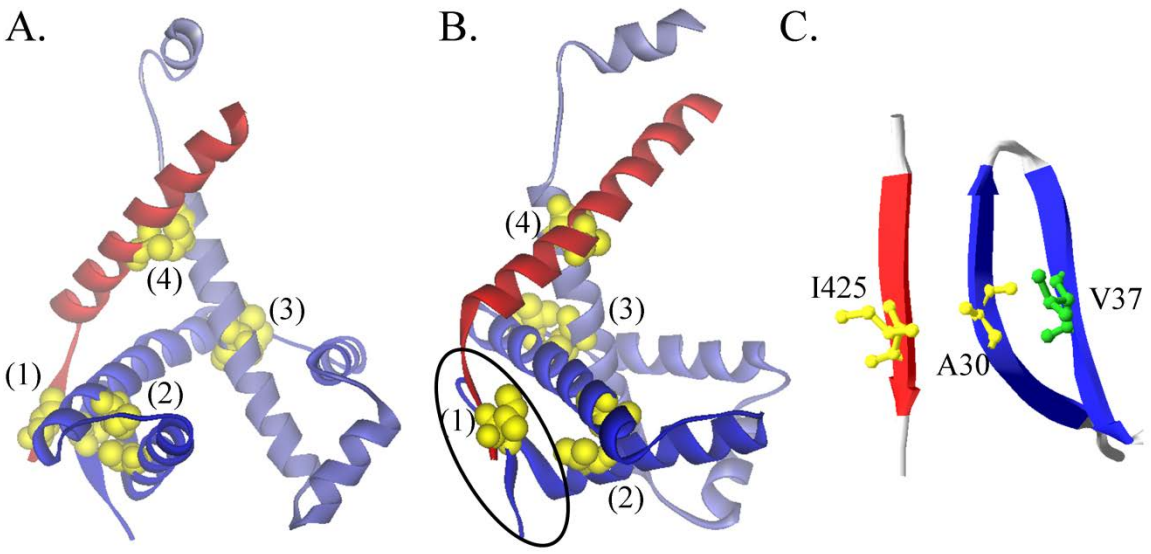

Figure 6.5 Structure of SurA. A. SurA N- (blue) and C- domain (red). Residues that are replaced by Cys to introduce disulfide bond were highlighted, A30-I425 (1), V42-I70 (2), V89-I137 (3), and V146-A410 (4). B. The same structure as in A, but rotated 90 degree along a vertical axis. The black oval indicated the location a three-stranded antiparallel β-sheet formed by two stands from the N-terminus and one strand from the C-terminus. C. A zoom in view of the β-sheet. Side chains of Ala30, Val37, and I425 are shown in ball-and-stick model.

I introduced two Cys at positions 30 and 425 in SurA sequence as a reporter Cys pair. According to the crystal structure of SurA, these two cysteines should be close enough to form disulfide bond. If the Val-37 to Gly mutation caused a significant change of the β-sheet structure, then the distance between the reporter Cys pair would be affected. Since disulfide bond formation is very sensitive to distance, I should be able to see a difference in the level of disulfide bond formation. I have developed an effective thiol trapping and fluorescent labeling protocol as reporters for protein structural change.[58] Using this method, I found that in $SurA_{A30C/I425C}$, disulfide bond formed completely between A30C and I425C (Figure 6. 6A).

However, when Val37Gly mutation was introduced to create $SurA_{A30C/I425C/V37G}$, the extent of disulfide bond formation was estimated to be approximately 50% (Figure 6. 6B). Therefore, Val37Gly did affect the local structure of the β-sheet.

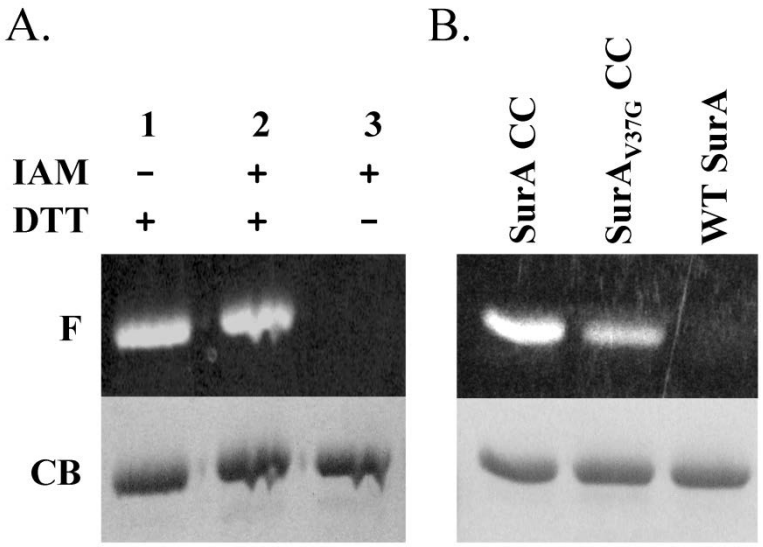

Figure 6.6 Characterization of $SurA_{V37G/A30C/I425C}$ ($SurA_{V37G}$ CC). A. Fluorescent image (F) and Commassie Blue (CB) stain of $SurA_{A30C/I425C}$ (SurA CC) after fluorescent labeling. Lane1 and lane3 were positive and negative controls, which were used to quantify the extent of disulfide bond formation (see text). B. Fluorescent image (F) and Commassie Blue (CB) stain of $SurA_{A30C/I425C}$ (SurA CC), $SurA_{V37G}$ CC, and WT SurA after fluorescent labeling. WT SurA was used as a control to confirm the absence of non-specific labeling under the current experimental condition.

6.3.4 Function loss in $SurA_{V37G}$ can be restored by a disulfide bond

When Ala30Cys/Ile425Cys mutations were introduced into $SurA_{V37G}$, the disulfide bond partially formed. I speculate that the disulfide bond may have stabilized SurA structure, and thus

partially compensated for the function loss caused by V37G mutation. To examine if this was actually the case, I performed drug susceptibility assay of $SurA_{V37G/A30C/I425C}$. Consistent with our expectation, MIC of $SurA_{V37G/A30C/I425C}$ toward novobiocin increased to 256 μg/mL, indicating that the disulfide bond did improve SurA stability and activity (Table 6. 1). Furthermore, to confirm that this increase of activity was actually caused by the formation of a disulfide bond, I also measured the MIC of $SurA_{V37G/A30C/I425C}$ toward novobiocin in the presence of 5 mM DTT, and found that the MIC reduced to a level comparable to $SurA_{V37G}$ (Table 6. 3). Under the same condition, 5 mM DTT had no effect on the MIC of $SurA_{V37G}$ or wild type SurA. If the disulfide bond improved the stability of SurA, there should be more full length SurA in the periplasm.

Table 6. 3 Novobiocin MIC of BW25113ΔsurA expressing plasmid encoded surA mutants.

Mutation	MIC (μg/mL)
A30C/I425C	256
A30C/I425C/V37G	256
A30C/I425C/V37G + 5 mM DTT	16
V37G + 5 mM DTT	16
WT SurA + 5 mM DTT	128

I measured the expression level of SurA in BW25113Δ*surA* containing plasmid-encoded $SurA_{V37G/A30C/I425C}$ and $SurA_{V37G}$ (Figure 6. 2). Similar to $SurA_{V37G}$, $SurA_{V37G/A30C/I425C}$ was partially degraded *in vivo*. However, there was still a significant fraction of full length protein in the case of $SurA_{V37G/A30C/I425C}$, which was clearly sufficient to maintain the wild type level SurA activity. Using quantitative Western blot analysis, I estimated that there were approximately

1,500 molecules of SurA per cell in BW25113 strain (Fig 5. 7).

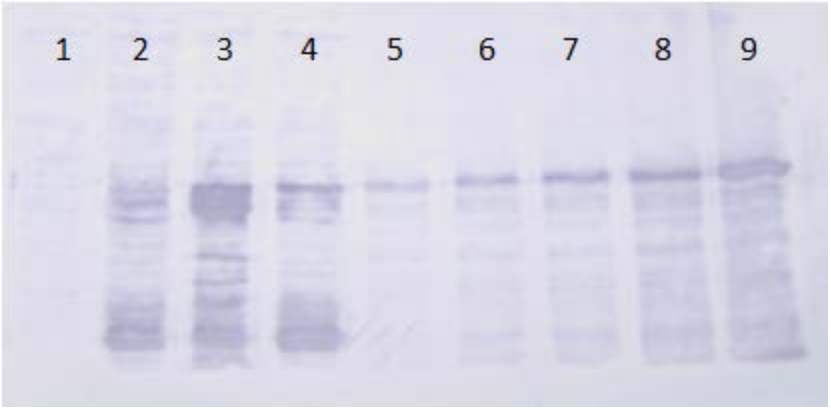

Figure 6.7 Quantitative western blot analysis of SurA expression level in BW25113Δ0052 strain expressing different plasmids. Western blot analysis of osmotic fluid from BW25113*ΔsurA* containing empty pMal-pIII, plasmid encoded WT SurA, $SurA_{V37G}$, $SurA_{V37G/A30C/I425C}$ ($SurA_{V37G}$ CC), 30 ng, 90 ng, 270 ng, 810 ng, 2430 ng purified SurA (lane 1-lane 9).

When BW25113Δ*surA* was transformed using the plasmid created in this study that encoded wild type SurA, under basal expression condition there were ~3,500 molecules of SurA per cell. However, this increase of SurA expression level did not further increase the MIC of the strain as compared to that of the BW25113. When BW25113Δ*surA* was transformed with plasmid encoding $SurA_{V37G/A30C/I425C}$, the copy number of full length SurA was approximately 1,000. However, the MIC of the strain was twice the level of the wild type strain or *surA* knockout strain transformed with plasmid encoded wild type SurA. This result revealed that *E. coli* need as little as 1,000 or fewer SurA per cell for normal SurA activity and maintaining membrane integrity. It is not clear why the MIC of BW25113Δ*surA* containing $SurA_{V37G/A30C/I425C}$ was twice as much as the MIC of the same strain containing wild type SurA. I have also tested the MIC of BW25113Δ*surA* containing $SurA_{A30C/I425C}$ and it was also twice as much at that of the wild type

strain (Table 6. 3).

As an alternative method to examine the activity of SurA, I measured the expression level of FimD in BW25113Δ*surA* expressing plasmid encoded WT SurA, $SurA_{V37G}$, or $SurA_{V37G/A30C/I425C}$ (Figure 6. 8). Studies have shown that the FimD expression level in the outer membrane depends on the function of SurA.[219] Consistent with the MIC assay, while the levels of FimD in cells containing WT SurA or $SurA_{V37G/A30C/I425C}$ were similar, the expression level in cells without SurA or $SurA_{V37G}$ were significantly lower.

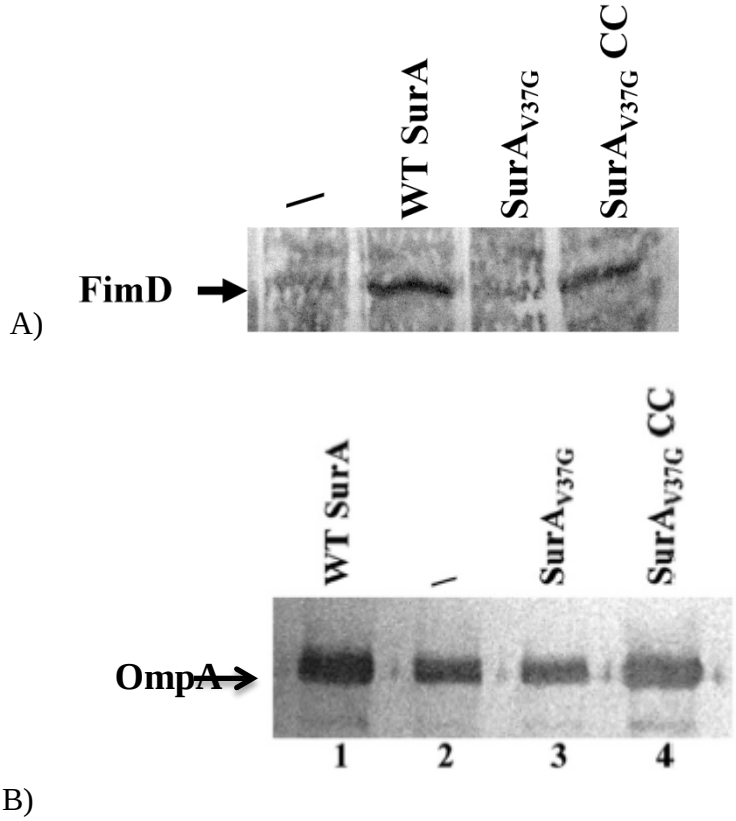

Figure 6.8 FimD and OmpA expression levels in different strains. Western blot analysis of outer membrane vesicles extracted from BW25113*ΔsurA* strain containing the empty vector (/) or plasmids encoding WT SurA, $SurA_{V37G}$, or $SurA_{V37G}$ CC. Anti-FimD and anti-OmpA primary antibody were used. The positions of FimD and OmpA were marked by an arrow, respectively.

6.3.5 Mutational Studies Of Hydrophobic Residues

Interaction between SurA and OMP precursors in the periplasm is reversible and non-covalent in nature. The interaction between SurA and OMPs is poly-specific, in which SurA interacts with various OMP precursors with different sequences and possibly various partially folded structures. Therefore, I expect SurA to function according to one or both of the following mechanisms: 1) The recognition and binding between SurA and OMPs rely heavily on hydrophobic interactions. Hydrophobic interaction has been shown to play critical roles in poly-specific binding scenarios, such as in the interaction between multidrug transporters and regulators and their array of diverse substrates.[110, 116] It has also been proposed as a major player in SurA-OMP interaction.[217, 218] 2) The structure of SurA is very flexible and therefore can adapt to bind to different substrates. To investigate the role played by hydrophobic interactions in SurA-OMP interaction, I mutated all aromatic residues in the NCt domain individually and examined the effect of such mutations on SurA function. Aromatic residues have bulky hydrophobic moieties that are usually abundant at sites of low specificity binding.[220] There are one Trp (W413), five Tyr (Y120, Y125, Y128, Y398, Y422), and one Phe (F406) in the NCt domain (Figure 6. 9).

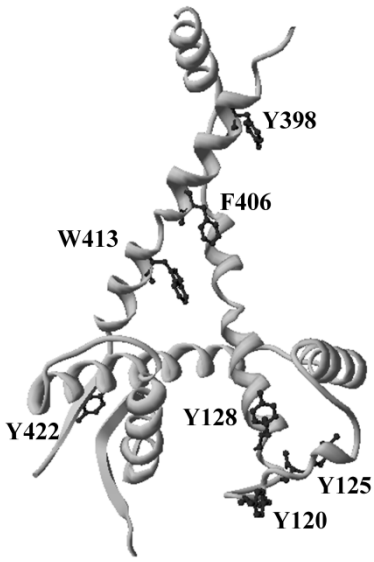

Figure 6. 9 Structure of the SurA NCt domain showing the side chains of aromatic residues.

I replaced each residue individually with Ala. When introduced into BW25113Δ*surA*, none of these mutations caused a significant decrease of MIC values. In addition, I have mutated Y120, Y125, and Y128 simultaneously to create a triple mutant SurAY120A/Y125A/Y128A. This triple mutant has similar activity as WT SurA as well. These results suggested that none of the aromatic residues investigated in this study played a dominant role in OMP binding. OMPs might interact with SurA at multiple sites.

6.3.6 SurA structure flexibility is not required for its chaperone function

I next examined the relationship between SurA function and its structure flexibility. I have shown earlier that a pair of Cys placed at positions 30 and 425 formed disulfide bond and the formation of the disulfide bond had no negative impact on the function of SurA. To investigate if disulfide bond introduced into other locations of SurA affect its activity, I introduced three additional cysteine pairs strategically placed at different locations in the NCt domain (Figures 6.

6A). According to SurA crystal structure, the distances between the α carbons of each Cys pair are within 6 Å, which allows the formation of disulfide bonds.[24] As shown in Figure 5. 10, Lanes 1 and 3 were positive and negative controls for the quantification of disulfide bond percentage. The extents of disulfide bond formation were calculated as described in Experimental and showed in Table 6. 4. Formation of disulfide bond was close to completion in all three pairs of Cys. Next, I tested the activity of these mutants using the drug susceptibility assay and found that they had similar activity as the WT SurA (Table 6. 5).

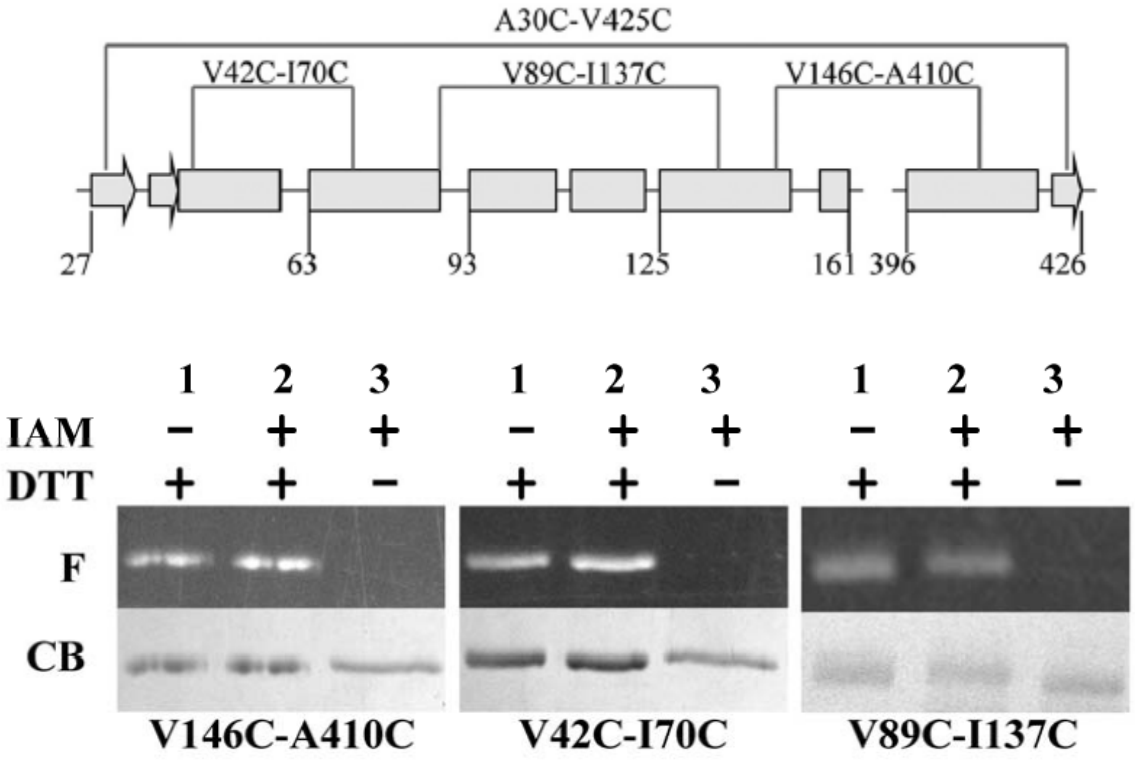

Figure 6.10 Secondary structure scheme of the NCt domain of SurA with theposition of disulfide bonds shown. Arrows and rectangles denote β-strandsand α-helices, respectively (Top).Fluorescent image (F) and Commassie Blue (CB) stain of three SurA cysteine pair mutants after fluorescent labeling (Bottom). Lane1 and lane3 were positive and negative controls, which were used to quantify the extent of disulfide bond formation

Table 6.4 Percentage disulfide formation in Cys pairs as revealed by the percentage of fluorescence labeling

Cysteine pair	Disulfide bond%
A30C-I425C	95.1±4.4
V42C-I70C	98.1±4.9
V89C-I137C	96.5±2.1
V146C-A410C	97.4±6.3

Table 6.5 Novobiocin MIC of three additional cysteine pair SurA mutants

Mutations	MIC (μg/mL)
V89C/I137C	128
V42C/I70C	128
V146C/A410C	128

Many chaperones, such as HSC70 and SecB, have been shown to undergo conformational changes upon binding with their substrates. [221, 222] Here I introduced a disulfide bond at four different locations in the functionally relevant NCt domain. To our surprise, while all four disulfide bond formed *in vivo*, none of them had a negative impact on SurA function. Therefore, SurA does not seem to undergo global conformational changes during its operation. Moreover, SurA may function more effectively with a rigid structure, as one disulfide bond containing mutant, $SurA_{A30C/V425C}$, was even more active than the wild type SurA. However, the exact

mechanism that caused the increase of MIC of cells containing this SurA mutant remains to be determined.

6.3.7 Outer Membrane Protein Level In Different Strains Containing SurA Mutations

SurA affects bacterial drug susceptibility by changing the outer membrane permeability. The outer membrane permeability is generally considered to be related to OMP level. However, there is no direct evidence indicating that a reduced OMP level is associated with compromised cell permeability. A reduced OMP level and decreased drug tolerance were observed simultaneously, whether there is a connection in between remains unknown.

Western blot analysis was performed to examine OmpA level in strains containing different SurA mutants. It has been demonstrated in a previous study that the two PPIase domains P1 and P2 could be deleted without changing SurA function in maintaining outer membrane integrity. Therefore, in this study, the SurA N-C construct was used. The antiparallel β-sheet has been shown to be important to SurA stability *in vivo*. A SurA mutant, $SurA_{10delN\text{-}C}$, has been identified to confer poor drug tolerance when introduced into surA gene knockout strain [cite Brent's thesis]. However, Western blot analysis showed that the level of $SurA_{10delN\text{-}C}$ was comparable to that of WT SurA. It is most likely that deleting the last ten amino acids caused SurA misfolding, which eventually leads to defective cell membrane. This was the first AcrB mutant that has been discovered with proper expression level and no activity. The discovery offered possibility to establish the relationship between SurA chaperone activity and cell permeability.

OmpA expression level was compared in four mutants, BW25113Δ*surA* strain expressing WT

SurA, pMal-pIII vector, $SurA_{10delN-C}$, and $SurA_{M2-9}$ (Figure 6.11). $SurA_{M2-9}$ was an active SurA mutant identified in a separate study.[223] First, MICs of novobiocin of the four strains were measured (Table 6. 6).

Table 6. 6 Novobiocin MIC of $SurA_{M2-9}$ and $SurA_{10delN-C}$

Plasmids	MIC (μg/mL)
WT SurA	128
pMal-pIII	16
$SurA_{M2-9}$	128
$SurA_{10delN-C}$	16

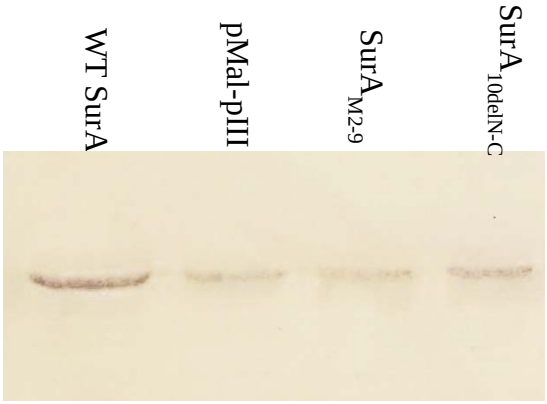

Figure 6. 11 OmpA expression level in BW25113ΔsurA strain expressing WT SurA, pMal-pIII vector, $SurA_{N-C}$, $SurA_{M2-9}$

BW25113*ΔsurA* transformed with the empty vector pMal-pIII exhibited a lower OmpA level in the outer membrane than cells expressing WT SurA. This finding is in agreement with published result. However, OmpA level was supposed to increase in $SurA_{M2-9}$ since it has the wild-type MIC level. My results proved the opposite. The mutant with the lowest MIC, $SurA_{10delN-C}$, had

the highest OmpA level among the three mutants. The observation implied that there might not necessarily be a connection between SurA chaperone activity and cell permeability. OMP levels might not be directly correlated with membrane permeability. It is possible that SurA could also be related to the biogenesis of some other components in cell membrane.

6.3.8 Interaction of SurA and OMPs under macromolecular crowding condition

An easy, sensitive, and convenient method to study SurA and OMPs binding is highly desirable. Mckay and coworker used ITC to investigate the interaction. However, this method requires large amount of proteins. here a fluorescence polarization based method was established in the study of SurA and OMPs interaction. First, OmpF was titrated into FITC-SurA, fluorescence polarized signal was collected. To prove the signal change does not result from non-specific binding, titration of BSA to SurA was used as a control (Figure 5.12). Kd of OmpF to SurA is 1.23±0.16 μM.

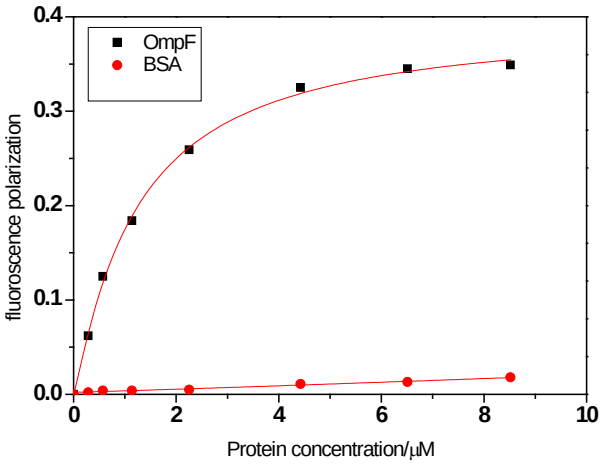

Figure 6. 12 Fluorescence polarization titration of OmpF (Black) and BSA (Red) into FITC labeled SurA.

The primary location of SurA activity is in the periplasm, which is filled with macromolecules such as proteins and sugars. It is often important to evaluate the chaperone function in the macromolecular crowding environment. I investigated whether the crowding condition affect SurA-OMP interaction. Two macromolecular crowding reagents were used, Ficoll and Dextran. The addition of Ficoll and Dextran increased the viscosity of the solutions. Consequently, the signal change was much smaller. However, it seemed that the crowding condition had little effect on the binding affinity between the two proteins. The Kds of SurA and OmpF in PB buffer, PB buffer containing 30% ficoll, and 30% Dextran were 4.59, 5.13, 3.29 μM (Figure 6.13) OmpF is dissolved in 8M urea, titration into PB buffer cause precipitation. The difference of Kd in Figure 6.12 and 6.13 might be resulted from the inaccurate concentration in buffer condition. In summary, a simple method was established to examine SurA and unfolded OMPs interaction. And this method can be used to measure the interaction under a crowding condition that resembles the real situation in the periplasm.

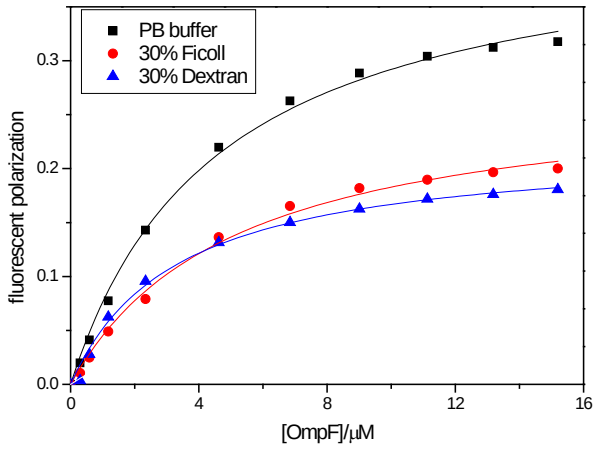

Figure 6. 13 Fluorescence polarization titration of OmpF in phosphate buffer (black) with the addition of 30% Ficoll (red) and 30% Dextran (blue) into FITC labeled SurA.

6. 4 CONCLUSION

SurA is the primary periplasmic molecular chaperone that facilitates the folding and assembling of the outer membrane proteins of Gram-negative bacteria. Deletion of SurA in *Escherichia coli* leads to a decrease in outer membrane density and an increase in bacterial drug susceptibility. In this study, the roles of structural flexibility and stability of SurA on its function were examined. Through mutagenesis studies, a single V37G mutation was first identified that drastically decreased the *in vivo* function of SurA. Further characterizations indicated that this mutation disrupted the interaction between two anti-parallel β-sheets located at the N- and C- terminus of SurA, respectively, which decreased the stability of the protein. SurA has no intrinsic cysteine. The loss of activity in V37G could be restored through the introduction of a pair of cysteine and the subsequent formation of a disulfide bond, which stabilized the interaction between the β-sheets and therefore the structure of SurA. To further investigate the mechanism of SurA function, I introduced four additional cysteine pairs distributed at different locations into the SurA structure and confirmed that they all formed disulfide bonds. Next, the function of SurA was examinedand the presence of disulfide bond was found to have no observable impact on SurA function. These results indicated that the drastic decrease of structural flexibility, as a result of disulfide bond formation, has little effect on SurA activity. Therefore, the function of SurA appears to not require large scale conformational change. Additionally, the investigation of OMP level and cell permeability further suggested that SurA affected cell permeability possibly by other mechanisms other than by OMP abundance.

CHAPTER VII. SITE SPECIFIC AND REVERSIBLE PROTEIN IMMOBILIZATION BY A DNA BINDING FUSION TAG

7.1 INTRODUCTION

Protein immobilization is the crucial first step for many applications including the construction of biosensors and protein microarrays, development of immunoassay methods, and employment of enzymes in biotechnology procedures.[224-227] Protein immobilization methods can be categorized as nonspecific and site-specific. Normally, nonspecific immobilization is achieved by physical adsorption or direct chemical reactions with amine, carboxyl, or thiol groups in the protein.[228, 229] It is difficult to control the extent of immobilization and orientation of the immobilized proteinsince there is usually more than one single functional group in the target protein. In addition, chemical modification of functional groups within a protein might change protein structure, leading to protein function loss. This effect has been demonstrated by the decrease of protein activities upon immobilization in many cases.[230, 231] On the other hand, physical adsorption is facilitatedbythe van der waals, electrostatic and hydrophobic interactions.[232] However, suchinteractions are weak, which can cause protein leaching.

A procedure that can produce a homogenous, stable, and active protein layer on a specific surface is highly desirable. Affinity tags and fusion proteins are widely used in order to achieve site-specific and oriented protein immobilization. After being modified with specific binding domains and tags, proteins can be captured by the corresponding affinity matrixes. Poly-histidine tag (histag) is a popular choice and has been used in the immobilization of proteins on the nickel nitrilotriacetic acid (Ni-NTA) resins.[233-235] However, there are several limitations of the binding specificity of the Ni-NTA resin. At least three*E. coli* endogenous proteins has showed certain degree of affinity to the resin.[236] Also, if a protein is rich in histidine, it could

interact with the resin nonspecifically; therefore compete with the target protein and complicate the immobilization procedure. Other fusion domains have also being used to immobilize target proteins, including the glutathione S-transferase, maltose binding protein, chitin binding protein, streptag and metal binding peptide .237-239

Compared to protein, oligonucleotides are easier to be modified and specifically immobilized due to its simpler structure and chemical composition.For example, DNA microarray is awell-established and commercialized routine technique. It has been used extensively to direct the assembly of proteins. In most of these studies, a ssDNA-target protein conjugation was first created whichthen was attached to a matrix modified with the complementary strand of the ssDNA.[239-243]These DNA-protein conjugates have been obtained through direct covalent links[244-249],a biotin-streptavidin bridge[250], or the expressed protein ligation[251].RNA-protein fusions have also been constructed for site specific protein immobilization[252, 253].However, there could be some negative impacts on protein activity caused by the chemical modification in formation process of the DNA/RNA-protein conjugate. In a more recent study, protein capture by a DNA functionalized matrix was accomplished through the coiled-coil association of an engineered pair of heterodimeric leucine zippers. One helix of the zipper was chemically linked to the DNA, and the other helix was expressed as a fusion tag to the protein.[254]

To prevent the negative effects of chemical modification to the target protein, Iinvestigatedthe incorporation ofa DNA binding protein as the fusion tag to direct the immobilization of the protein of interest. Recently Gang and coworkers had shown that surface-bound DNAs could serve as anchoring sites to immobilize DNA binding proteins.[255]Herein, I constructed a fusion protein containing an N-terminus super-folder green fluorescent protein (sfGFP) and a C-terminus single-strand DNA binding protein (SSB). In this work, sfGFP was used as a reporter

group to facilitate convenient characterization of immobilization, while SSB facilitated high affinity binding toward single-stranded DNA. The fusion protein sfGFP-SSB retained the properties from both domains, being fluorescent and binding to single stranded DNA. In this work, I have also demonstrated that SSB could be used as a fusion tag to facilitate fast and convenient protein immobilization through the coupling with an ssDNA modified surface.

7.2 MATERIALS AND METHODS

Cloning, Protein Expression and Purification

The SSB and sfGFP gene was amplified by PCR. For SSB, the *E. coli* genomic DNA was used as the template. The gene encoding sfGFP was obtained from Theranostech Inc. (Albuquerque, NM, USA). The PCR products weregel purified, digested and inserted into similarly digested pET28a expression vector to generate plasmid pET28a-SSB and pET28a-sfGFP, which introduced a histag at the N-terminus of the proteins. Next, the gene of sfGFP was cloned into the plasmid pET28a-SSB to generateplasmid pET28a-sfGFP-SSB. All sequences were confirmed by DNA sequencing (Retrogen, CA, USA).

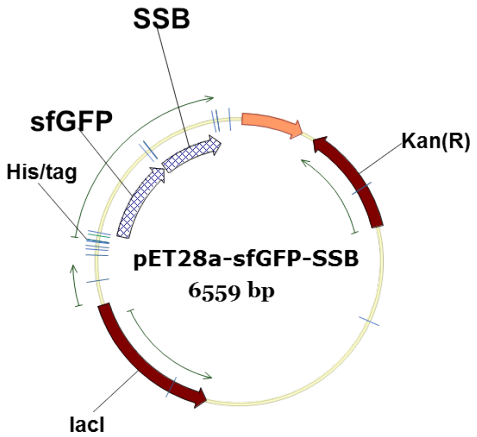

Figure 7.1 Vector map of sfGFP-SSB, pET28a vector was used. Gene encoding sfGFP and SSB were inserted between BamHI/NdeI and BamHI/XhoI restriction enzyme sites, respectively.

Plasmids pET28a-sfGFP-SSB, pET28a-sfGFP and pET28a-SSB were used to transform *E. coli* strain ER2566 for protein production. The cells were grown at 37°C in LB medium containing 100 μg/mL kanamycin to an OD_{600nm} of 0.6, and then induced with 1mM IPTG. Three hours after induction, the cells were harvested by centrifugation at 7,000rpm for 10 min. The cell pellets were resuspended in a binding buffer (100 mM Tris-Cl, 0.5 M NaCl and 10% glycerol, pH 8.1) and lysed by sonication on ice for 10 mins with 10s on-off intervals. The cell debris was removed by centrifugation at 12,000rpm for 15 min. DNaseI was added to the cleared lysate to digest DNA at room temperature for 30 min. The cleared lysate was incubated with Ni-NTA resin (Qiagen, Huntsville, AL) with shaking at room temperature for 45 min and afterward loaded to an empty column. The resin was then washed witha buffer containing 100 mM Tris-Cl, 0.5 M NaCl, 10% glycerol and 50 mM imidazole (pH 8.1). Finally the protein was eluted with a buffer containing 100 mM Tris-Cl buffer, 0.5 M NaCl, 10% glycerol and 500mM imidazole (pH 8.1). Purified sfGFP-SSB, sfGFP and SSB weredialyzed extensively against the binding buffer to remove excess imidazole.

The purified proteins were analyzed using the SDS-PAGE with a 10% homogeneous polyacrylamide gel and visualized with Coomassie Blue stain. Protein concentrations were determined using the Bradford protein assay.

Fluorescence Spectroscopy

Fluorescence emission spectra were collected using a PerkinElmer LS-55 fluorescence spectrometer (PerkinElmer, Waltham, MA) at 20°C. The buffer used for all fluorescence measurements contains 100 mM NaCl and 100 mM Tris-Cl (pH 8.1).

Fluorescence quenching titration was used to measure binding affinity between sfGFP-SSB, SSB, and ssDNA dT_{37}. All oligonucleotideswere obtained from Integrated DNA Technology (San Diego, CA), including dT_{37}, dA_{35},the 5' amine-derivatized dT_{37} (H_2N-dT_{37}), and the 5' thiol-derivatized dT_{37} (RSS-dT_{37}). $dT_{37}$was titratedinto the protein solution and the tryptophan fluorescence weremonitored at excitation and emission wavelengths of 282and 355nm, respectively.

Protein immobilization

H_2N-dT_{37} was attached to the NHS-resin (Sigma-Aldrich, St. Louis, MO). The NHS-resin was first washed with 100 mM sodium-phosphate buffer (pH 7.4),and then incubated with H_2N-dT_{37}(25μmol/L) at room temperature for 2 hours. Finally, Tris-HCl buffer was added to a final concentration of 20 mM to quench the unreacted NHS groups. The modified resin was washed 3 times with 10 times the bed volume using 100mM Tris-HCl buffer (pH 8.1).

RSS-dT_{37} was attached to the DVS-A activated resin (Adar Biotech LTD, Rehovot, Israel). The resin was washed using 100mM sodium phosphate buffer (pH 7.4). RSS-dT_{37} was first reduced to form free thiols using 10mM TCEP in 100mM HAc-NaAc buffer(pH 5.4), and thenincubated with the DVS-A resinat room temperature for 2 hours in 100mM sodium phosphate buffer (pH 7.4). The reaction was then quenched using 20mM DTT. The DNA modified resin was washedusing the same phosphate buffer.

To examine site-specific protein immobilization, sfGFP-SSB or sfGFP was incubated with the DNA modified resins for 15 minutes, in which sfGFP was used as a negative control. Then the resin was collected through centrifugation and washed3 times with 10 bed volumes of thesame Tris-Cl buffer each time. Protein bound to the resin was quantifiedby subtracting the amount of protein left unbound from the total amount of protein added. After protein immobilization and washing, the resins were also examined directly under a fluorescent microscope (Nikon Eclipse 55i, Nikon Instrument Inc., Elgin, IL).

Reversibility of protein immobilization

After sfGFP-SSB was immobilized on NHS-dT_{37} and DVS-A-dT_{37} activated resins in a Tris-Cl buffer (pH 8.1), the effect of different pHs on protein-substrate dissociation was examined. HAc-NaAc buffer was used for pHs 4, 4.5 and 5.0. Sodium phosphate buffer was used for pHs 5.5, 6, 6.5 and 7. Tris-HCl buffer wasused for pHs 7.5, 8, and 8.5. Sodium-glycine buffer was used for pHs 9, 9.5, 10 and 10.5. The indicated buffer (100 mM) was added to sfGFP-SSB modified resin and incubated at room temperature for 30 min. The fluorescence intensity in the supernatant was determined to estimate the quantity of protein dissociated from the beads. The effect of pH on the intrinsic fluorescence of sfGFP-SSB was characterized and adjusted for.

7.3 RESULTS AND DISCUSSION

7.3.1 Construction of fusion protein sfGFP-SSB

Aiming at developing a reversible and site specific method for protein immobilization, I examined the prospect of immobilizing proteins through a DNA binding fusion tag. I created a

fusion protein containing the protein of interest and a ssDNA binding module. To facilitate convenient detection and characterization, I have chosen sfGFP as the model target protein. sfGFP was fused with SSB at the C-terminus. Furthermore, a histag was introduced at the N-terminus of the fusion protein to facilitate convenient purification. As controls, pET28a-histag-sfGFP and pET28a-SSB were also constructed.

Figure 7.2 The construct of the fusion protein, which contains a N-terminus histag, followed by sfGFP, and a C-terminus SSB.

7.3.2 Purification and activity assay of sfGFP-SSB

I was able to express and purify the fusion protein as well as individual modules, sfGFP and SSB, in high yield. Both sfGFP and SSB will be used as controls in future experiments. Figure 7.3 showed the SDS-PAGE analysis of all three proteins. The calculated molecular weights of the proteins using amino acid sequence are 29.0 kDa (sfGFP), 22.5 kDa (SSB) and 48.1 kDa (sfGFP-SSB).

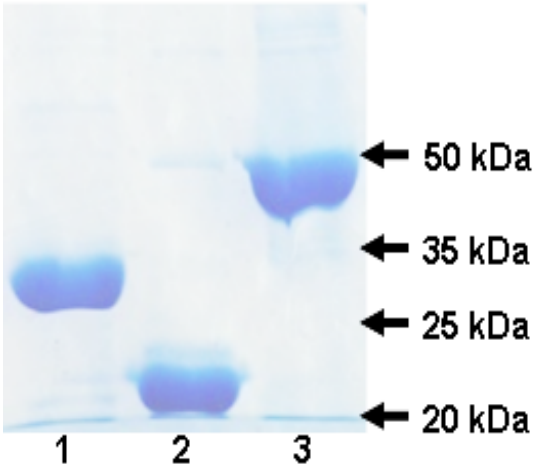

Figure 7.3 SDS-PAGE analysis of purified sfGFP (lane 1), SSB (lane 2) and the sfGFP-SSB fusion protein (lane 3). The molecular weight of the three proteins are 29.0 (sfGFP), 22.5 (SSB) and 48.1 (sfGFP-SSB) kDa. Positions of the molecular weight markers are indicated by arrows.

It is critical to prove SSB is a tetramer, which is responsible for its interaction with ssDNA. I examined the quaternary structure of the fusion protein using the size exclusion chromatography (Figure 7. 4). The retention time of the fusion protein is around 20.4 min, close to the second peak of molecular weight standard (20.7 min). The shorter retention time indicated the size of protein is slightly larger than the molecular weight of the second standard, which is 158 kDa. Since the molecular weight of each sfGFP-SSB subunit is 48.1, this result suggests that the fusion protein is likely to be a tetramer.

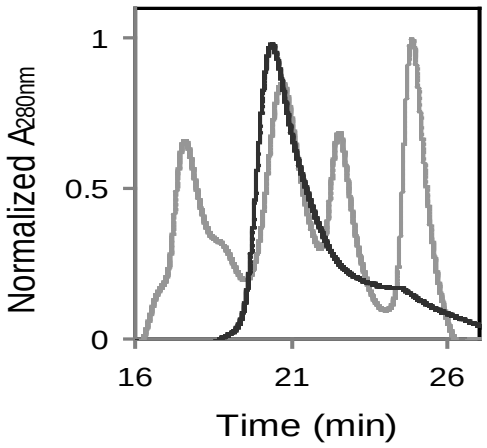

Figure 7.4 Size exclusion chromatography analysis of the fusion protein (black trace). The grey trace is the molecular weight standard. From left to right, the peaks correspond to 670, 158, 44, and 17 kDa, respectively.

To examine the influence of fusing on properties of each individual module, I measured the fluorescence emission as well as the ssDNA binding affinity of the fusion protein. I first compared the fluorescent emissions of sfGFP and sfGFP-SSB. There is a red shift of the emission peak, from 509 nm for sfGFP to 512 nm for sfGFP-SSB (Figure 7.5). The peak shift is likely due to the local environmental change with the addition of SSB at the C-terminus.

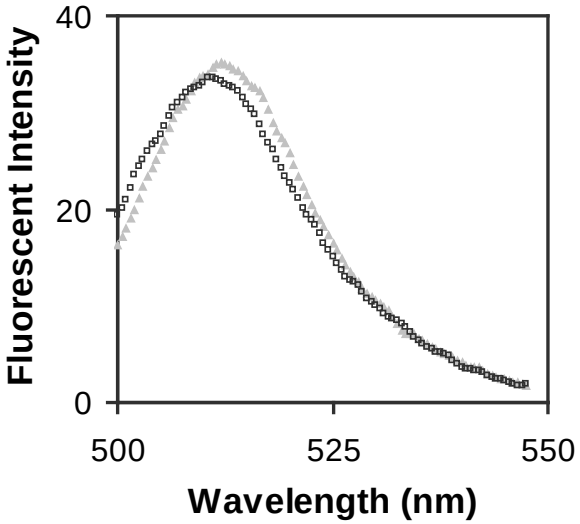

Figure 7.5 Fluorescent emission spectra of sfGFP (open square) and sfGFP-SSB (filled triangle) measured with the excitation wavelength of 490 nm. The concentration of both proteins is 45 nM. The maximum emission wavelengths of sfGFP-SSB and sfGFP are 512nm and 509nm, respectively.

Figure 7.6 shows the plots of fluorescent intensity of each protein at increasing concentrations. Linear fitting of the plots for sfGFP and sfGFP-SSB yielded slopes of 0.752 and 1.436, respectively. The linear range of fluorescence vs. protein concentration was from 1 nM to 1 μM. Slopes of the two lines show that the fluorescent intensity of the fusion protein is enhanced by approximately one fold compared to that of the sfGFP.

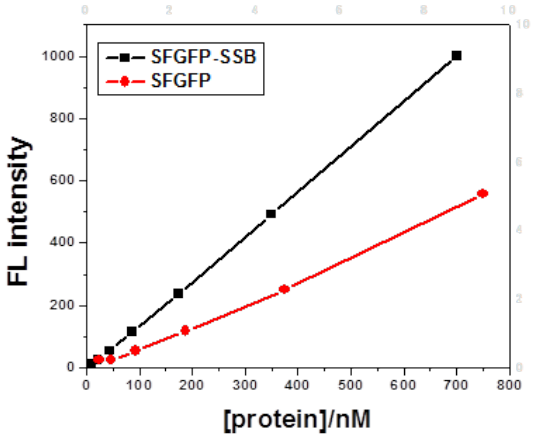

Figure 7.6 Fluorescent intensity of different concentration of sfGFP-SSB and SFGFP concentration. Linear curve for sfGFP is Y=0.752[sfGFP]-16.205, linear curve for sfGFP-SSB is Y=1.436[sfGFP-SSB]-8.850.

I then examined the ssDNA binding affinity of sfGFP-SSB, SSB was used as a control. Previous studies showed that when SSB bound to dT_{37},the tryptophan fluorescence of the protein decreased.[256]Based on the percentage of fluorescent quenching, the binding affinity between SSB and dT_{37} could be determined. sfGFP has one tryptophan, W57. Intrinsic tryptophan fluorescence emission of sfGFP is very small compared to that of SSB, which won't interfere with the SSB tryptophan fluorescence titration (Figure 7.7a). The excitation and emission wavelengths were 282 and 355 nm, respectively. Under our experimental condition, the intensity of sfGFP emission was about 3% of the intensity of SSB emission. Furthermore, the addition of dT_{37} had no effect on the emission of sfGFP (Figure 7.7b).

Finally, I compared the effect of dT_{37} on sfGFP-SSB and SSB tryptophan fluorescence (Figure 7.7c). The fluorescence quenching curvesof the two proteins superimposed well in the concentration range examined (between $10^{-9.5}$M to 10^{-7}M), and matched the result from the

literature for SSB.[257] This result indicates that the ssDNA binding affinity of SSB was not affected in the fusion protein.

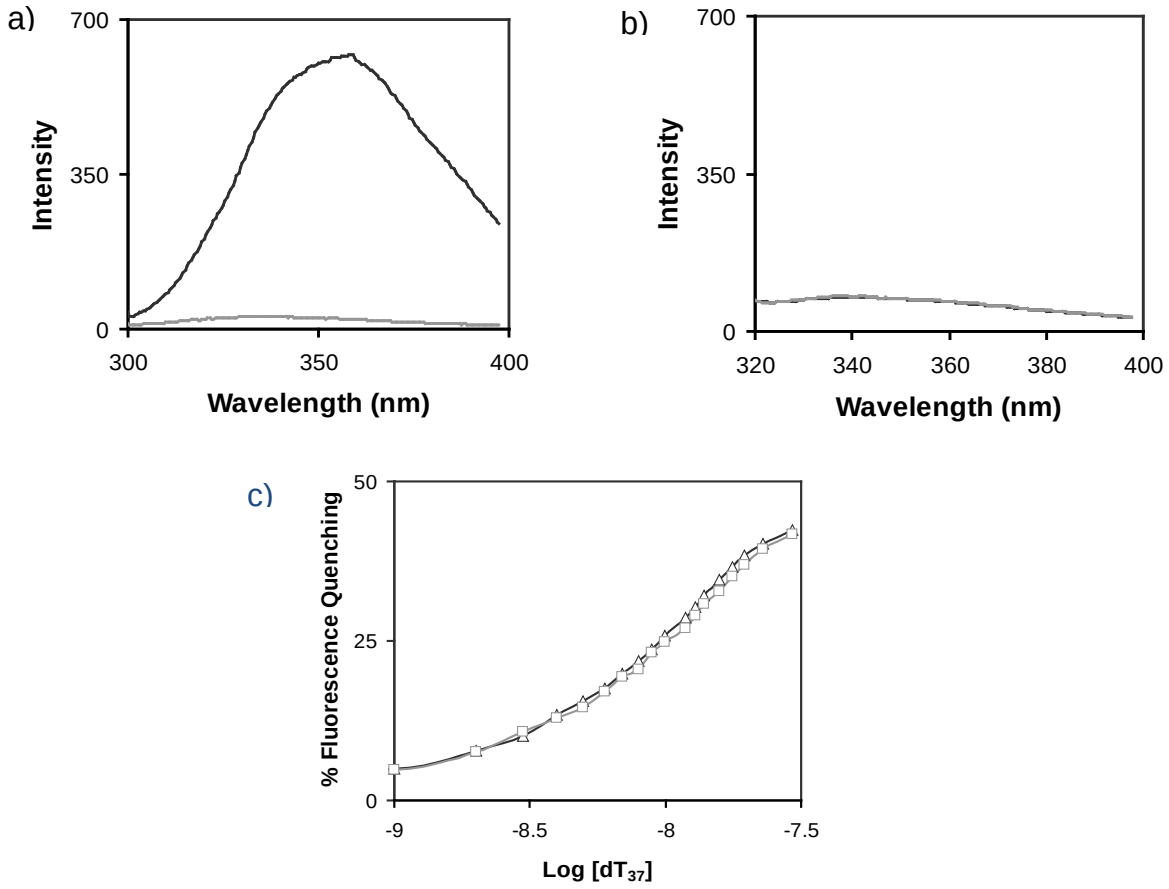

Figure 7.7 a) Tryptophan fluorescence spectra of sfGFP (grey) and SSB (black) when excited at 282 nm. b) Tryptophan fluorescence spectra of sfGFP before (black) and after adding $3.75*10^{-7}$ dT_{37} (gray). b) Fluorescence quenching of sfGFP-SSB (grey) and SSB (black) in the presence of dT_{37}. The excitation and emission wavelengths are 282 and 357 nm, respectively. The concentrations of both proteins are 4.2×10^{-7} M.

7.3.3 Cation, pH dependent sFGFP-SSB and resin binding

Interaction between SSB and ssDNA was highly dependent on pH and cation concentration.[258-260] I expect the binding of sfGFP-SSB to dT_{37} to be sensitive to changes of pH and cationic concentration as well. Therefore, Icharacterized their interaction at different pHs (pH 8.1 and pH 10) and NaCl and $MgCl_2$ concentrations, aiming at identifying conditions that could enable reversible protein immobilization. There were two major binding modes between SSB and dT_{37}, named $(SSB)_{35}$ and $(SSB)_{65}$. The subscripts refer to the length of the oligonucleotides interactingwithone SSB tetramer (35). In the $(SSB)_{35}$ binding mode, ssDNA only interacts with two of the four SSB subunits in a tetramer. On the other hand, in the $(SSB)_{65}$ binding mode, all four subunits participate in DNA binding. The switch between the two binding modes is sensitive tochanges in pH, temperature, andcation concentrations. For example, when the concentration of Na^+ is less than 10mM, the main binding mode is the $(SSB)_{35}$ mode. And, $(SSB)_{65}$ mode is the main binding mode when Na^+ concentration is higher than 200mM. For $MgCl_2$, such a switch happens at a much lower Mg^{2+} concentration, usually the switch to $(SSB)_{65}$ mode occurs at 5 mM $MgCl_2$. I examined the effect of NaCl and $MgCl_2$ on the ssDNA binding of the fusion protein. I found that sfGFP-SSB behaved very much like the free SSB. ssDNA titration experiment using dT_{37} showed that fluorescence quenching reached a plateau at 60% in 1 mM NaCl. While in the presence of 2.5mM $MgCl_2$, 90% of the tryptophan emission was quenched (Figure 7.8A).

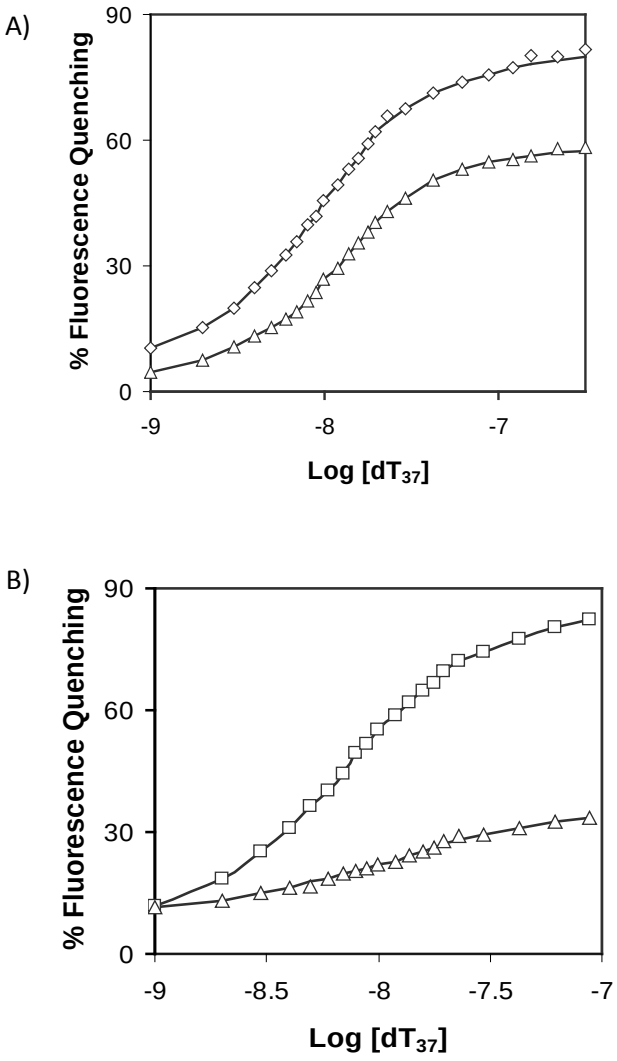

Figure 7.8 A) sfGFP-SSB and dT_{37} binding monitored as tryptophan fluorescence quenching in the presence of 1 mM NaCl, 25 mM Tris-Cl, pH 8.1 (triangle) or 1 mM $MgCl_2$, 25 mM Tris-Cl, pH 8.1 (diamond). The concentration of sfGFP-SSB is 1.4×10^{-7} M. B) sfGFP-SSB and dT_{37} binding at pH 6.9 with 2.5 mM $MgCl_2$ (square) or pH 10 with 1 mM NaCl (triangle).

These results indicate that the fusion protein also has two binding modes, similar to the two binding modes of SSB. There are two binding sites per SSB tetramer (each binding site contains two SSB subunits). A negative cooperation exists between bindings at these two sites.[260] As salt

concentration decreases, this negative cooperation increases. This explains why the percentage fluorescence quenching upon binding was different in the presence of 1mM NaCl or 2.5 mM $MgCl_2$.

Next, I examined a series of pH and cation concentrations and their combinations to identify conditions that maximize or minimize the interaction between sfGFP-SSB and dT_{37}. These two conditions could be used potentially as the binding and elution conditions during protein immobilization experiments. I found that pH6.9, 2.5mM $MgCl_2$ was the best condition for sfGFP-SSB and dT_{37} binding, while pH 10, 1mM NaCl minimized this binding (Figure 7.8 B).

7.3.4 Reversible immobilization of sfGFP-SSB on NHS- and DVS-A activated resin

To examine the binding of sfGFP-SSB with immobilized ssDNA, I first covalently attached chemically derivatized dT_{37} to a solid matrix. Two kinds of chemical reactions were tested for the attachment: amine-derivatized ssDNA to NHS functionalized resin and thiol-derivatized ssDNA to DVS-A activated resin. After the modification, the resins were washed extensively to remove the unreacted ssDNA. Next, sfGFP-SSB or sfGFP were incubated under the same experimental condition in the presence of the modified resins. I used sfGFP as a negative control to examine the effect of non-specific interaction between the protein and the beads. After incubation, the resins were separated from excess proteins by centrifugation and washed extensively using the binding buffer. The white color of the modified resins indicated that nonspecific binding of sfGFP was very weak compared to the SSB facilitated specific binding (Figure 7.9).

a) 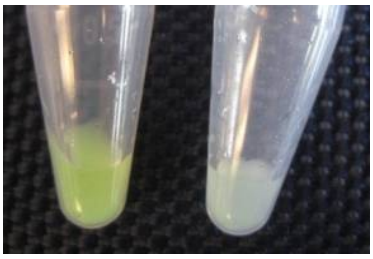 b) 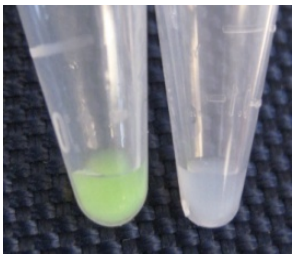

Figure 7.9 Protein immobilization on NHS-dT_{37} (a) or DVS-A-dT_{37} (b) resins. In each panel, the resins in the microcentrifuge tubes were incubated with sfGFP-SSB (left) or sfGFP (right), and then washed extensively.

Next, fluorescent microscope was used to further characterize both types of resins incubated with sfGFP or sfGFP-SSB (Figure 7. 10). The control resins were not fluorescent, further confirming the lack of nonspecific interaction. The amount of sfGFP-SSB immobilized was determined to be around 2.6or 1.8 mg protein per ml of drained NHS or DVS-A activated resins.

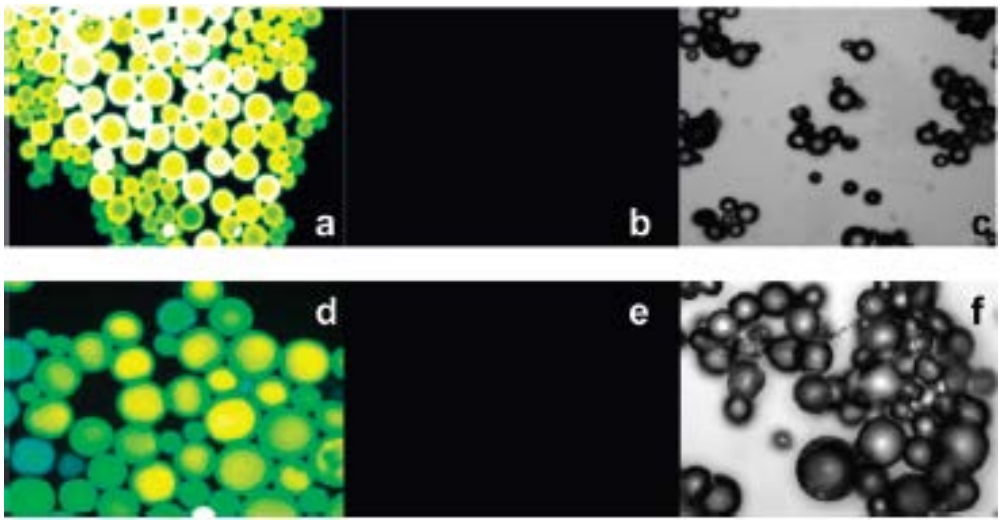

Figure 7.10 Protein modified NHS-dT_{37} (a, b and c) and DVS-A-dT_{37} (d, e and f) imaged using fluorescent light (a, b, d and e) or normal white light (c and f). Resins in panels a and d were treated with sfGFP-SSB. Resins in panels b, c, e and f were treated with sfGFP.

An immobilization method that is reversible is highly desirable as it introduced an additional level of flexibility to the process. I evaluated twoapproaches to elute the protein off the resins: addition of the complementary dA_{35} oligonucleotideand change of pH/salt concentration. I first

examined the reversibility of sfGFP-SSB interaction with the immobilized dT_{37} through the addition of dA_{35}. Binding of the two oligonucleotides generated double stranded DNA, which did not bind to SSB. Eluted sfGFP-SSB was quantified through its fluorescence emission. In the presence 125μM dA_{35}, 82.4% of bound protein was eluted within the first 10 min of incubation (Figure 7.11).

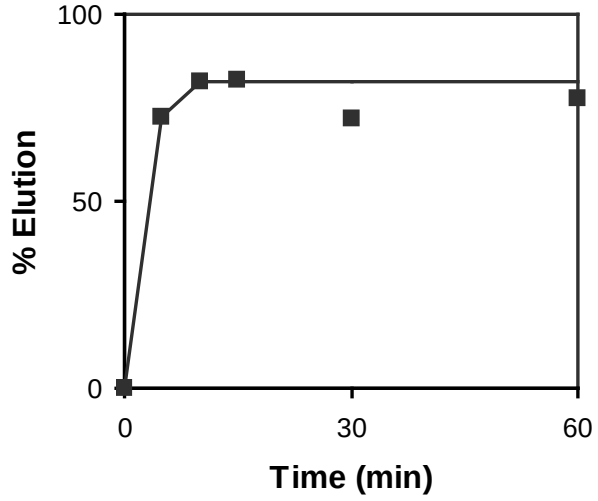

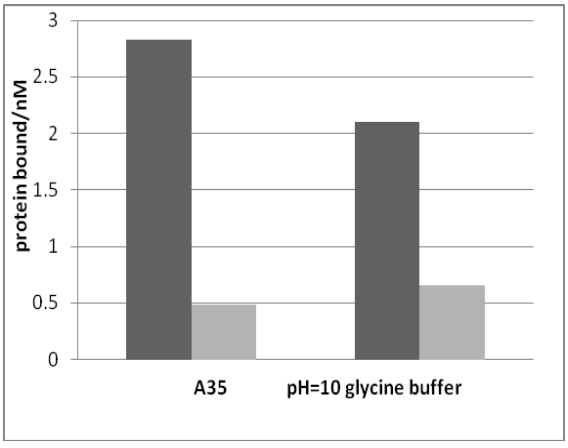

Figure 7.11 Effect of incubation time on protein elution by dA_{35} and glycine buffer (pH=10). 82.4% and 68.4% of protein could be eluted by dA_{35} and glycine buffer in 10 minutes, respectively.

In addition, the resin could be regenerated by the treatment of free dT_{37}, which competitively bound to dA_{35} and removed them from the resin. Addition of fresh sfGFP-SSB changed the color of the resins from white to green again (Figure 7.12).

Figure 7.12 Reversible immobilization of sfGFP-SSB on NHS-resin. NHS-dT_{37} resins modified with sfGFP-SSB (left), elutedusing dA_{35} (middle), and then regenerated and incubated with fresh sfGFP-SSB (right).

To identify a more cost effective and convenient method to release the fusion protein from the resin, I examined the effect of pH/salt concentration on the elution of the fusion protein. I found that 68.4% of sfGFP-SSB could be eluted by the condition identified above (Na-glycine buffer, 1 mM NaCl, pH 10). To examine the reversibility of binding, the pH value of the protein eluate was adjusted to 8.1 and mixed with fresh resins. In parallel, fresh sfGFP-SSB was added to the resinafter pH mediated elution and re-equilibration. In both cases, sfGFP effectively bound to the resin.

7.7 CONCLUSION

In summary, I have demonstrated that SSB could serve as a versatile fusion tag to facilitate ssDNA-mediated protein immobilization. SSB is very stable and shows no negative effect of the overall expression and stability of the fusion protein. The binding between SSB and ssDNA is very tight, with nM affinity. And yet such interaction can be attenuated through the change of pH/salt concentration, which could serve as a convenient method to elute the immobilized

protein and regenerate the surface without denaturing the fusion protein. Compared to other DNA- or RNA-mediated protein immobilization methods, our approach has the advantage of not requiring additional chemical modification. And thus, an array of potential complications related to chemical modifications is avoided, including selectivity, specificity, extent of chemical reaction, purification of the modified protein, and protein denaturation issues.

REFERENCE

1. Wainwright, M. (1989). Moulds in ancient and more recent medicine. *Mycologist* **3**, 21-3.
2. Diggins, F. (1999). The true history of the discovery of penicillin, with refutation of the misinformation in the literature. *BrJ Biomed Sci* **56**, 83-93.
3. Weiss, R., & McMichael A. (2004). Social and environmental risk factors in the emergence of infectious diseases. *Nat Med* **10**, S70-6.
4. Thomson, C., Power, E., Ruebsamen-Waigmann, H., & Labischinski, H. (2004). Antibacterial research and development in the 21st century – an industry perspective of the challenges. *Curr Opin Microbiol* **7**, 445-50.
5. Mingeot-Leclercq, M., Glupczynski, Y., & Tulkens, P. (1999). Aminoglycosides: activity and resistance. *Antimicrob Agents Chemother* **43**, 727-37.
6. Demain, A., & Elander R. (1999). The β-lactam antibiotics: past, present, and future. *Antonie Van Leewenhoek* **75**, 5-19.
7. Chen J., & Stubbe J. (2005). Bleomycins: towards better therapeutics. *Nat Rev Cancer* **5**, 102-12.
8. Peschel A. & Sahl H. (2006). The co-evolution of host cation antimicrobial peptides and microbial resistance. *Nat Rev Microbiol* **4**, 529-36.
9. McDonnell, G., & Russell, A. (1999). Antiseptics and disinfectants: activity, action and resistance. *Clin Microbiol Rev* **12**, 147-79.
10. Koehn, F., & Carter G. (2005). The evolving role of natural products in drug discovery. *Nat Rev Drug Discov* **4**, 206-220.
11. Butler, M. (2004). The role of natural product chemistry in drug discovery. *J Nat Prod* **67**, 2141-2153.

12. Hermann, T. (2005). Drugs targeting the ribosome. *Curr Opin Struc Biol* **15**, 355-66.
13. Acred, P., Brown, D., Knudsen, E., Rolinson, G., & Sutherla, R. (1967). New semi-synthetic penicillin active against pseudomonas pyocyanea. *Nature* **215**, 25-30.
14. Walsh, C. (2003).Where will new antibiotics come from? *Nat Rev Microbiol* **1**, 65-70.
15. Wright, G. (2007). The antibiotic resistome: the nexus of chemical and genetic diversity. *Nat Rev Microbiol* **5**, 175-86.
16. Fernandes, P. (2006). Antibacterial discovery and development – the failure of success? *Nat Biotechnol* **24**, 1497-1503.
17. Barrett, J. (2005). Can biotech deliver new antibiotics? *Curr Opin Microbiol* **8**, 498-503.
18. Coates A., Halls G., & Hu Y. (2011). Novel classes of antibiotics or more of the same? Br. *J Pharmacol* **163**, 184-194.
19. Baltz, R., Miao V., & Wrigley, S. (2005). Natural products to drugs: daptomycin and related lipopeptide antibiotics. *Nat Prod Rep* **22**, 717-41.
20. Livermore, D. (2005). Tigecycline: what is it, and where should it be used? *J Antimicrob Chemother* **56**, 611-614.
21. Shinabarger, D., Marotti, K., Murray, R., Lin A., Melchior, E., Swaney, S., Dunyak, D., Demyan, W., & Buysse, J. (1997). Mechanism of action of oxazolidinones: effects of linezolid and eperezolid on translation reactions. *Antimicrob Agents Chemother* **41**, 2132-6.
22. Mullane, K., Miller, M., Weiss, K., Lentnek, A., Golan, Y., Sears, P., Shue, Y., Louie, T. & Gorbach, S. (2011). Efficacy of fidaxomicin versus vancomycin as therapy for Clostridium difficile infection in individuals taking concomitant antibiotics for other concurrent infections. *Clin Infect Dis* **53**, 440-7.

23. Fraise, A. (2002). Biocide abuse and antimicrobial resistance – a cause for concern? *J Antimicrob Chemother* **49**, 11-2.
24. Huovinen, P., & Cars, O. (1998). Control of antimicrobial resistance: time for action. The essentials of control are already well known. *BMJ* **317**, 613-4.
25. Levy, SB (1998). The challenge of antibiotic resistance. Sci. Am. 278, 46-53.
26. McEwen, S., & Fedorka-Cray P. (2002). Antimicrobial use and resistance in animals. *Clin Infect Dis* **34**, 93-106.
27. Leclercq, R., & Courvalin, P. (1991). Intrinsic and unusual resistance to macrolide, lincosamide, and streptogramin antibiotics in bacteria. *Antimicrob Agents Chemother* **35**, 1273-6.
28. Hancock, R. (1998). Resistance mechanisms in *Pseudomonas aeruginosa* and other nonfermentative gram-negative bacteria. *Clin Infect Dis* **27**, 93-99.
29. Alonso, A., Sanchez, P., & Martinez, J. (2001). Environmental selection of antibiotic resistance genes. *Enviorn Microbiol* **3**, 1-9.
30. Ochman, H., Lawrence, J., & Groisman, E. (2000). Lateral gene transfer and the nature of bacterial innovation. *Nature* **405**, 299-304.
31. Aminov, R. (2010). A brief history of the antibiotic era: lessons learned and challenges for the future. *Front Microbiol* **1**, 134.
32. Grundmann, H, Aires-de-Sousa, M, Boyce, J, and Tiemersma, E (2006) Emergence and resurgence of meticillin-resistant Staphylococcus aureus as a public-health threat. *Lancet* **368**, 874-885.
33. Moellering, R. C., Jr. (2010). NDM-1--a cause for worldwide concern. *N Engl J Med* **363**, 2377-9.

34. Hsueh, P. R. (2010). New Delhi metallo-ss-lactamase-1 (NDM-1): an emerging threat among Enterobacteriaceae. *J Formos Med Assoc* **109**, 685-7.

35. Gupta, N., Limbago, B. M., Patel, J. B. &Kallen, A. J. (2011). Carbapenem-resistant Enterobacteriaceae: epidemiology and prevention. *Clin Infect Dis* **53**, 60-7.

36. Walsh, C. (2000). Molecular mechanisms that confer antibacterial drug resistance. *Nature* **406**, 775-81.

37. Seward, R. J., Lambert, T. & Towner, K. J. (1998). Molecular epidemiology of aminoglycoside resistance in Acinetobacter spp. *J Med Microbiol* **47**, 455-62.

38. Baba, T., Takeuchi, F., Kuroda, M., Yuzawa, H., Aoki, K., Oguchi, A., Nagai, Y., Iwama, N., Asano, K., Naimi, T., Kuroda, H., Cui, L., Yamamoto, K. &Hiramatsu, K. (2002). Genome and virulence determinants of high virulence community-acquired MRSA. *Lancet* **359**, 1819-27.

39. Davies, J. (1994). Inactivation of antibiotics and the dissemination of resistance genes. *Science* **264**, 375-82.

40. Bradford, P. A. (2001). Extended-spectrum beta-lactamases in the 21st century: characterization, epidemiology, and detection of this important resistance threat. *ClinMicrobiol Rev* **14**, 933-51, table of contents.

41. Longley, D. B. & Johnston, P. G. (2005). Molecular mechanisms of drug resistance. *J Pathol* **205**, 275-92.

42. Ge, M., Chen, Z., Onishi, H. R., Kohler, J., Silver, L. L., Kerns, R., Fukuzawa, S., Thompson, C. &Kahne, D. (1999). Vancomycin derivatives that inhibit peptidoglycan biosynthesis without binding D-Ala-D-Ala. *Science* **284**, 507-11.

43. Nikaido, H. (1996). Multidrug efflux pumps of gram-negative bacteria. *J Bacteriol* **178**, 5853-9.

44. Nikaido, H. (1994). Prevention of drug access to bacterial targets: permeability barriers and active efflux. *Science* **264**, 382-8.

45. Coates, A., Hu, Y., Bax, R. & Page, C. (2002). The future challenges facing the development of new antimicrobial drugs. *Nat Rev Drug Discov* **1**, 895-910.

46. Vollmer, W. (2012). Bacterial outer membrane evolution via sporulation? *Nat Chem Biol* **8**, 14-8.

47. Nikaido, H. &Vaara, M. (1985). Molecular basis of bacterial outer membrane permeability. *Microbiol Rev* **49**, 1-32.

48. Hancock, R. E. (1997). The bacterial outer membrane as a drug barrier. *Trends Microbiol* **5**, 37-42.

49. Marquez, B. (2005). Bacterial efflux systems and efflux pumps inhibitors. *Biochimie* **87**, 1137-47.

50. Webber, M. A. &Piddock, L. J. (2003). The importance of efflux pumps in bacterial antibiotic resistance. *J AntimicrobChemother* **51**, 9-11.

51. Eswaran, J., Koronakis, E., Higgins, M. K., Hughes, C. &Koronakis, V. (2004). Three's company: component structures bring a closer view of tripartite drug efflux pumps. *CurrOpinStructBiol* **14**, 741-7.

52. Koronakis, V., Sharff, A., Koronakis, E., Luisi, B. & Hughes, C. (2000). Crystal structure of the bacterial membrane protein TolC central to multidrug efflux and protein export. *Nature* **405**, 914-9.

53. Koronakis, V., Eswaran, J. & Hughes, C. (2004). Structure and function of TolC: the bacterial exit duct for proteins and drugs. *Annu Rev Biochem* **73**, 467-89.

54. Sharff, A., Fanutti, C., Shi, J., Calladine, C. & Luisi, B. (2001). The role of the TolC family in protein transport and multidrug efflux. From stereochemical certainty to mechanistic hypothesis. *Eur J Biochem* **268**, 5011-26.

55. Yu, E. W., Aires, J. R. & Nikaido, H. (2003). AcrB multidrug efflux pump of Escherichia coli: composite substrate-binding cavity of exceptional flexibility generates its extremely wide substrate specificity. *J Bacteriol* **185**, 5657-64.

56. Nakamura, H., Hachiya, N. & Tojo, T. (1978). Second acriflavine sensitivity mutation, acrB, in Escherichia coli K-12. *J Bacteriol* **134**, 1184-7.

57. Murakami, S., Nakashima, R., Yamashita, E. & Yamaguchi, A. (2002). Crystal structure of bacterial multidrug efflux transporter AcrB. *Nature* **419**, 587-93.

58. Lu, W., Zhong, M. & Wei, Y. (2011). Folding of AcrB Subunit Precedes Trimerization. *J Mol Biol* **411**, 264-74.

59. Symmons, M. F., Bokma, E., Koronakis, E., Hughes, C. & Koronakis, V. (2009). The assembled structure of a complete tripartite bacterial multidrug efflux pump. *Proc Natl Acad Sci U S A* **106**, 7173-8.

60. Schuldiner, S. (2006). Structural biology: the ins and outs of drug transport. *Nature* **443**, 156-7.

61. Murakami, S., Nakashima, R., Yamashita, E., Matsumoto, T., & Yamaguchi, A. (2006). Crystal structures of a multidrug transporter reveal a functionally rotating mechanism. *Nature* **443**, 173-9.

62. Seeger, M., Schiefner, A., Eicher, T., Verrey, F., Diederichs, K., & Pos, K.M. (2006). Structural asymmetry of AcrB trimer suggests a peristaltic pump mechanism. *Science* **313**, 1295-8.

63. Murakami, S. (2008). Multidrug efflux transporter, AcrB--the pumping mechanism. *Curr Opin Struct Biol* **18**, 459-65.

64. Guan, L. & Nakae, T. (2001). Identification of essential charged residues in transmembrane segments of the multidrug transporter MexB of Pseudomonas aeruginosa. *J Bacteriol* **183**, 1734-9.

65. Elkins, C. A. & Nikaido, H. (2002). Substrate specificity of the RND-type multidrug efflux pumps AcrB and AcrD of Escherichia coli is determined predominantly by two large periplasmic loops. *J Bacteriol* **184**, 6490-8.

66. Yu, E. W., Aires, J. R., McDermott, G. & Nikaido, H. (2005). A periplasmic drug-binding site of the AcrB multidrug efflux pump: a crystallographic and site-directed mutagenesis study. *J Bacteriol* **187**, 6804-15.

67. Bohnert, J. A., Karamian, B. & Nikaido, H. (2010). Optimized Nile Red efflux assay of AcrAB-TolC multidrug efflux system shows competition between substrates. *Antimicrob Agents Chemother* **54**, 3770-5.

68. Husain, F. & Nikaido, H. (2010). Substrate path in the AcrB multidrug efflux pump of Escherichia coli. *Mol Microbiol* **78**, 320-30.

69. Husain, F., Bikhchandani, M. & Nikaido, H. (2011). Vestibules are part of the substrate path in the multidrug efflux transporter AcrB of Escherichia coli. *J Bacteriol* **193**, 5847-9.

70. Nikaido, H. (2003). Molecular basis of bacterial outer membrane permeability revisited. *Microbiol Mol Biol Rev* **67**, 593-656.

71. Tommassen, J., van Tol, H. & Lugtenberg, B. (1983). The ultimate localization of an outer membrane protein of Escherichia coli K-12 is not determined by the signal sequence. *EMBO J* **2**, 1275-9.

72. Ruiz, N., Kahne, D. & Silhavy, T. J. (2006). Advances in understanding bacterial outer-membrane biogenesis. *Nat Rev Microbiol* **4**, 57-66.

73. Andersen, C. L., Matthey-Dupraz, A., Missiakas, D. & Raina, S. (1997). A new Escherichia coli gene, dsbG, encodes a periplasmic protein involved in disulphide bond formation, required for recycling DsbA/DsbB and DsbC redox proteins. *Mol Microbiol* **26**, 121-32.

74. Bos, M. P., Robert, V. & Tommassen, J. (2007). Biogenesis of the gram-negative bacterial outer membrane. *Annu Rev Microbiol* **61**, 191-214.

75. Hagan, C. L., Kim, S. & Kahne, D. (2010). Reconstitution of outer membrane protein assembly from purified components. *Science* **328**, 890-2.

76. Sklar, J. G., Wu, T., Kahne, D. & Silhavy, T. J. (2007). Defining the roles of the periplasmic chaperones SurA, Skp, and DegP in Escherichia coli. *Genes Dev* **21**, 2473-84.

77. Wu, S., Ge, X., Lv, Z., Zhi, Z., Chang, Z. & Zhao, X. S. (2011). Interaction between bacterial outer membrane proteins and periplasmic quality control factors: a kinetic partitioning mechanism. *Biochem J* **438**, 505-11.

78. De Las Penas, A., Connolly, L. & Gross, C. A. (1997). SigmaE is an essential sigma factor in Escherichia coli. *J Bacteriol* **179**, 6862-4.

79. Vertommen, D., Ruiz, N., Leverrier, P., Silhavy, T. J. & Collet, J. F. (2009). Characterization of the role of the Escherichia coli periplasmic chaperone SurA using differential proteomics. *Proteomics* **9**, 2432-43.

80. Rouviere, P. E. & Gross, C. A. (1996). SurA, a periplasmic protein with peptidyl-prolyl isomerase activity, participates in the assembly of outer membrane porins. *Genes Dev* **10**, 3170-82.

81. Webb, H. M., Ruddock, L. W., Marchant, R. J., Jonas, K. & Klappa, P. (2001). Interaction of the periplasmic peptidylprolyl cis-trans isomerase SurA with model peptides. The N-terminal region of SurA id essential and sufficient for peptide binding. *J Biol Chem* **276**, 45622-7.

82. Bitto, E. & McKay, D. B. (2003). The periplasmic molecular chaperone protein SurA binds a peptide motif that is characteristic of integral outer membrane proteins. *J Biol Chem* **278**, 49316-22.

83. Xu, X., Wang, S., Hu, Y. X. & McKay, D. B. (2007). The periplasmic bacterial molecular chaperone SurA adapts its structure to bind peptides in different conformations to assert a sequence preference for aromatic residues. *J Mol Biol* **373**, 367-81.

84. Rondelet, A. & Condemine, G. (2012). SurA is involved in the targeting to the outer membrane of a Tat signal sequence-anchored protein. *J Bacteriol* **194**, 6131-42.

85. Alcock, F. H., Grossmann, J. G., Gentle, I. E., Likic, V. A., Lithgow, T. & Tokatlidis, K. (2008). Conserved substrate binding by chaperones in the bacterial periplasm and the mitochondrial intermembrane space. *Biochem J* **409**, 377-87.

86. Weinstein, R. A. (2001). Controlling antimicrobial resistance in hospitals: infection control and use of antibiotics. *Emerg Infect Dis* **7**, 188-92.

87. Hancock, R. E. & Patrzykat, A. (2002). Clinical development of cationic antimicrobial peptides: from natural to novel antibiotics. *Curr Drug Targets Infect Disord* **2**, 79-83.

88. Hancock, R. E. (1984). Alterations in outer membrane permeability. *Annu Rev Microbiol* **38**, 237-64.

89. Girard, M. P., Cherian, T., Pervikov, Y. & Kieny, M. P. (2005). A review of vaccine research and development: human acute respiratory infections. *Vaccine* **23**, 5708-24.

90. Summers, W. C. (2001). Bacteriophage therapy. *Annu Rev Microbiol* **55**, 437-51.

91. Pages, J. M., Masi, M. & Barbe, J. (2005). Inhibitors of efflux pumps in Gram-negative bacteria. *Trends Mol Med* **11**, 382-9.

92. Meng, J., Bai, H., Jia, M., Ma, X., Hou, Z., Xue, X., Zhou, Y. & Luo, X. (2012). Restoration of antibiotic susceptibility in fluoroquinolone-resistant Escherichia coli by targeting acrB with antisense phosphorothioate oligonucleotide encapsulated in novel anion liposome. *J Antibiot (Tokyo)* **65**, 129-134.

93. Spellberg, B., Powers, J., Brass, E., Miller, L., & Edwards, J. Jr. (2004). Trends in antimicrobial drug development: Implications for the future. *Clin Infect Dis* **38**, 1279-86.

94. Jarvis, L. (2007). Imminent threat: As gram-negative bacteria become resistant to current antibiotics, the search for new drugs accelerates. *Chem Eng News* **86**, 21-4.

95. Livermore, D. (2009) Has the era of untreatable infections arrived? *J Antimicrob Chemother* **64** (Suppl. 1), i29–i36.

96. Lee, J., Jeong, S., Cha, S., & Lee, S. (2007) A lack of drugs for antibiotic-resistant Gram-negative bacteria. *Nat Rev Drug Discov* **6**, 938-9.

97. Ma, D., Cook, D., Alberti, M., Pon, N., Nikaido, H., & Hearst, J. (1995) Genes acrA and acrB encode a stress-induced efflux system of *Escherichia coli*. *Mol Microbiol* **16**, 45-55

98. Lomovskaya, O., & Watkins, W. (2001) Inhibition of efflux pumps as a novel approach to combat drug resistance in bacteria. *J Mol Microbiol Biotechnol* **3**, 225-36.

99. Lomovskaya, O., Bostian, K. (2006) Practical applications and feasibility of efflux pump inhibitors in the clinic - A vision for applied use. *Biochem Pharmacol* **71**, 910-18.

100. Bremner, J. (2007) Some approaches to new antibacterial agents. *Pure Appl Chem* **79**, 2143-53.

101. Vergidis, P., & Falagas, M. (2008) Multidrug-resistant Gram-negative bacterial infections: The emerging threat and potential novel treatment options. *Curr Opin Investig Drugs* **9**, 176-83.

102. Pages, J. & Amaral, L. (2009) Mechanisms of drug efflux and strategies to combat them: Challenging the efflux pump of Gram-negative bacteria. *Biochim Biophys Acta* **1794**, 826-33.

103. Lobedanz, S., Bokma, E., Symmons, M., Koronakis, E., Hughes, C., & Koronakis, V. (2007) Periplasmic coiled-coil interface underlying TolC recruitment and the assembly of bacterial drug efflux pumps. *Proc Natl Acad Sci U. S. A.* **104**, 4612-17.

104. Murakami, S., Tamura, N., Saito, A., Hirata, T., & Yamaguchi, A. (2004) Extramembrane central pore of multidrug exporter AcrB in *Escherichia coli* plays an important role in drug transport. *J Biol Chem* **279**, 3743-48.

105. Tikhonova, E., & Zgurskaya, H. (2004). AcrA, AcrB, and TolC of *Escherichia Coli* form a stable intermembrane multidrug efflux complex. *J Biol Chem* **279**, 32116-24.

106. Touzé, T., Eswaran, J., Bokma, E., Koronakis, E., Hughes, C., & Koronakis, V. (2004) Interactions underlying assembly of the *Escherichia coli* AcrAB–TolC multidrug efflux system. *Mol Microbiol* **53**, 697–706.

107. Tamura, N., Murakami, S., Oyama, Y., Ishiguro, M., & Yamaguchi, A. (2005) Direct interaction of multidrug efflux transporter AcrB and outer membrane channel TolC detected via site-directed disulfide cross-linking. *Biochemistry* **44**, 11115-21.

108. Su, C., Li, M., Gu, R., Takatsuka, Y., & McDermott, G., Nikaido, H.& Yu, E. (2006) Conformation of the AcrB multidrug efflux pump in mutants of the putative proton relay pathway. *J Bacteriol* **188**, 7290-6.

109. Takatsuka, Y., Nikaido, H. (2006) Threonine-978 in the transmembrane segment of the multidrug efflux pump AcrB of *Escherichia Coli* is crucial for drug transport as a probable component of the proton relay network. *J Bacteriol* **188**, 7284-9.

110. Bohnert, J., Schuster, S., Seeger, M., Fahnrich, E., Pos, K., & Kern, W. (2008) Site-directed mutagenesis reveals putative substrate binding residues in the *Escherichia Coli* RND efflux pump AcrB. *J Bacteriol* **190**, 8225-9.

111. Seeger, M., von Ballmoos, C., Verrey, F., & Pos, K. (2009). Crucial role of Asp408 in the proton translocation pathway of multidrug transporter AcrB: Evidence from site-directed mutagenesis and carbodiimide labeling. *Biochemistry* **48**, 5801-12.

112. Tikhonova, E., Dastidar, V., Rybenkov, V., & Zgurskaya, H. (2009). Kinetic control of TolC recruitment by multidrug efflux complexes. *Proc Natl Acad Sci U. S. A.* **106**, 16416-21.

113. Zgurskaya, H. (2009). Multicomponent drug efflux complexes: architecture and mechanism of assembly. *Future Microbiol* **4**, 919-92.

114. Zgurskaya, H., & Nikaido, H. (1999). Bypassing the periplasm: reconstitution of the AcrAB multidrug efflux pump of *Escherichia coli*. *Proc Natl Acad Sci U. S. A.* **96**, 7190-5.

115. Takatsuka, Y., & Nikaido, H. (2009) Covalently linked trimer of the AcrB multidrug efflux pump provides support for the functional rotating mechanism. *J Bacteriol* **191**, 1729-37.

116. Yu, E., McDermott, G., Zgurskaya, H., Nikaido, H., & Koshland, D. (2003). Structural basis of multiple drug-binding capacity of the AcrB multidrug efflux pump. *Science* **300**, 976-80.

117. Sennhauser, G., Amstutz, P., Briand, C., Storchenegger, O., & Grutter, M. (2007) Drug export athway of multidrug exporter AcrB revealed by DARPin inhibitors. *PLoS Biol* **5**, 106-13.

118. Takatsuka, Y., & Nikaido, H. (2007). Site-directed disulfide cross-linking shows that cleft flexibility in the periplasmic domain is needed for the multidrug efflux pump Acrb of *Escherichia coli*. *J Bacteriol* **189**, 8677-84.

119. Seeger, M., von Ballmoos, C., Eicher, T., Brandstatter, L., Verrey, F., Diederichs, K., & Pos, K. (2008). Engineered disulfide bonds support the functional rotation mechanism of multidrug efflux pump AcrB. *Nat Struc Mol Biol* **15**, 199-205.

120. Schulz, R., Vargiu, A., Collu, F., Kleinekathofer, U., & Ruggerone, P. (2010) Functional rotation of the transporter AcrB: insights into drug extrusion from simulations. *PLoS Comput Biol* **6**: e1000806.

121. Riemer, J., Bulleid, N., & Herrmann, J. (2009). Disulfide formation in the ER and mitochondria: Two solutions to a common process. *Science* **324**, 1284-7.

122. Ruiza, N., Chngb, S., Hinikera, A., Kahne, D., & Silhavy, T. (2001). Nonconsecutive disulfide bond formation in an essential integral outer membrane protein. *Proc Natl Acad Sci U. S. A.*, **107**, 12245-50

123. Leichert, L., & Jakob, U. (2004). Protein thiol modifications visualized *in vivo*. *PLoS Biol* **2**, 1723-37.

124. Rasband, W. ImageJ (1997-2009) U. S. National Institutes of Health, Bethesda, Maryland, USA, http://rsb.info.nih.gov/ij/

125. Abramoff, M., Magelhaes, P., & Ram, S. (2004). Image processing with ImageJ. *Biophotonics Int* **11**, 36-42.

126. Careaga, C., & Falke, J. (1992) Structure and dynamics of *Escherichia coli* chemosensory receptors. Engineered sulfhydryl studies. *Biophys J* **62**, 209-16.

127. Careaga, C., & Falke, J. (1995) Thermal motions of surface alpha-helices in the D-galactose chemosensory receptor. Detection by disulfide trapping. *J Mol Biol* **226**, 1219-35.

128. Careaga, C., & Falke, J. (1995) Large amplitude twisting motions of an interdomain hinge: A disulfide trapping study of the galactose-glucose binding protein. *Biochemistry* **34**, 3048-55.

129. Falke, J., & Koshland, D. (1987). Global flexibility in a sensory receptor-A site directed cross-linking approach. *Science* **237**, 1596-600.

130. Akabas, M., Stauffer, D., Xu, M., & Karlin, A. (1992) Acetylcholine-receptor channel structure probed in cysteine-substitution mutants. *Science* **258**, 307-10.

131. Chervitz, S., Falke, J. (1996). Molecular mechanism of transmembrane signaling by the aspartate receptor: A model. *Proc Natl Acad Sci U S A* **93**, 2545-50.

132. Hughson, A., & Hazelbauer, G. Detecting the conformational change of transmembrane signaling in a bacterial chemoreceptor by measuring effects on disulfide cross-linking *in vivo*. *Proc Natl Acad Sci U S A* **93**, 11546-51.

133. Pakula, A., & Simon, M. (1992) Determination of transmembrane protein structure by disulfide cross-linking-The *Escherichia coli* Tar receptor. *Proc Natl Acad Sci U S A* **89**, 4144-8.

134. Bass, R., Butler, S., Chervitz, S., Gloor, S., & Falke, J. (2007) Use of site-directed cysteine and disulfide chemistry to probe protein structure and dynamics: Applications to soluble and transmembrane receptors of bacterial chemotaxis, *Methods Enzymol* **423**, 25-51.

135. Milanesi, L., Jelinska, C., Hunter, C., Hounslow, A., Staniforth, R., & Waltho, J. (2008) A method for the reversible trapping of proteins in non-native conformations. *Biochemistry* **47**, 13620-34.

136. Ali, M. & Imperiali, B. (2005). Protein oligomerization: how and why. *Bioorg Med Chem* **13**, 5013-20.

137. Goodsell, D. & Olson, A. (2000). Structural symmetry and protein function. *Annu Rev Biophys Biomol Struct* **29**, 105-53.

138. Hong, H., Joh, N., Bowie, J. & Tamm, L. (2009). Methods for measuring the thermodynamic stability of membrane proteins. *Methods Enzymol* **455**, 213-36.

139. Naveed, H., Jackups, R., Jr. & Liang, J. (2009). Predicting weakly stable regions, oligomerization state, and protein-protein interfaces in transmembrane domains of outer membrane proteins. *Proc Natl Acad Sci U S A* **106**, 12735-40.

140. Haltia, T. & Freire, E. (1995). Forces and factors that contribute to the structural stability of membrane proteins. *Biochim Biophys Acta* **1228**, 1-27.

141. Chen, W., Helenius, J., Braakman, I. & Helenius, A. (1995). Cotranslational folding and calnexin binding during glycoprotein synthesis. *Proc Natl Acad Sci U S A* **92**, 6229-33.

142. Copeland, C. , Zimmer, K., Wagner, K. , Healey, G. , Mellman, I. & Helenius, A. (1988). Folding, trimerization, and transport are sequential events in the biogenesis of influenza virus hemagglutinin. *Cell* **53**, 197-209.

143. Prabakaran, D., Kim, P., Dixit, V. & Arvan, P. (1996). Oligomeric assembly of thrombospondin in the endoplasmic reticulum of thyroid epithelial cells. *Eur J Cell Biol* **70**, 134-41.

144. Bulleid, N., Dalley, J. & Lees, J. (1997). The C-propeptide domain of procollagen can be replaced with a transmembrane domain without affecting trimer formation or collagen triple helix folding during biosynthesis. *Embo J* **16**, 6694-701.

145. Xu, D., Tsai, C. & Nussinov, R. (1998). Mechanism and evolution of protein dimerization. *Protein Sci* **7**, 533-44.

146. Wallin, E. & von Heijne, G. (1998). Genome-wide analysis of integral membrane proteins from eubacterial, archaean, and eukaryotic organisms. *Protein Sci* **7**, 1029-38.

147. Green, W. N. & Claudio, T. (1993). Acetylcholine receptor assembly: subunit folding and oligomerization occur sequentially. *Cell* **74**, 57-69.

148. Lu, W., Zhong, M. & Wei, Y. (2011). A reporter platform for the monitoring of in vivo conformational changes in AcrB. *Protein Pept. Lett*. **18**, 863-71

149. Wittig, I., Braun, H. P. & Schagger, H. (2006). Blue native PAGE. *Nat Protoc* **1**, 418-28.

150. Heuberger, E., Veenhoff, L., Duurkens, R., Friesen, R. & Poolman, B. (2002). Oligomeric state of membrane transport proteins analyzed with blue native electrophoresis and analytical ultracentrifugation. *J Mol Biol* **317**, 591-600.

151. Stroebel, D., Sendra, V., Cannella, D., Helbig, K., Nies, D. & Coves, J. (2007). Oligomeric behavior of the RND transporters CusA and AcrB in micellar solution of detergent. *Biochim Biophys Acta* **1768**, 1567-73.

152. Touze, T., Eswaran, J., Bokma, E., Koronakis, E., Hughes, C. & Koronakis, V. (2004). Interactions underlying assembly of the Escherichia coli AcrAB-TolC multidrug efflux system. *Mol Microbiol* **53**, 697-706.

153. Curnow, P. & Booth, P. J. (2007). Combined kinetic and thermodynamic analysis of alpha-helical membrane protein unfolding. *Proc Natl Acad Sci U S A* **104**, 18970-5.

154. Fontana, A., de Laureto, P., Spolaore, B., Frare, E., Picotti, P. & Zambonin, M. (2004). Probing protein structure by limited proteolysis. *Acta Biochim Pol* **51**, 299-321.

155. Zappacosta, F., Pessi, A., Bianchi, E., Venturini, S., Sollazzo, M., Tramontano, A., Marino, G. & Pucci, P. (1996). Probing the tertiary structure of proteins by limited proteolysis and mass spectrometry: the case of Minibody. *Protein Sci* **5**, 802-13.

156. Dokudovskaya, S., Williams, R., Devos, D., Sali, A., Chait, B. T. & Rout, M. (2006). Protease accessibility laddering: a proteomic tool for probing protein structure. *Structure* **14**, 653-60.

157. Fontana, A., Polverino de Laureto, P., De Filippis, V., Scaramella, E. & Zambonin, M. (1997). Probing the partly folded states of proteins by limited proteolysis. *Fold Des* **2**, R17-26.

158. Cohen, S., Ferre-D'Amare, A., Burley, S. & Chait, B. (1995). Probing the solution structure of the DNA-binding protein Max by a combination of proteolysis and mass spectrometry. *Protein Sci* **4**, 1088-99.

159. Su, C., Li, M., Gu, R., Takatsuka, Y., McDermott, G., Nikaido, H. & Yu, E. (2006). Conformation of the AcrB multidrug efflux pump in mutants of the putative proton relay pathway. *J Bacteriol* **188**, 7290-6.

160. Bowie, J. (2005) Solving the membrane protein folding problem. *Nature* **438**, 581-89

161. Zgurskaya, H., & Nikaido, H. (2012). Multidrug resistance mechanisms: drug efflux across two membranes. *Mol Microbiol* **37**, 219-25

162. Nikaido, H., & Pages, J. (2012). Broad-specificity efflux pumps and their role in multidrug resistance of Gram-negative bacteria. *FEMS Microbiol Rev* **36**, 340-63

163. Paulsen, I., Brown, M., & Skurray, R. (1996). Proton-dependent multidrug efflux systems. Microbiol. *Mol Biol Rev* **60**, 575-608

164. Pos, K. (2009). Drug transport mechanism of the AcrB efflux pump. Biochim Biophys Acta **5**, 782-93

165. Eicher, T., Brandstatter, L., & Pos, K. (2009). Structural and functional aspects of the multidrug efflux pump AcrB. *Biol Chem* **390**, 693-9

166. Eicher, T., Cha, H., Seeger, M., Brandstatter, L., El-Delik, J., Bohnert, J., Kern, W., Verrey, F., Grutter, M., Diederichs, K., & Pos, K. (2012). Transport of drugs by the multidrug transporter AcrB involves an access and a deep binding pocket that are separated by a switch-loop. *Proc Natl Acad Sci U. S. A.* **109**, 5687-92

167. Nakashima, R., Sakurai, K., Yamasaki, S., Nishino, K., & Yamaguchi, A. (2011). Structures of the multidrug exporter AcrB reveal a proximal multisite drug-binding pocket. *Nature* **480,** 565-9

168. Takatsuka, Y., Chen, C, & Nikaido, H. (2010). Mechanism of recognition of compounds of diverse structures by the multidrug efflux pump AcrB of Escherichia coli. *Proc Natl Acad Sci U. S. A.* **107**, 6559-65

169. Pos,, K., Schiefner, A., Seeger, M., & Diederichs K. (2004). Crystallographic analysis of AcrB. *FEBS Lett* **564**, 333-9

170. Yu, L., Lu, W., & Wei, Y. (2011). AcrB Trimer Stability and Efflux Activity, Insight from Mutagenesis Studies. *PLoS ONE* **6**, e28390

171. Middlemiss, J., & Poole, K.(2004). Differential impact of MexB mutations on substrate selectivity of the MexAB-OprM multidrug efflux pump of Pseudomonas aeruginosa. *J Bacteriol* **186**, 1258-69

172. Zgurskaya, H., & Nikaido, H. (2000). Cross-linked complex between oligomeric periplasmic lipoprotein AcrA and the inner-membrane-associated multidrug efflux pump AcrB from Escherichia coli. *J Bacteriol* **182**, 4264-7

173. Rasila, T., Pajunen, M., & Savilahti, H. (2009). Critical evaluation of random mutagenesis by error-prone polymerase chain reaction protocols, Escherichia coli mutator strain, and hydroxylamine treatment. *Anal Biochem* **388**, 71-80

174. Klumpp, S., Zhang, Z., & Hwa, T. (2009). Growth rate-dependent global effects on gene expression in bacteria. *Cell* **139**, 1366-75

175. Chen, D., & Texada, D. (2006). Low-usage codons and rare codons of Escherichia coli. *Gene Ther Mol Biol* **10**, 1-12

176. Rand, J., Danby, S., Greenway, D., & England, R. (2002). Increased expression of the multidrug efflux gene acrAB occurs during slow growth of Escherichia coli. *FEMS Microbiol Lett* **207**, 91-5

177. Ferrandez, Y., Monlezun, L., Phan, G., Benabdelhak, H., Benas, P., Ulryck, N., Falson, P., Ducruix, A., Picard, M., & Broutin, I. (2012). Stoichiometry of the MexA-OprM binding, as investigated by blue native gel electrophoresis. *Electrophoresis* **33**, 1282-7

178. Dresler, J., Klimentova, J., & Stulik, J. (2011). Francisella tularensis membrane complexome by blue native/SDS-PAGE. *J Proteomics* **75**, 257-69

179. Radzicka, A., & Wolfenden, R. (1987) Comparing the polarities of the amino acids: side-chain distribution coefficients between the vapor phase, cyclohexane, 1-Octanol, and neutral aqueous solution. *Biochemistry* **27**, 1664-70

180. Schlessinger, J. (2002). Ligand-induced, receptor-mediated dimerization and activation of EGF receptor. *Cell* **110**, 669-72

181. Ayoub, M., Couturier, C., Lucas-Meunier, E., Angers, S., Fossier, P., Bouvier, M., & Jockers R. (2002). Monitoring the ligand-independent dimerization and ligand induced conformational changes of melatonin receptors in living cells by bioluminescence resonance energy transfer. J. Biol. Chem. **277** 21522-8

182. Goodwin, C. & Armstrong, J. (1990). Microbiological aspects of Helicobacter pylori (Campylobacter pylori). *Eur J Clin Microbiol Infect Dis* **9**, 1-13.

183. Sipponen, P. (1991). Helicobacter pylori and chronic gastritis: an increased risk of peptic ulcer? A review. *Scand J Gastroenterol Suppl* **186**, 6-10.

184. Peek, R. M., Jr. & Blaser, M. J. (2002). Helicobacter pylori and gastrointestinal tract adenocarcinomas. *Nat Rev Cancer* **2**, 28-37.

185. Vaira, D. & Vakil, N. (2001). Blood, urine, stool, breath, money, and Helicobacter pylori. *Gut* **48**, 287-9.

186. Cutler, A. F. (1997). Diagnostic tests for Helicobacter pylori infection. *Gastroenterologist* **5**, 202-12.

187. Graham, D. Y., Lew, G. M., Klein, P. D., Evans, D. G., Evans, D. J., Jr., Saeed, Z. A. & Malaty, H. M. (1992). Effect of treatment of Helicobacter pylori infection on the long-term recurrence of gastric or duodenal ulcer. A randomized, controlled study. *Ann Intern Med* **116**, 705-8.

188. West, A. P., Millar, M. R. & Tompkins, D. S. (1992). Effect of physical environment on survival of Helicobacter pylori. *J Clin Pathol* **45**, 228-31.

189. Andersen, L. P. & Rasmussen, L. (2009). Helicobacter pylori-coccoid forms and biofilm formation. *FEMS Immunol Med Microbiol* **56**, 112-5.

190. Walsh, E. J. & Moran, A. P. (1997). Influence of medium composition on the growth and antigen expression of Helicobacter pylori. *J Appl Microbiol* **83**, 67-75.

191. Dumon, C., Priem, B., Martin, S. L., Heyraud, A., Bosso, C. & Samain, E. (2001). In vivo fucosylation of lacto-N-neotetraose and lacto-N-neohexaose by heterologous expression of Helicobacter pylori alpha-1,3 fucosyltransferase in engineered Escherichia coli. *Glycoconj J* **18**, 465-74.

192. Ge, Z., Chan, N. W., Palcic, M. M. & Taylor, D. E. (1997). Cloning and heterologous expression of an alpha1,3-fucosyltransferase gene from the gastric pathogen Helicobacter pylori. *J Biol Chem* **272**, 21357-63.

193. Graham, D. Y., Hammoud, F., El-Zimaity, H. M., Kim, J. G., Osato, M. S. & El-Serag, H. B. (2003). Meta-analysis: proton pump inhibitor or H2-receptor antagonist for Helicobacter pylori eradication. *Aliment Pharmacol Ther* **17**, 1229-36.

194. Stedman, C. A. & Barclay, M. L. (2000). Review article: comparison of the pharmacokinetics, acid suppression and efficacy of proton pump inhibitors. *Aliment Pharmacol Ther* **14**, 963-78.

195. Gerrits, M. M., van Vliet, A. H., Kuipers, E. J. & Kusters, J. G. (2006). Helicobacter pylori and antimicrobial resistance: molecular mechanisms and clinical implications. *Lancet Infect Dis* **6**, 699-709.

196. Graham, D. Y. & Fischbach, L. (2010). Helicobacter pylori treatment in the era of increasing antibiotic resistance. *Gut* **59**, 1143-53.

197. De Francesco, V., Giorgio, F., Hassan, C., Manes, G., Vannella, L., Panella, C., Ierardi, E. & Zullo, A. (2010). Worldwide H. pylori antibiotic resistance: a systematic review. *J Gastrointestin Liver Dis* **19**, 409-14.

198. Nishimura, A., Morita, M., Nishimura, Y. & Sugino, Y. (1990). A rapid and highly efficient method for preparation of competent Escherichia coli cells. *Nucleic Acids Res* **18**, 6169.

199. Srikumar, R., Kon, T., Gotoh, N. & Poole, K. (1998). Expression of Pseudomonas aeruginosa multidrug efflux pumps MexA-MexB-OprM and MexC-MexD-OprJ in a multidrug-sensitive Escherichia coli strain. *Antimicrob Agents Chemother* **42**, 65-71

200. Bos, M. P., & Tommassen, J. (2004) Biogenesis of the Gram-negative bacterial outer membrane, *Curr Opin Microbiol* **7**, 610-616

201. Nikaido, H. (2001) Preventing drug access to targets: cell surface permeability barriers and active efflux in bacteria, *Semin Cell Dev Biol* **12**, 215-223

202. Gold, V. A. M., Duong, F., & Collinson, I. (2007) Structure and function of the bacterial Sec translocon, *Mol Membr Biol* **24**, 387-394.

203. Rizzitello, A. E., Harper, J. R., & Silhavy, T. J. (2001) Genetic evidence for parallel pathways of chaperone activity in the periplasm of *Escherichia coli*, *J Bacteriol* **183**, 6794-6800

204. Leverrier, P., Vertommen, D., & Collet, J. (2010) Contribution of proteomics toward solving the fascinating mysteries of the biogenesis of the envelope of *Escherichia coli*, *Proteomics* **10**, 771-784

205. Vertommen, D., Ruiz, N., Leverrier, P., Silhavy, T. J. & Collet, J. (2011) Characterization of the role of the *Escherichia coli* periplasmic chaperone SurA using differential proteomics, *Proteomics* **9**, 2432-2443

206. Lazar, S. W., Almiron, M., Tormo, A., & Kolter, R. (1996) Role of the *Escherichia coli* SurA protein in stationary phase survival, *J Bacteriol* **180**, 5704-5711

207. Tormo, A., Almiron, M., & Kolter, R. (1990) SurA, an *Escherichia coli* gene essential for survival in stationary phase, *J Bacteriol* **172**, 4339-4347

208. Lazar, S. W., & Kolter, R. (1996) SurA, assists the folding of *Escherichia coli* outer membrane proteins, *J Bacteriol* **178**, 1770-1773

209. Dominique, M., Jean-Michel, B., &Satish, R. (1996) New components of protein folding in extracytoplasmic compartments of *Escherichia coli* SurA, FkpA and Skp/OmpH, *Mol Microbiol* **21**, 871-884

210. Tamae, C., Liu, A., Kim, K., Sitz, D., Hong, J., Becket, E., Bui, A., Solaimani, P., Tran, H. P., Yang, H. J., & Miller, J. H. (2008) Determination of Antibiotic Hypersensitivity among 4,000 Single-Gene-Knockout Mutants of *Escherichia coli*, *J Bacteriol* **190**, 5981-5988

211. Hennecke, G., Nolte, J., Volkmer-Engert, R., Schneider-Mergener, J., & Behrens, S. (2005) The periplasmic chaperone SurA exploits two features characteristic of integral outer membrane proteins for selective substrate recognition *J Biol Chem* **280**, 23540- 23548

212. Bitto, E., & Mckay, D. B. (2004) Binding of phage-display-selected peptides to the periplasmic chaperone protein SurA mimics binding of unfolded outer membrane proteins *FEBS Lett* **568**, 94-98

213. Behrens-Kneip, S. (2010) The role of SurA factor in outer membrane protein transport and virulence *Int J Med Microbiol* **300**, 421-428

214. Ruiz, N., Chng, S., Hiniker, A., Kahne, D., & Silhavy, T. J. (2010) Nonconsecutive disulfide bond formation in an essential integral outer membrane protein, *Proc Natl Acad Sci U S A* **107**, 12245-12250

215. Muller, M., Koch, H. G., Beck, K., & Schafer, U. (2001) Protein traffic in bacteria: multiple routes from the ribosome to and across the membrane, Prog. Nucleic Acid Res. *Mol Biol* **66**, 107-157

216. Alcock, F.H., Grossmann, J.G., Gentle, I.E., Likic, V.A., Lithgow, T., & Tokatlidis, K. (2008) Conserved substrate binding by chaperones in the bacterial periplasm and the mitochondrial inter-membrane space. *Biochem J* **409**, 377–387.

217. Sydenham, M., Douce, G., Bowe, F., Ahmed, S., Chatfield, S., & Dougan, G. (2000) *Salmonella enterica serovartyphimurium* surA mutants are attenuated and effective live oral vaccines, *Infect Immun* **68**, 1109–1115

218. Notredame, C., Higgins, D. G., & Heringa, J. (2000) T-coffee: A novel methods for fast and accurate multiple sequence alignment, *J Mol Biol* **302**, 205-217

219. Palomino, C., Marin, E., & Fernandez, L. A. (2011) The fimbrial usher FimD follows the SurA-BamB pathway for its assembly in the outer membrane of *Escherichia coli*., *J Bacteriol* **193**, 5222-5230.

220. Dougherty, D. A. (1996) Cation-π interactions in chemistry and biology: A new view of benzene, Phe, Tyr, and Trp, *Science* **271**, 163-168.

221. Park, K., Fasman, G. D., Flynn, G. C., & Rothman, J. E. (1993) Conformational change of chaperone Hsc70 upon binding to a decapeptide: A circular dichroism study. *Protein Sci* **2**, 325–330.

222. Haimann, M. M., Akdogan, Y., Philipp, R., Varadarajan, R., Hinderberger, D., & Trommer, W.E. (2011) Conformational changes of the chaperone SecB upon binding to a model substrate--bovine pancreatic trypsin inhibitor (BPTI). *Biol Chem* **392**, 849-58

223. Ferrell, B. (2011) Investigation of the critical residues in the C-terminus of the E.coli periplasmic chaperone, SurA. *Thesis and Dissertation—Chemistry* paper 8

224. Eugenii, K., &Itamar. W. (2003) Probing Biomolecular Interactions at Conductive and Semiconductive Surfaces by Impedance Spectroscopy: Routes to Impedimetric Immunosensors, DNA-Sensors, and Enzyme Biosensors. *Electroanalysis* **15**, 913-47

225. Kohn, M. (2009) Immobilization strategies for small molecule, peptide and protein microarrays. *J Pept Sci* **15**, 393-397

226. Yamaguchi, H., Miyazaki, M., Honda, T., Briones-Nagata, M. P., Arima, K. & Maeda, H. (2009). Rapid and efficient proteolysis for proteomic analysis by protease-immobilized microreactor. *Electrophoresis* **30**, 3257-64.

227. Wang, Z. & Jin, G. (2003). Feasibility of protein A for the oriented immobilization of immunoglobulin on silicon surface for a biosensor with imaging ellipsometry. *J Biochem Biophys Methods* **57**, 203-11.

228. Tan, Y. H., Liu, M., Nolting, B., Go, J. G., Gervay-Hague, J. & Liu, G. Y. (2008). A nanoengineering approach for investigation and regulation of protein immobilization. *ACS Nano* **2**, 2374-84.

229. Batalla, P., Fuentes, M., Mateo, C., Grazu, V., Fernandez-Lafuente, R. & Guisan, J. M. (2008). Covalent immobilization of antibodies on finally inert support surfaces through their surface regions having the highest densities in carboxyl groups. *Biomacromolecules* **9**, 2230-6.

230. Yewle, J. N., Wei, Y., Puleo, D. A., Daunert, S. & Bachas, L. G. (2012). Oriented immobilization of proteins on hydroxyapatite surface using bifunctional bisphosphonates as linkers. *Biomacromolecules* **13**, 1742-9.

231. Cha, T., Guo, A. & Zhu, X. Y. (2005). Enzymatic activity on a chip: the critical role of protein orientation. *Proteomics* **5**, 416-9.

232. Fuentes, M., Mateo, C., Pessela, B. C., Batalla, P., Fernandez-Lafuente, R. & Guisan, J. M. (2007). Solid phase proteomics: dramatic reinforcement of very weak protein-protein interactions. *J Chromatogr B Analyt Technol Biomed Life Sci* **849**, 243-50.

233. Hochuli, E. (1988). Large-scale chromatography of recombinant proteins. *J Chromatogr* **444**, 293-302.

234. Khan, F., He, M. & Taussig, M. J. (2006). Double-hexahistidine tag with high-affinity binding for protein immobilization, purification, and detection on ni-nitrilotriacetic acid surfaces. *Anal Chem* **78**, 3072-9.

235. Fischer, N. O., Blanchette, C. D., Chromy, B. A., Kuhn, E. A., Segelke, B. W., Corzett, M., Bench, G., Mason, P. W. & Hoeprich, P. D. (2009). Immobilization of His-tagged proteins on nickel-chelating nanolipoprotein particles. *Bioconjug Chem* **20**, 460-5.

236. Hengen, P. (1995). Purification of His-Tag fusion proteins from Escherichia coli. *Trends Biochem Sci* **20**, 285-6.

237. Shao, W. H., Zhang, X. E., Liu, H., Zhang, Z. P. & Cass, A. E. (2000). Anchor-chain molecular system for orientation control in enzyme immobilization. *Bioconjug Chem* **11**, 822-6.

238. Kacar, T., Zin, M. T., So, C., Wilson, B., Ma, H., Gul-Karaguler, N., Jen, A. K., Sarikaya, M. & Tamerler, C. (2009). Directed self-immobilization of alkaline phosphatase on micro-

patterned substrates via genetically fused metal-binding peptide. *Biotechnol Bioeng* **103**, 696-705.

239. Rusmini, F., Zhong, Z. & Feijen, J. (2007). Protein immobilization strategies for protein biochips. *Biomacromolecules* **8**, 1775-89.

240. Niemeyer, C. M. (2002). The developments of semisynthetic DNA-protein conjugates. *Trends Biotechnol* **20**, 395-401.

241. Weng, S., Gu, K., Hammond, P. W., Lohse, P., Rise, C., Wagner, R. W., Wright, M. C. & Kuimelis, R. G. (2002). Generating addressable protein microarrays with PROfusion covalent mRNA-protein fusion technology. *Proteomics* **2**, 48-57.

242. Hendrickson, E. R., Truby, T. M., Joerger, R. D., Majarian, W. R. & Ebersole, R. C. (1995). High sensitivity multianalyte immunoassay using covalent DNA-labeled antibodies and polymerase chain reaction. *Nucleic Acids Res* **23**, 522-9.

243. Schweitzer, B., Wiltshire, S., Lambert, J., O'Malley, S., Kukanskis, K., Zhu, Z., Kingsmore, S. F., Lizardi, P. M. & Ward, D. C. (2000). Immunoassays with rolling circle DNA amplification: a versatile platform for ultrasensitive antigen detection. *Proc Natl Acad Sci U S A* **97**, 10113-9.

244. Howorka, S., Cheley, S. & Bayley, H. (2001). Sequence-specific detection of individual DNA strands using engineered nanopores. *Nat Biotechnol* **19**, 636-9.

245. Kozlov, I. A., Melnyk, P. C., Stromsborg, K. E., Chee, M. S., Barker, D. L. & Zhao, C. (2004). Efficient strategies for the conjugation of oligonucleotides to antibodies enabling highly sensitive protein detection. *Biopolymers* **73**, 621-30.

246. Glynou, K., Ioannou, P. C. & Christopoulos, T. K. (2003). Affinity capture-facilitated preparation of aequorin- oligonucleotide conjugates for rapid hybridization assays. *Bioconjug Chem* **14**, 1024-9.

247. Boozer, C., Ladd, J., Chen, S., Yu, Q., Homola, J. & Jiang, S. (2004). DNA directed protein immobilization on mixed ssDNA/oligo(ethylene glycol) self-assembled monolayers for sensitive biosensors. *Anal Chem* **76**, 6967-72.

248. Boozer, C., Ladd, J., Chen, S. & Jiang, S. (2006). DNA-directed protein immobilization for simultaneous detection of multiple analytes by surface plasmon resonance biosensor. *Anal Chem* **78**, 1515-9.

249. Schlapak, R., Pammer, P., Armitage, D., Zhu, R., Hinterdorfer, P., Vaupel, M., Fruhwirth, T. & Howorka, S. (2006). Glass surfaces grafted with high-density poly(ethylene glycol) as substrates for DNA oligonucleotide microarrays. *Langmuir* **22**, 277-85.

250. Niemeyer, C. M., Boldt, L., Ceyhan, B. & Blohm, D. (1999). DNA-Directed immobilization: efficient, reversible, and site-selective surface binding of proteins by means of covalent DNA-streptavidin conjugates. *Anal Biochem* **268**, 54-63.

251. Takeda, S., Tsukiji, S. & Nagamune, T. (2004). Site-specific conjugation of oligonucleotides to the C-terminus of recombinant protein by expressed protein ligation. *Bioorg Med Chem Lett* **14**, 2407-10.

252. Roberts, R. W. & Szostak, J. W. (1997). RNA-peptide fusions for the in vitro selection of peptides and proteins. *Proc Natl Acad Sci U S A* **94**, 12297-302.

253. Biyani, M., Husimi, Y. & Nemoto, N. (2006). Solid-phase translation and RNA-protein fusion: a novel approach for folding quality control and direct immobilization of proteins using anchored mRNA. *Nucleic Acids Res* **34**, e140.

254. Schweller, R. M., Constantinou, P. E., Frankel, N. W., Narayan, P. & Diehl, M. R. (2008). Design of DNA-conjugated polypeptide-based capture probes for the anchoring of proteins to DNA matrices. *Bioconjug Chem* **19**, 2304-7.

255. Lee, S. K., Maye, M. M., Zhang, Y. B., Gang, O. & van der Lelie, D. (2009). Controllable g5p-protein-directed aggregation of ssDNA-gold nanoparticles. *Langmuir* **25**, 657-60.

256. Meyer, R. R. & Laine, P. S. (1990). The single-stranded DNA-binding protein of Escherichia coli. *Microbiol Rev* **54**, 342-80.

257. Lohman, T. M. & Bujalowski, W. (1988). Negative cooperativity within individual tetramers of Escherichia coli single strand binding protein is responsible for the transition between the $(SSB)_{35}$ and $(SSB)_{56}$ DNA binding modes. *Biochemistry* **27**, 2260-5.

258. Lohman, T. M. & Ferrari, M. E. (1994). Escherichia coli single-stranded DNA-binding protein: multiple DNA-binding modes and cooperativities. *Annu Rev Biochem* **63**, 527-70.

259. Overman, L. B., Bujalowski, W. & Lohman, T. M. (1988). Equilibrium binding of Escherichia coli single-strand binding protein to single-stranded nucleic acids in the $(SSB)_{65}$ binding mode. Cation and anion effects and polynucleotide specificity. *Biochemistry* **27**, 456-71.

260. Raghunathan, S., Kozlov, A. G., Lohman, T. M. & Waksman, G. (2000). Structure of the DNA binding domain of E. coli SSB bound to ssDNA. *Nat Struct Biol* **7**, 648-52.

Vita

Meng Zhong

EDUCATION

- B.S. in Chemistry (Analytical Chemistry), 2008
  College of Chemistry and Molecular Engineering
  Peking University, Beijing, China

PUBLICATION

- Zhong, M., Ferrell, B., Lu, W., Wu, M., Chai Q., & Wei Y. (2012). Insights into the Function and Structural Flexibility of the Periplasmic Molecular Chaperone SurA. *J. Bacteriol*., 195, 1061-7
- Zhong, M., Fang, J., & Wei, Y. (2010) Site Specific and reversible protein immobilization facilitated by a DNA binding fusion tag. *Bioconjugate Chemistry*, 21, 1177-82
- Zhong, M., Ferrell, B., Lu, W., Wu, M., & Wei, Y. Evidence for increased cell permeability in SurA deficient strain unrelated to outer membrane protein level. In preparation
- Zhong, M., Cui, Y., Lu, W., Wu, M., Yu, L., & Wei, Y. Characterization of mutations in $AcrB_{P223G}$ restoring trimerization, substrate binding and interaction with AcrA. In preparation.
- Cui, Y., Chai, Q., Zhong, M. & Wei, Y. (2012) Effect of crowding by Ficolls on OmpA and OmpT refolding and membrane insertion. *Prot. Sci.* 22, 239-45
- Lu, W., Chai, Q., Zhong, M., Yu, L., Fang, J., Wang, T., Li, H., Zhu, H., & Wei Y. (2012) Assembling of AcrB trimer in cell membrane. J. Mol. Biol. 423, 123-34
- Lu, W., Zhong, M., Wei, Y. (2011) Folding of AcrB subunit precedes trimerization. *J. Mol. Biol.*, 411, 264-74
- Lu, W., Zhong, M., Wei, Y. (2011) A reporter platform for the monitoring of in vivo conformational changes in AcrB. *Protein Pept. Lett.*, 18, 863-71
- Yu, L., Zhong, M., Wei, Y. (2010) Direct fluorescence polarization assay for the detection of glycopeptide antibiotics. *Analytical Chemistry*, 82, 7044-48

CONFERENCE PRESENTATIONS

- Poster presentation, Gibbs Conference, Carbondale, IL (2012)
- Poster presentation and graduate research award presentation, ASBMB Annual Meeting, Washington D. C. (2011)
- Naff Symposium, University of Kentucky, Lexington, KY (2010, 2011)
- Poster presentation, Gibbs Conference, Carbondale, IL (2009)
- Oral presentation, Kentucky Academy of Science Meeting, Highland Heights, KY (2009)
-

AWARDS AND HONORS

- Kentucky Opportunity Fellowship, 2009-2010
- Research Challenge Trust Fund, University of Kentucky, 2010-2011
- Presidential Fellowship, University of Kentucky, 2011-2012
- Academic Year Fellowship, University of Kentucky, 2012-2013
- 100 & plus Award for best graduate student, Department of Chemistry, 2012
- Graduate Travel Award, 2011 ASBMB annual meeting, Washington D. C., 2011
- 2^{nd} prize graduate presentation award, 94^{th} KAS meeting, Highland Heights, KY, 2009